ORNL/TM-6832
ENDF-281

Measurement of $^{238}U(n,n'\gamma)$ and $^{7}Li(n,n'\gamma)$ Gamma-Ray Production Cross Sections

D. K. Olsen
G. L. Morgan
J. W. McConnell

OAK RIDGE NATIONAL LABORATORY
OPERATED BY UNION CARBIDE CORPORATION · FOR THE DEPARTMENT OF ENERGY

Printed in the United States of America. Available from
National Technical Information Service
U.S. Department of Commerce
5285 Port Royal Road, Springfield, Virginia 22161
Price: Printed Copy $6.50; Microfiche $3.00

ORNL/TM-6832
ENDF-281
Dist. Category UC-79d

Contract No. W-7405-eng-26

Engineering Physics Division

MEASUREMENT OF $^{238}U(n,n'\gamma)$ AND $^{7}Li(n,n'\gamma)$ GAMMA-RAY PRODUCTION CROSS SECTIONS

D. K. Olsen, G. L. Morgan,* and J. W. McConnell

Manuscript Completed - May 7, 1979

Date Published: September 1979

* Present Address: Los Alamos Scientific Laboratory

Prepared by the
OAK RIDGE NATIONAL LABORATORY
Oak Ridge, Tennessee 37830
operated by
UNION CARBIDE CORPORATION
for the
DEPARTMENT OF ENERGY

CONTENTS

ABSTRACT

Time-of-flight techniques and a 95-cm^3 Ge(Li) detector positioned 20 m from the ORELA white neutron source have been utilized to measure 125° cross sections for the production of gamma rays in ^{238}U and ^{7}Li samples by 0.48- to 5.0-MeV neutrons. The incident neutron flux was determined with a proton-recoil telescope which used a solid-state, recoil-proton detector. Altogether, 28 cross sections for ^{238}U transitions from levels with 680 to 1224 keV of excitation were measured. In addition, 7 branching ratios for weak ^{238}U transitions and the $^{7}Li(n,n'\gamma)$ $^{7}Li^*$ (478 keV) cross section were measured. From these data and other level-decay information, preliminary neutron inelastic scattering cross sections were constructed and compared with those at 680, 732, 827, 965, 1048, and 1170-keV of excitation from the proposed ENDF/B-V evaluation.

I. INTRODUCTION

Accurate knowledge of neutron inelastic scattering cross sections on ^{238}U is important for fast reactor design. Although these cross sections do not determine neutron balance directly, they influence fast-critical and reactor parameters through the energy transfer mechanism they provide for the neutron flux. For example, the sensitivities of the neutron multiplication and the ^{238}U to ^{239}Pu fission ratio of the ZPR-6/7 fast critical are - 0.043 and - 0.243, respectively, with respect to the total ^{238}U inelastic cross section,[1] which is known with perhaps a 7 to 10% accuracy.[2] More importantly, the excitation-energy distribution must be accurately known, since, depending on the flux shape, a small cross section giving a large energy transfer may be as important as a large cross section giving a small energy transfer. Accurate knowledge of these cross sections has been elusive since the cross sections are both difficult to measure due to resolution-intensity problems and difficult to calculate due to simultaneous compound and direct components because ^{238}U is highly deformed.

The most recent evaluation of these cross sections is described in ref. 2 and intended for inclusion in the ENDF/B-V file. The evaluators[2] first determined the total inelastic cross section as the difference between precisely determined partial cross sections and the accurately measured total cross section. Figure 1 shows part of the ^{238}U energy level diagram from the 1977 compilation by Ellis.[3] Inelastic scattering measurements[4-11] with Van de Graaff neutrons independently determined the important cross sections for the 2^+(44.9 keV) and 4^+(148.4 keV) members of the ground-state (GS) rotational band shown in Fig. 1

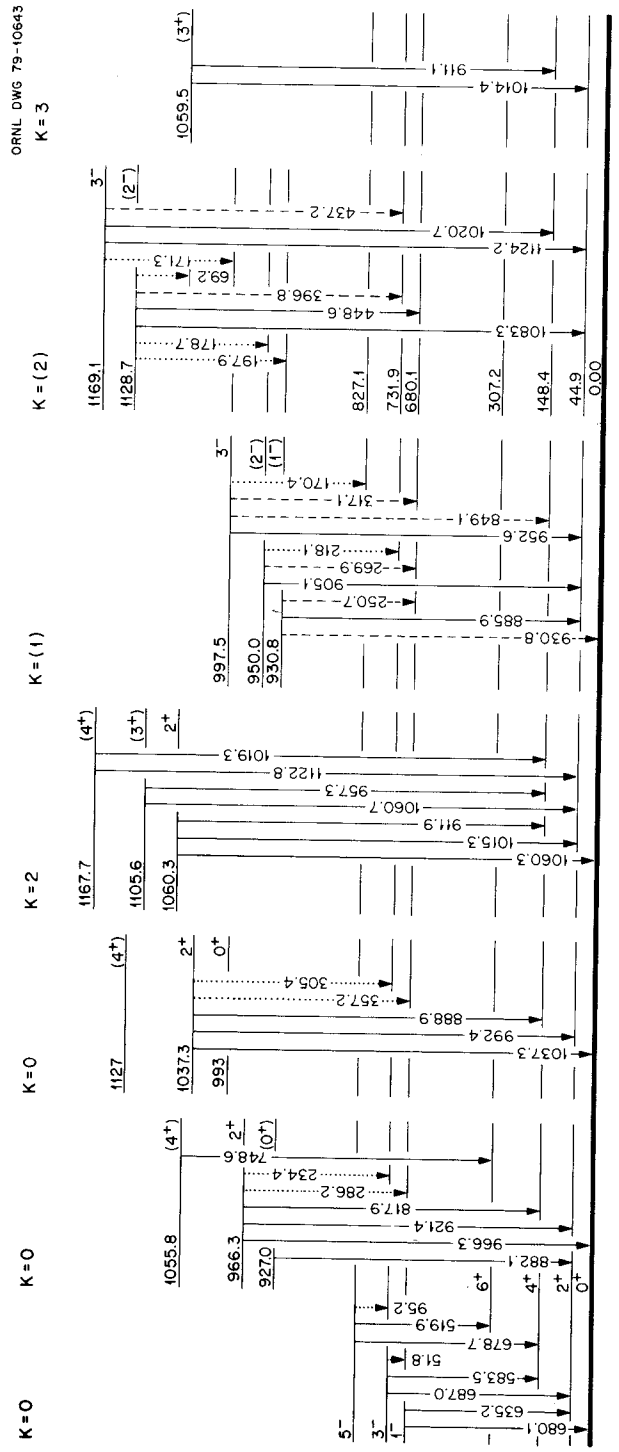

Fig. 1. Proposed ^{238}U rotational-band structure of Ref. 3.

Cross sections for the higher levels from 680 keV to about 1.3 MeV of excitation were determined with Van de Graaff measurements[4,5,7,8,12] mostly at one angle, the $^{238}U(n,n'\gamma)$ results of McMurray et al.,[13] the total inelastic constraint, and theoretical considerations. The 680.1, 731.9, and 927.1 keV levels of Fig. 1 have unique evaluated[2] cross sections. Levels from 927 keV and upwards are clustered into pseudolevels and evaluated[2] as groups. The correspondence between the 965, 1048, and 1170 keV pseudolevels of ref. 2 with the low-spin levels[3] of Fig. 1 are listed in Table 1. Above $\sim$ 1.5 MeV the remaining unassigned inelastic cross section was distributed over excitation energy following theoretical considerations. The resultant ^{238}U inelastic cross sections along with others were tested against ZPR-6-7 criticality, ^{238}U-reflected clean spherical critical, and ^{238}U pulsed-sphere emergent spectra.[2]

This technical memorandum reports the measurement of gamma-ray production cross sections from ^{238}U inelastic scattering. From these data and other level-decay information[3,14-18] inelastic scattering cross sections were constructed and compared with those from the 680, 732, 827 keV levels and the 965, 1048, and 1170 keV pseudolevels of the proposed ENDF/B-V evaluation.[2] In particular, time-of-flight techniques and a 95-cm^3 Ge(Li) detector positioned 20 m from the Oak Ridge Electron Linear Accelerator (ORELA) white neutron source were utilized to measure 125° cross sections for the production of gamma rays in ^{238}U samples by 0.48- to 5.0-MeV neutrons. The incident neutron flux was determined with a proton-recoil telescope which used a solid state, recoil-proton detector.[19] Simultaneously, the $^{7}Li(n,n'\gamma)$ $^{7}Li^{*}$(478 keV) cross section was measured in order to verify the ^{238}U results. Altogether, 28 cross

TABLE I. Correspondence Between ENDF/B-V (Ref. 2) Pseudolevels and Nuclear Data Sheets Energy Levels* (Ref. 3)

ENDF/B-V	Nuclear Data Sheets	
965 keV	927.0 keV	(0^+)
	930.8	(1^-)
	950.0	(2^-)
	966.3	2^+
	993	0^+
	997.5	3^-
1048 keV	1037.3 keV	2^+
	1055.8	(4^+)
	1059.5	(3^+)
	1060.3	2^+
1170 keV	1105.6 keV	(3^+)
	1127	(4^+)
	1128.7	(2^-)
	1167.7	(4^+)
	1169.1	3^-

*High spins and the 998.3-keV levels not listed

sections for ^{238}U transitions from levels with 680 to 1224 keV of excitation were measured with an additional 7 branching ratios for weak transitions. These transitions are shown as solid lines and dashed lines, respectively, on the Fig. 1 energy level diagram. The dotted lines show transitions needed to calculate inelastic scattering cross sections and were obtained from other sources.[3,14-18]

Section II of this report describes the experimental aspects of the measurement. Section III describes the data reduction procedure and Section IV presents the resultant gamma-ray production cross sections which are listed in Appendix A. Appendix B contains figures of some measured gamma-ray spectra. Finally, in Section V the inelastic scattering cross sections are constructed and compared with those of the proposed ENDF/B-V evaluation.[2] This section is considered preliminary since incompleted Coulomb excitation work[18,20] may provide improved spectral decay information. Some conclusions from the present work are discussed in Section VI.

II. EXPERIMENTAL APPARATUS AND PROCEDURE

A. Beam Line

The measurement was performed at the 20-m station of ORELA[21] flight path[22] number 8 with the beam conditions summarized in Table II. Eight hundred electron pulses per second were incident on the ORELA water-cooled tantalum target-moderator,[23] producing neutron bursts with a FWHM of 35 nsec. This neutron flux was collimated by three sets of standard apertures to produce a 7-cm diameter beam spot at the sample position. In order to maximize the intensity of high-energy neutrons no shadow bar was employed and in order to minimize the intensity of very low-energy neutrons the 14.0-cm diameter collimator at 3m, collimator A, contained a 22.9-cm long brass sleeve with a 6.4-cm diameter aperture. The 5-m filter changer contained a 0.93 gm/cm^2 ^{10}B filter to prevent time overlap from successive bursts, a 5.1-cm thick carbon filter to provide a verification of the energy scale, and fourteen 1.27-cm thick thorium filters used to reduce the gamma flash to a tolerable level. Final data were taken with eleven of the fourteen thorium filters in the beam. The beam line was evacuated from the ORELA target to the beam dump except for a $\sim$ 2.5-m air gap over the optical bench[22] at 20 m.

A proton recoil (PR) telescope and a scattering sample were mounted on the optical bench. Figure 2 shows a schematic diagram of the PR telescope whose radiator consisted of a 6.9-mgm/cm^2 aluminum absorber foil sandwiched between 2.0 and 0.67-mgm/cm^2 polyethylene radiator foils. Recoil protons from the radiators were counted with a 0.30-mm thick silicon solid-state detector whose geometry was defined by a 1.27-cm^2 aperture

TABLE II. Neutron Beam Conditions

H_2O cooled Ta target
Flight path length - 22.181 m
Pulse rate - 800 Hertz
Pulse width - 35 nsec (FWHM)
Electron beam power - 35 kW
Time overlap filter - 0.93 gm/cm^2 of ^{10}B
Gamma flash filter - 14.0 cm of Th

located 30.6 cm from the radiator center at an angle of 15° with respect to the beam direction. In order to obtain a recoil-proton energy calibration for the solid state detector and verification of counting losses, an ^{241}Am alpha source was mounted near the radiator. This telescope was positioned upstream from the scattering sample with its radiator foil 21.420 m from the ORELA target center.

A flat scattering sample was mounted in a vertical plane at a 50° angle with respect to the beam direction with its center positioned 22.181 m from the ORELA target center. Both a ^{238}U and a ^{7}Li scattering sample were employed. The 0.003760-atom/barn ^{238}U sample consisted of a 11.11-cm diameter, 0.76-mm thick, 99.92% isotopically enriched disk. The 0.02912-atom/barn highly-enriched ^{7}Li sample consisted of a 78.77-gm, 15.2 x 15.2 x 0.63-cm isotopically enriched plate enclosed in an airtight stainless steel can with 0.05-mm thick windows.

Photons produced in the sample were counted with a 95-cm^3 Ge(Li) detector with its front face positioned 28 cm from the sample center and shielded from low-energy photons with 1.8 mm of lead. The sides of the crystal were shielded with a 5-cm thick lead sleeve. This detector

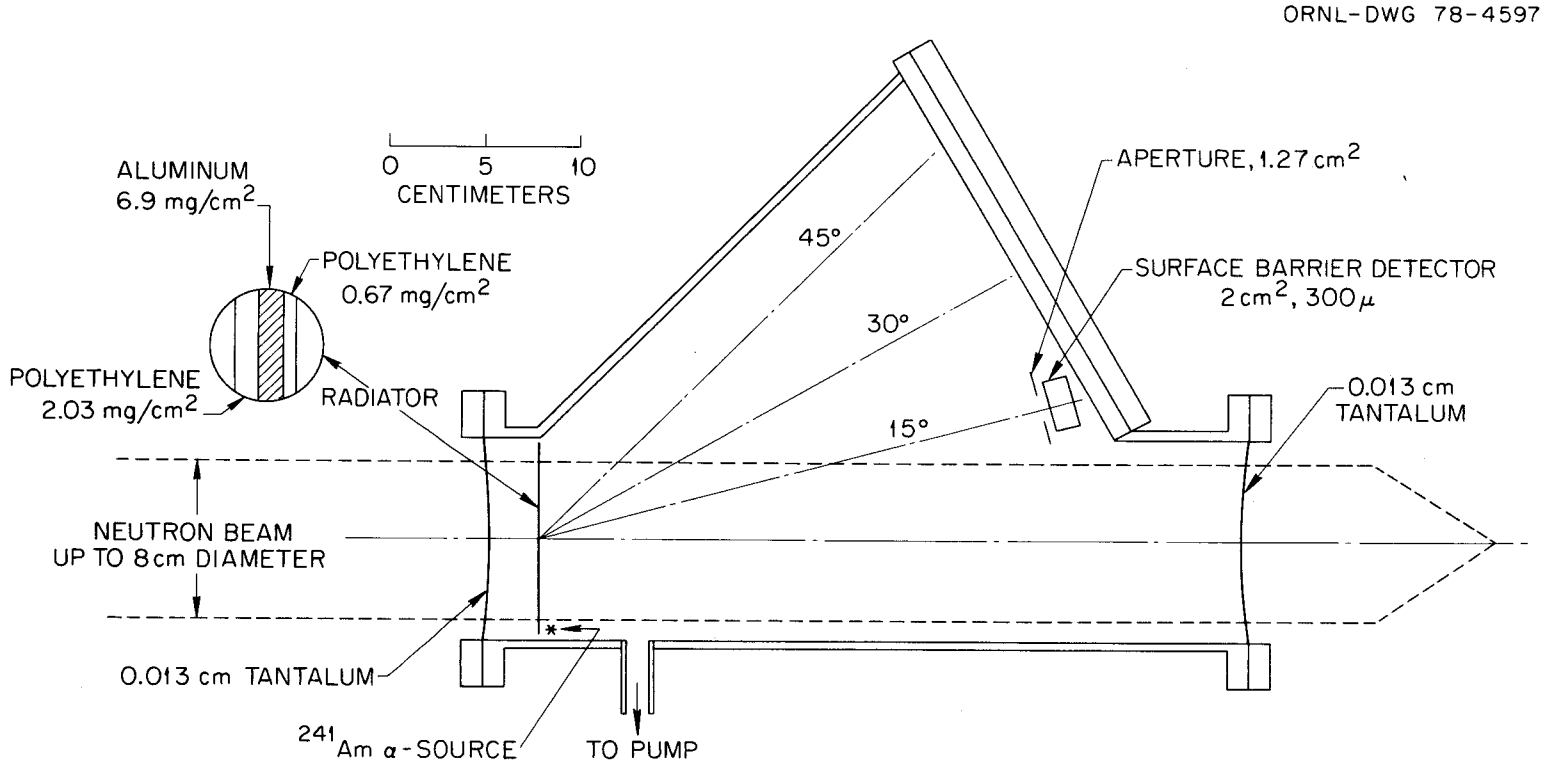

Fig. 2. Schematic diagram of the proton-recoil telescope, which was mounted upstream from the scattering sample and Ge(Li) detector, with its radiator foil 21.43 m from the ORELA target center.

was mounted so that its axis was at 125° and 15° angles with respect to the beam direction and sample-disk normal, respectively. In order to eliminate RF interference, both the detector and associated electronics were contained in a copper-screened cage. In order to measure counting losses and line-shape distortion during the ORELA burst, a ^{137}Cs source was mounted near the sample to provide a 662-keV photon source of constant and known intensity.

B. Electronic Apparatus

Both fast and slow signals were obtained from the Ge(Li) and PR detectors. The fast signals were combined in an OR circuit and used to stop a time digitizer operated in a single stop mode so that no more than one event from either the Ge(Li) or PR detector could be processed per ORELA burst. Figure 3 shows a schematic of the electronic apparatus.

In particular, the Ge(Li) detector was an ORTEC 95-cm^3 true coaxial crystal operated at a bias of + 4800 V. Slow signals from this detector were integrated and shaped with a TC205A amplifier, and the resulting bipolar output was pulse-height analyzed into 2048 channels with an ORTEC 800 ADC. Fast signals from this detector were amplified with an ORTEC 454 timing-filter amplifier whose output fed an ORTEC 473A constant fraction discriminator (CFD) operated in the slow-risetime reject (SRR) mode.

The PR telescope employed an ORTEC 0.30-mm thick, surface-barrier, solid-state detector operated at + 100 V of bias with an ORTEC 124 preamplifier. Using a twin-axial cable the "E output" of the preamplifier fed a TC217 differential amplifier, followed by a CI1410 double delay line amplifier whose delayed output was pulse-height analyzed into 256

ORNL–DWG 79-9940

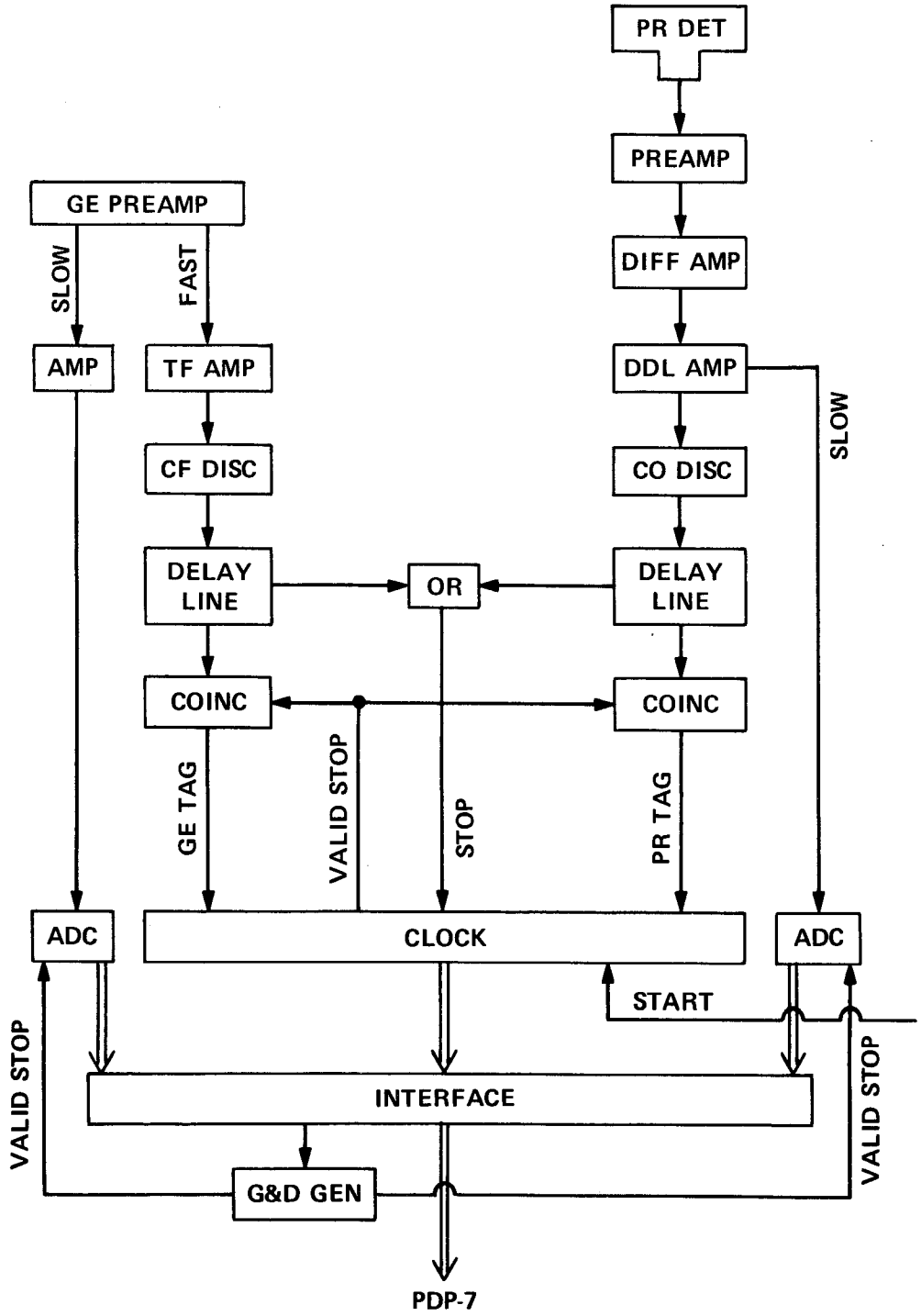

Fig. 3. Major electronic components of data acquisition system.

channels with a TMC 217A ADC. From the prompt output of the amplifier a fast signal was generated using an ORNL Q3066B crossover discriminator.

The fast signal from each detector was split. One set of fast signals was combined in an EG&G C315/NL OR circuit and used to stop an EG&G TDC100 clock operated in a single-stop mode. Start signals for the clock were obtained from the usual ORELA gamma-flash detector.[24] If the stop signal was in the correct time range, the clock valid-stop output signal was coincidenced with the other set of fast signals and returned to the clock to supply tags to distinguish which detector initiated the event. Nineteen bits of tag and time-of-flight information were discharged from the clock to the PDP-7 interface which then triggered the ADC's to also discharge their pulse-height information.

The resulting word was sent sequentially to the laboratory E PDP-7 computer which controlled the measurement, stored summed flight-time and pulse-height spectra for each detector, read and update various hardware and software scalers, and acted as a buffer to the SEL810B computer. The SEL computer stored[25] the event on a random-access fast disk. Each event from either the Ge(Li) or PR detector was stored in separate two-parameter arrays of pulse height versus TOF: one array of 2048 pulse-height channels per TOF channel for the Ge(Li) detector and another array of 256 pulse-height channels per TOF channel for the PR detector. Table III gives the TOF channel structure common to both detectors. In addition, pulse-height-summed TOF spectra with 1 nsec channel widths from the two detectors were stored.

TABLE III. Time-of-flight Channel Structure

Number of Spectra	Channel Width (nsec)	Clock Time (μsec)	Ge(Li) Energy (MeV)
1	40	0.0 - 0.040	-
1	1160	0.040 - 1.200	Background
1	184	1.200 - 1.384	Gamma flash
1	370	1.384 - 1.754	∞ - 8.184
50	36	1.754 - 3.554	8.184 - 0.462
1	498	3.554 - 4.052	0.462 - 0.315
1	1260	4.052 - 5.312	0.315 - 0.152
5	1200	5.312 - 65.312	0.152 - 0.0006

C. Experimental Procedure

Considerable beam time was used investigating pileup, deadtime, photopeak line shape, and timing line-shape problems associated with the Ge(Li) detector. In particular, it was assumed that the line shape of the gamma flash photons scattered from the sample into the Ge(Li) detector was indeed the Ge(Li) timing resolution function. Without the SRR circuit of the CFD an ORELA burst width of 5 nsec (FWHM) produced a gamma flash group 8 nsec wide which was more than adequate; however, $\sim$ 50% of the events were contained in a large tail trailing hundreds of nsec behind the main group. Use of the SRR with proper discriminator adjustment removed this tail, reducing the count rate by 50% and selectively discriminating against low-energy photons. Figure 4 shows a Ge(Li), pulse-height summed, TOF spectrum for 35 nsec wide ORELA burst and 4 nsec wide channels. The gamma-flash group is also $\sim$ 35 nsec wide with no trailing tail.

ORNL-DWG. 78-11945

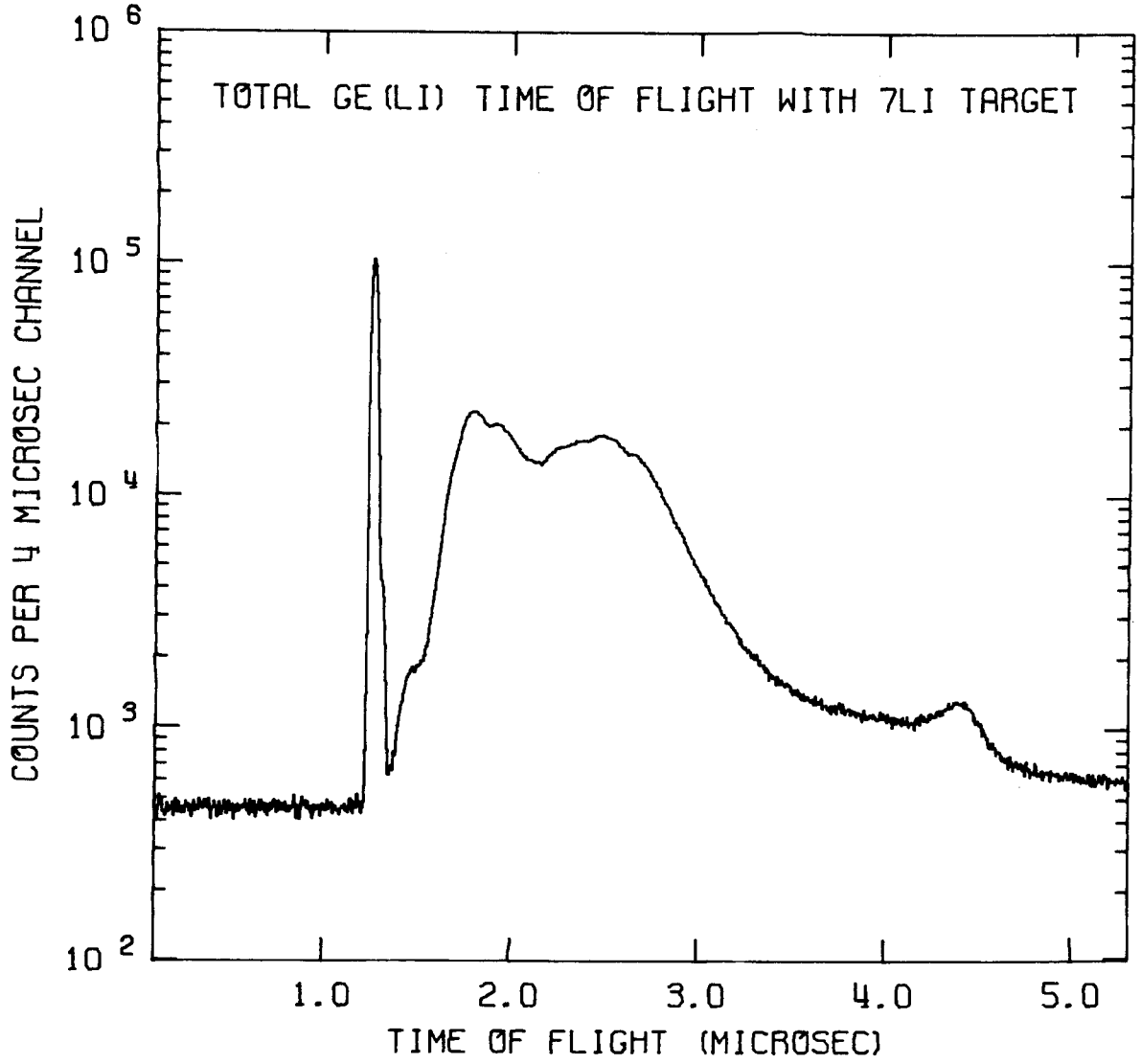

Fig. 4. Ge(Li) pulse-height-summed, TOF spectrum for 35-nsec FWHM ORELA burst on ^{7}Li. Photons of interest produced by 5.0 to 0.5-MeV neutrons span clock times from 1.9 to 3.5 μsec, respectively. Gamma-flash photons occur at 1.3 μsec and neutron scattering from the 0.25-MeV ^{7}Li resonance produces the peak observed at 4.4 μsec.

With this resolution function, pileup and deadtime problems were investigated by varying the neutron intensity and ratio to gamma flash by changing the Th filter thickness and observing the intensity and photopeak line shape of the ^{137}Cs group counted during various time intervals following the gamma flash. At very long times the ^{137}Cs line had the same shape and count rate, within 1% with the appropriate clock deadtime correction, as counting with ORELA off. However, at very short times, corresponding to 0.5 to 5.0 MeV, this was not the case; the ^{137}Cs line shape was slightly distorted with a high-energy tail and the count rate was significantly smaller than the beam off measurement. This loss of counts was expected because the clock recorded only events as determined by the CFD with SRR. Events which did not fire the CFD went undetected causing pileup on the slow pulses and thus removing them from the full-energy peaks. The clock deadtime correction could not account for this pileup. Using various Th filter thicknesses this missing count rate was found to be proportional to the count rate indicating a pileup problem. The fact that the ^{241}Am group measured in the PR detector had the correct count rate after the clock deadtime correction indicated that the problem was in the Ge(Li) detector.

At 35 kW of ORELA electron beam power, a suitable compromise between count rate and missing count rate was obtained with 14.0 cm of thorium filter. With the ^{238}U sample the Ge(Li) detector counted a gamma-flash photon for $\sim$ 3% of the beam bursts and counted a photon in the neutron energy range of interest for $\sim$ 3% of the bursts. Over this neutron energy region the electronic deadtime and pileup correction was measured to be 10%. Ge(Li) spectra from the ^{7}Li sample also required a 10% correction.

Because of possible uncertainties in this correction and to account for uncertainties in extracting counts from slightly distorted line shapes a 5% uncorrelated uncertainty was added quadratically to the statistical uncertainty for each photon group in each energy bin. This uncertainty represents a major source of error in the measurement.

With the beam conditions of Table II, final data were taken over parts of four ORELA cycles, each of ten days duration. The ^{238}U and ^{7}Li samples were alternated in the beam for intervals on the order of one day with the ^{238}U sample occupying $\sim$ 75% of the available beam time. The output of a NDS36 clock was counted to insure that the system was operating correctly over long periods of time. After each of these counting intervals various consistency checks were made and the data transferred to a PDP-10 disk. After completion of a cycle the ^{238}U and ^{7}Li data were summed giving a separate measurement for each of the four cycles. At the end of each interval the events in the various spectra were summed and compared to the scalers to insure that the data had been transferred correctly from the clock and ADC's to the PDP-7 computer and to the SEL disk. In addition, the number of ^{137}Cs events and ^{241}Am events at long and short times, the number of either ^{238}U 635-keV or ^{7}Li 478-keV events, and an integrated number of monitor events were calculated, ratioed, and compared to insure that the system was stable. Prior to this measurement, the efficiency of the Ge(Li) detector was measured in situ with ^{137}Cs, ^{88}Y, ^{22}Na, ^{60}Co, ^{152}Eu, and ^{106}Ru sources. At the end of each cycle the efficiency was checked with the ^{152}Eu source to insure that it was stable with time. In addition, the permanently mounted ^{137}Cs source verified the efficiency on a continuous basis.

III. DATA REDUCTION

A. Energy Scales

Altogether four energy scales were established; the TOF energies for the incident neutrons producing events in the Ge(Li) and PR detectors, the recoil proton energy in the PR detector, and the photon energy in the Ge(Li) detector. In particular, the relativistic neutron energies in MeV were calculated from the flight path length L in meters, the "clock" time t in nsec, and the measured centroid of the spectral γ-flash group t_γ in nsec using the equations

$$E = 939.549\{[1-(V/.299792)^2]^{-1/2}-1\} \tag{1a}$$

$$V = L/(t-t_\gamma+L/0.299792) \ . \tag{1b}$$

Gamma flash centroids of 1281 and 1267 nsec and path lengths of 21.726 and 22.181 m were used for the PR and Ge(Li) detectors, respectively. A small correction was made for the reduced recoil-proton velocity over its 0.306-m flight path. The Ge(Li) TOF energy scale was verified by observing the sharp 2.078 MeV ^{12}C transmission dip.[26]

A linear energy scale for the proton detector was determined using the 5.48-MeV alpha particles from the ^{241}Am source. For the Ge(Li) detector the linear energy scale 0.9362 x (channel number) + 2.9 keV was found to reproduce within 0.4 keV both gamma-ray energies[27] from standard sources and the ^{238}U gamma-ray energies given in ref. 3.

B. Deadtime Correction

In principle the data required no clock deadtime correction because the desired cross sections were a ratio of Ge(Li) to PR events, both measured through a common clock. However, a clock deadtime correction was applied because an incident neutron energy in the two detectors corresponded to slightly different clock times and a common flux measurement was renormalized for use with both the ^{238}U and ^{7}Li samples which produces count rates differing by a factor of two. Because the clock was operated in the single-stop mode the required deadtime correction for timing channel i simply equalled $(1-N_i/B)^{-1}$ where N_i was the summed clock events for both detectors which preceded channel i in time and B was the number of bursts employed for the measurement. For the energy region of interest the clock deadtime correction for both samples was always less than 5%.

C. Fluence Measurement

A schematic of the fluence monitor is shown in Fig. 2 and is described in detail in ref. 19. Only a brief description will be given here. The radiator consisted of a 6.9 mg/cm^2 Al absorber sandwiched between 2.03 mg/cm^2 and 0.65 mg/cm^2 polyethylene foils. The Al foil thickness corresponds to the range of about 2.0 MeV protons. Thus at high-neutron energies where the fluence is small and the proton range large the solid state detector counted recoils from both polyethylene foils, whereas at low-neutron energies where the proton range is less then 6.9 mg/cm^2 of Al the solid state detector counted only recoils from the thin polyethylene foil.

Figures 5 to 7 show typical recoil proton spectra for one cycle. Upper Fig. 5 is a spectrum for a 0.43-MeV wide bin with 4.5-MeV neutrons. A $\sim$ 2% background has been subtracted which was estimated by performing a short measurement with only the Al foil in place. All the counts above the arrow were taken as recoil-proton events. Lower Fig. 5 is a spectrum for a 0.23-MeV wide bin with 2.9-MeV neutrons. Recoil protons from the two foils are well separated and both groups are used for the fluence measurement. Below this energy the recoils from the thick foil merge with the background and only the recoils from the thin foil can be employed.

Figure 6 shows spectra for 0.13 and 0.03-MeV wide bins for 2.0 and 0.7-MeV, respectively. These spectra are very clean and the recoil events from the thin foil can be determined unambiguously. Knowing the areal H density of the radiators and the H total cross section[28] and assuming an isotropic center of mass angular distribution, the efficiency of the telescope was calculated by averaging the differential cross section for proton recoils and the detector solid angle over the geometry of the radiator-detector system. With this efficiency and the number of recoils per channel the fluence was determined. Figure 7 shows a spectrum for a 0.02-MeV wide bin from 0.59 MeV neutrons where some recoil-proton energy ranges are less than 0.65 mg/cm^2 which results in a more complicated analysis. The histogram is a Monte Carlo calculation of the absolute recoil proton energy distribution which should be detected using the stopping powers of Bichsel.[29] The data have been normalized to the calculation above the 0.22-MeV bias level and the neutron fluence was taken as the ratio of the measured number of recoils above the bias to the

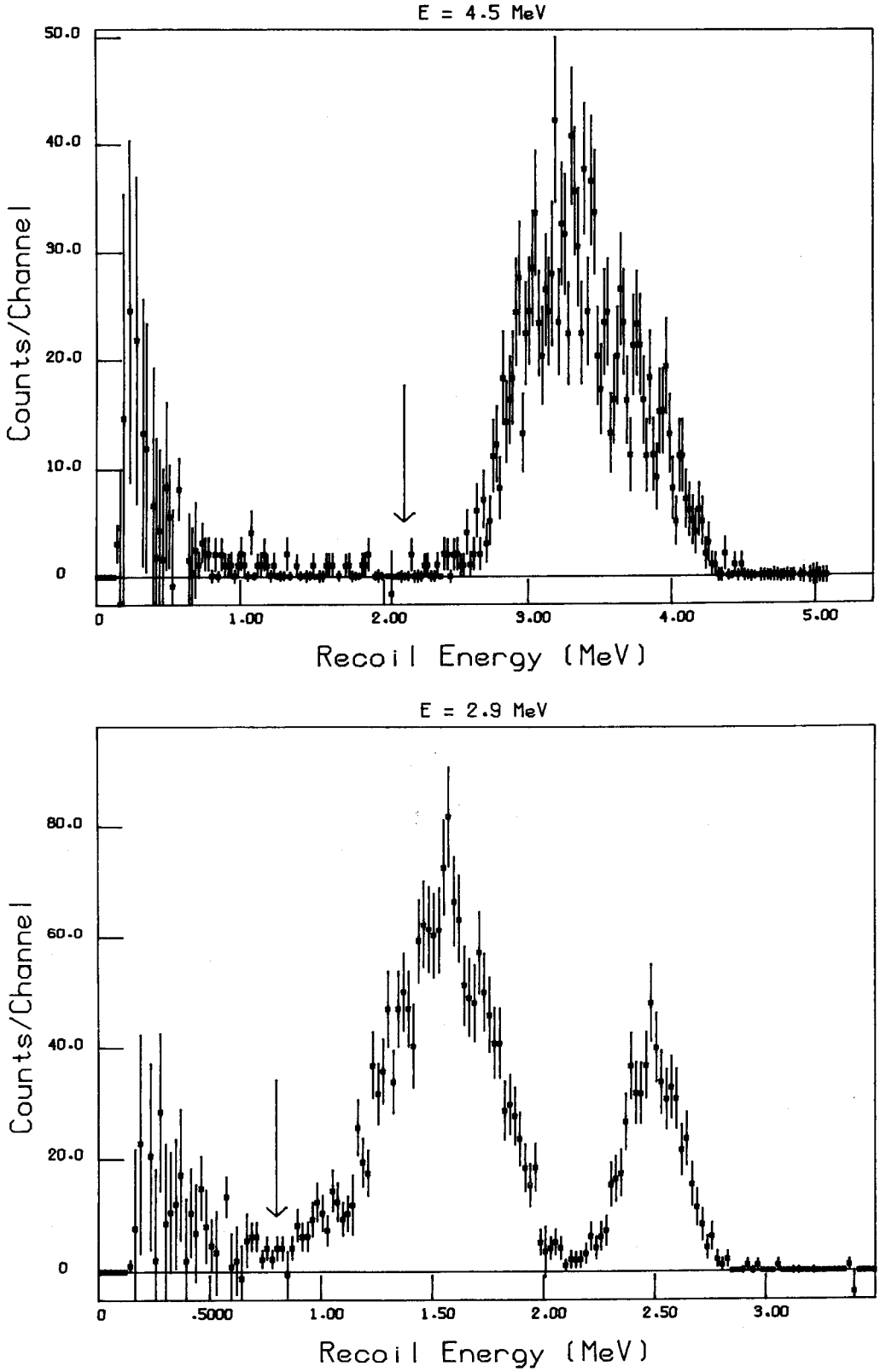

Fig. 5. Net recoil proton spectra for 0.43 and 0.23-MeV wide bins for 4.5 and 2.9-MeV incident neutrons, respectively. The subtracted background was $\sim$ 2%, and events above the arrows were assumed to be recoil protons. With 2.9 MeV neutrons the recoils from the two foils are separated, whereas with 4.5 MeV neutrons they are not.

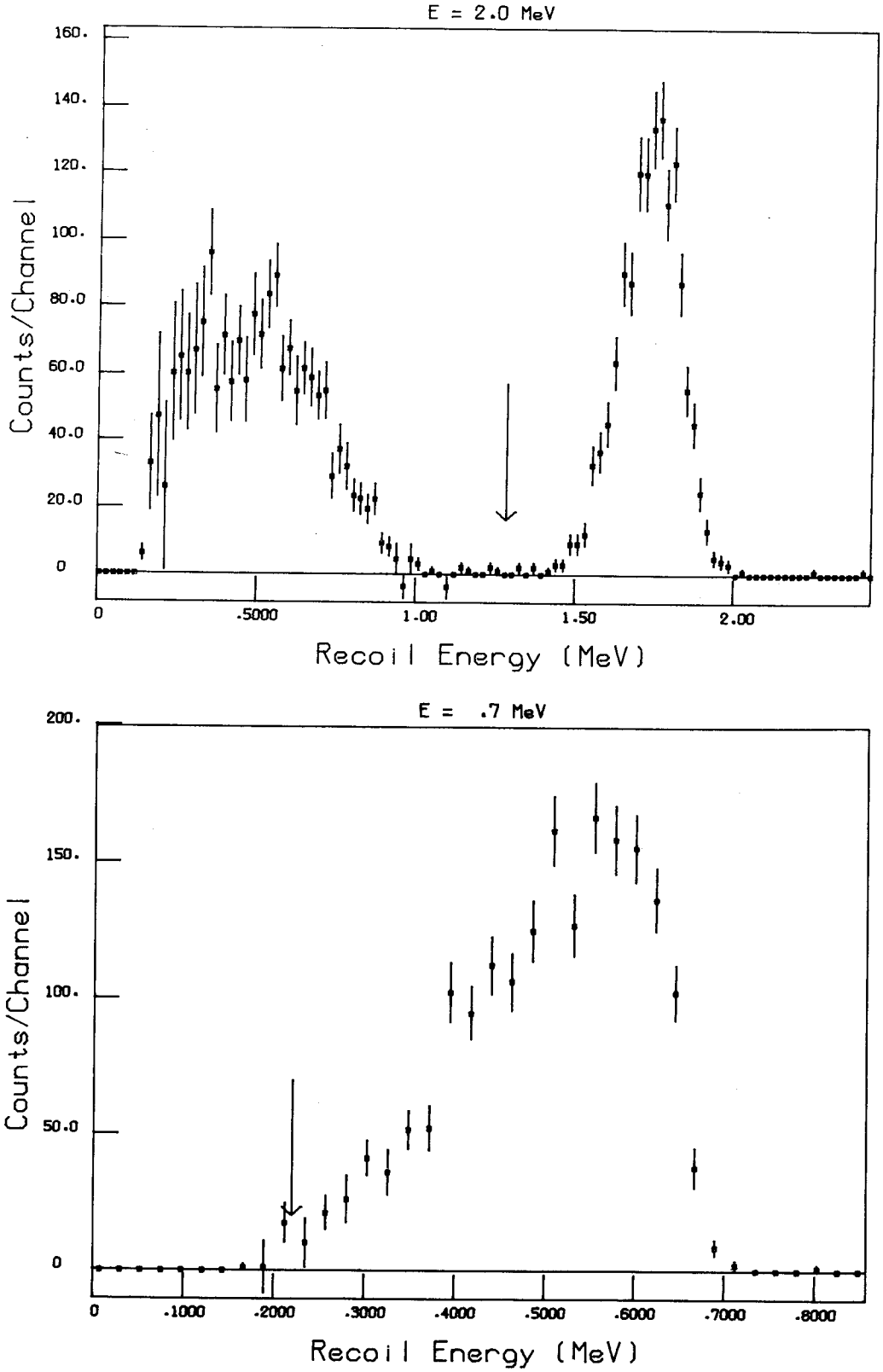

Fig 6. Net recoil proton spectra for 0.13 and 0.03-MeV wide bins for 2.0 and 0.7-MeV incident neutrons, respectively. The subtracted background was $\sim$ 2% and events above the arrows were assumed to be recoils from only the thin foil. Some recoil protons from incident neutrons less than 0.7 MeV could not escape the thin foil.

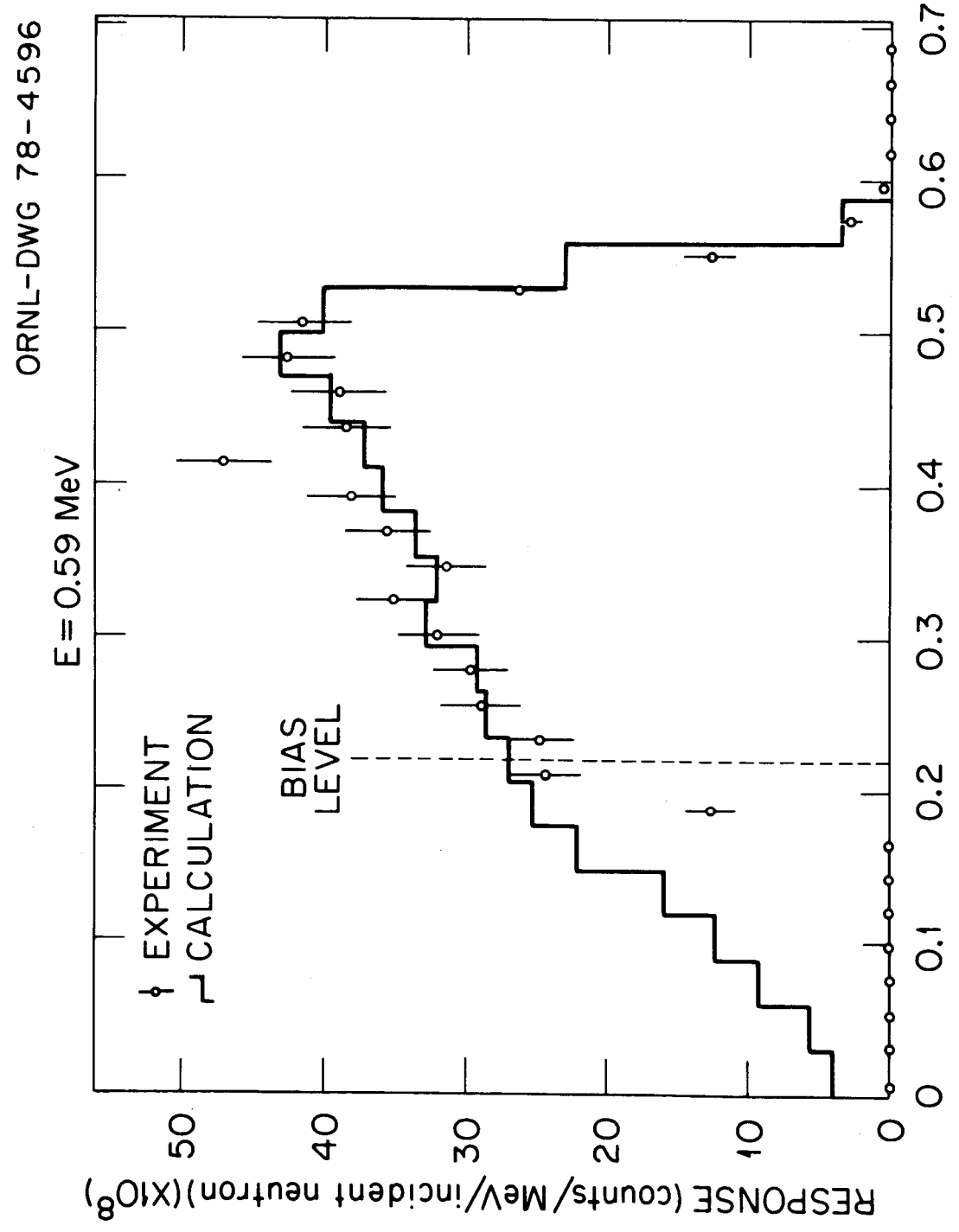

Fig. 7 Net recoil proton spectrum for a 0.02-MeV wide bin from 0.59-MeV incident neutrons normalized to a Monte-Carlo calculated spectrum. The PR detector efficiency was taken as the calculated area above the bias level.

calculated area above the bias level. The resulting fluence was rebinned to the energy bins of the Ge(Li) detector by integrating piecewise polynomial fits and is shown in Fig. 8. A more complete description of the fluence measurement can be found in ref. 19.

D. Ge(Li) Efficiency

The photopeak efficiency of the Ge(Li) detector was measured in situ with standard gamma-ray sources of known intensities. In particular, the sources were attached to an Al plate at the center of the sample position and spectra were measured for fixed time intervals. The CFD output was used to gate the ADC, shown on Fig. 3, so the efficiency calibration includes the effect of the LRR circuit. With known source strengths, the deadtime-corrected photopeak areas gave directly the detector efficiency with respect to 4π steradians. The resulting efficiency is shown in Fig. 9 where the solid data points are from ^{137}Cs (# A3062), ^{88}Y (# B9643), and ^{106}Ru sources. The crossed data points have been normalized by a factor of 1.020 and are from ^{22}Na (# A3259) and ^{60}Co (# A3117) sources and the open data points have been normalized by a factor of 0.985 and are from a ^{152}Eu source (# LMR2423).

E. Gamma-ray Production Cross Sections

Gamma-ray production cross sections were calculated from the fifty ^{7}Li and ^{238}U deadtime-corrected Ge(Li) pulse-height spectra and the corresponding neutron fluences over the same energy bins. A common fluence measurement for both samples was made for each cycle and was normalized to a particular sample with ratios of recoil events integrated over incident neutron energy. The ^{238}U 635-keV and ^{7}Li 478-keV gamma-ray production cross sections were calculated for each cycle to insure consistency.

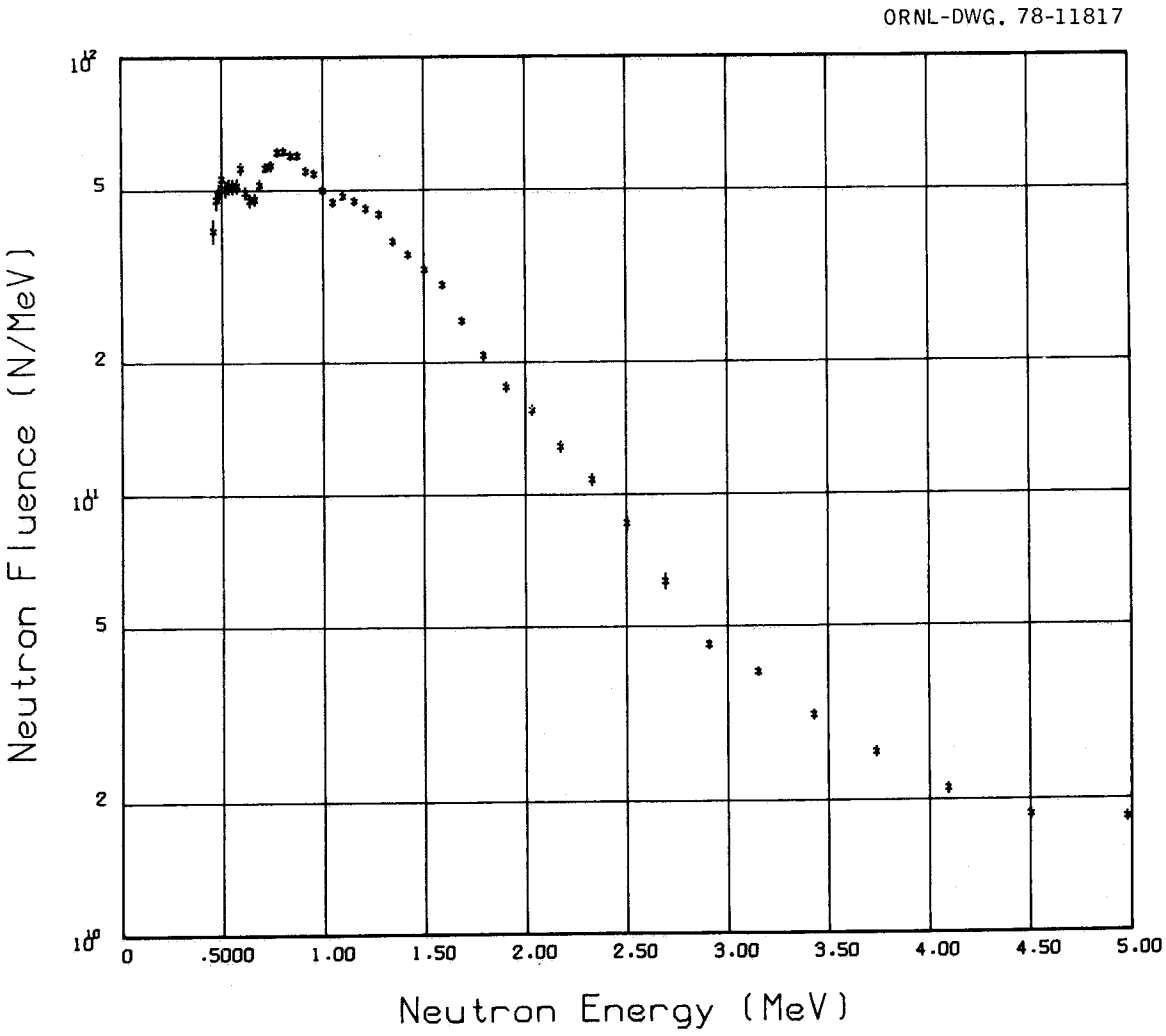

Fig. 8. PR-measured neutron fluence from ORELA for ∿ 260 hours of operation.

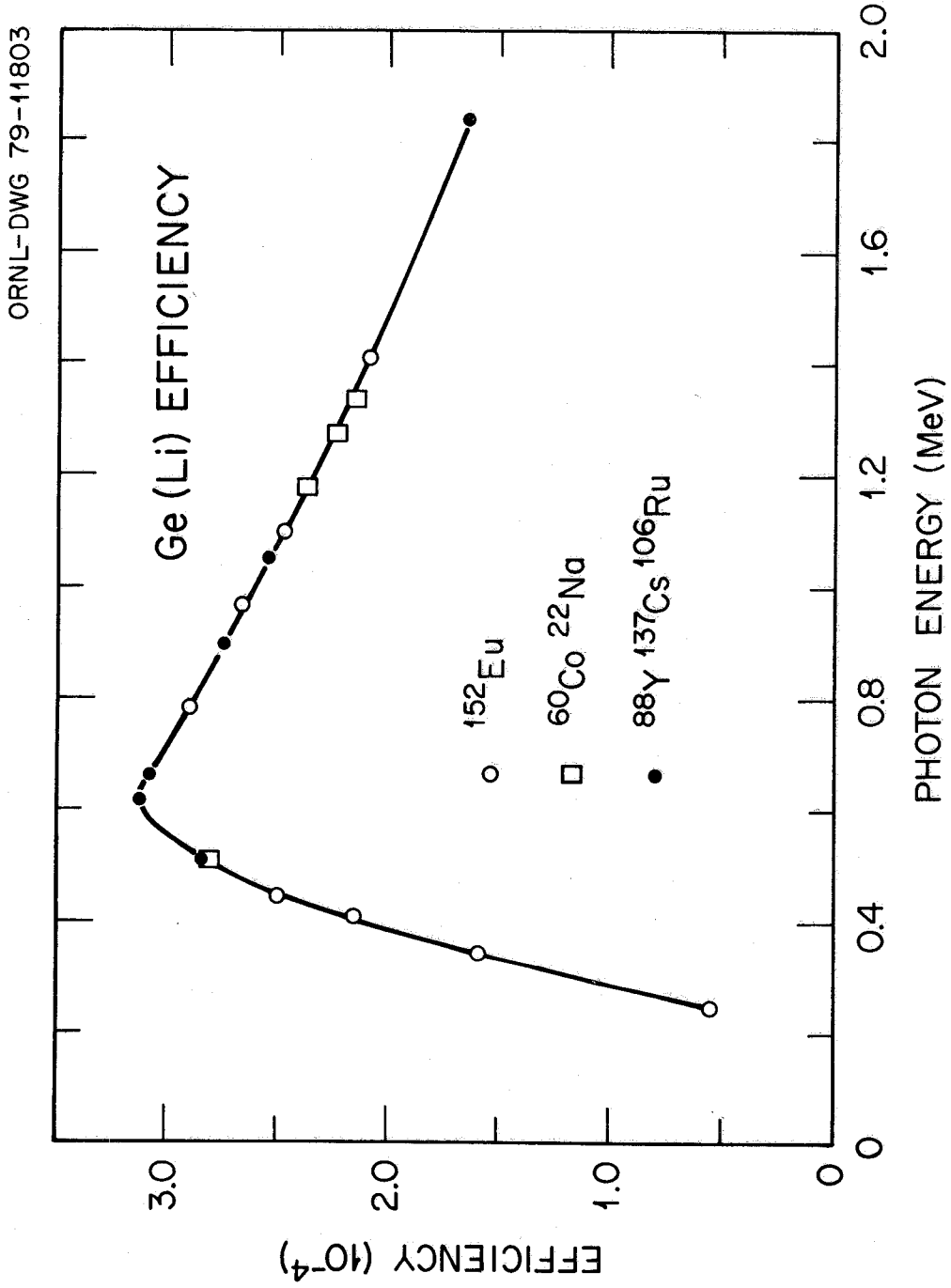

Fig. 9. Measured photopeak efficiency with respect to 4π steradians of 95 cm^3 Ge(Li) detector in situ with LRR and 1.8 mm Pb shield.

Within statistical error the four cycles gave identical cross sections. The other ^{238}U cross sections were obtained from analysis of the sum of the four data sets.

In particular, assuming isotropic gamma emission, the absolute 4π-steradian gamma-ray production cross section for a given bin, σ_γ, can be written as

$$\sigma_\gamma = \frac{NM}{F\ \varepsilon n COS(40°)} \tag{2}$$

where N = peak area or detected number of photons, M = correction for multiple scattering and flux and gamma-ray attenuation, F = fluence, ε = photon detection efficiency with respect to 4π steradians and peak definition of N, and n = areal number density of sample. The quantities σ_γ, N, MSC, and F are all functions of the incident neutron energy.

The number of deadtime-corrected photopeak events were obtained from the Ge(Li) spectra employing either linear-background summing routines using OPRODF,[30] or the computer program TPASS,[31] or the function listed as examples for the nonlinear least-squares fitting program LSFODF.[32] Figure 10 shows a LSFODF shape fit of a Gaussian resolution function, integrated over the finite channel widths, to the 882.1, 885.9, and 888.9-keV triplet for the 1.30-MeV bin. Whenever possible care was taken to insure that the photopeak-area definition employed to obtain the number of photons was consistent between the efficiency calculation, pileup-correction calculation and cross-section calculation. The resulting photopeak areas used for the cross-section calculation were increased by 10% to account for the measured pileup correction.

The correction factor M accounted for neutron flux attenuation, gamma-ray self-absorbtion, neutron multiple scattering, and solid angle variations from the finite sample size and was calculated with Monte Carlo procedures. The required ^{7}Li and ^{238}U cross sections were taken from ENDF/B-IV, and above the ^{238}U fission threshold the contribution to the correction from fission neutrons was included. The flux-attenuation contribution to the correction was $\sim$ 4 and 2% respectively for the ^{7}Li and ^{238}U samples. The gamma-ray self-absorbtion contribution depended on the photon energy through its total absorbtion cross section which was taken from the tabulation of Storm and Israel.[33] Their ^{238}U total absorbtion cross section values for various gamma-ray energies were verified experimentally with $\sim$ 5% accuracy using ^{88}Y and ^{152}Eu sources and a 38 mm-thick ^{238}U sample in transmission. For the 478-keV ^{7}Li line the contribution to the finite sample correction from gamma-ray self-absorbtion was $\sim$ 2%. For 0.4, 0.8, and 1.2 MeV photons from the ^{238}U sample this contribution was $\sim$ 24, 6, and 5%, respectively. The contribution from multiple scattering was of the order of 5% or less, and the contributions from solid angle variations and fission neutrons were almost negligible. With this finite sample correction computed for each gamma ray of interest for each neutron energy bin, Eq. (2) yielded the measured production cross sections which are presented below.

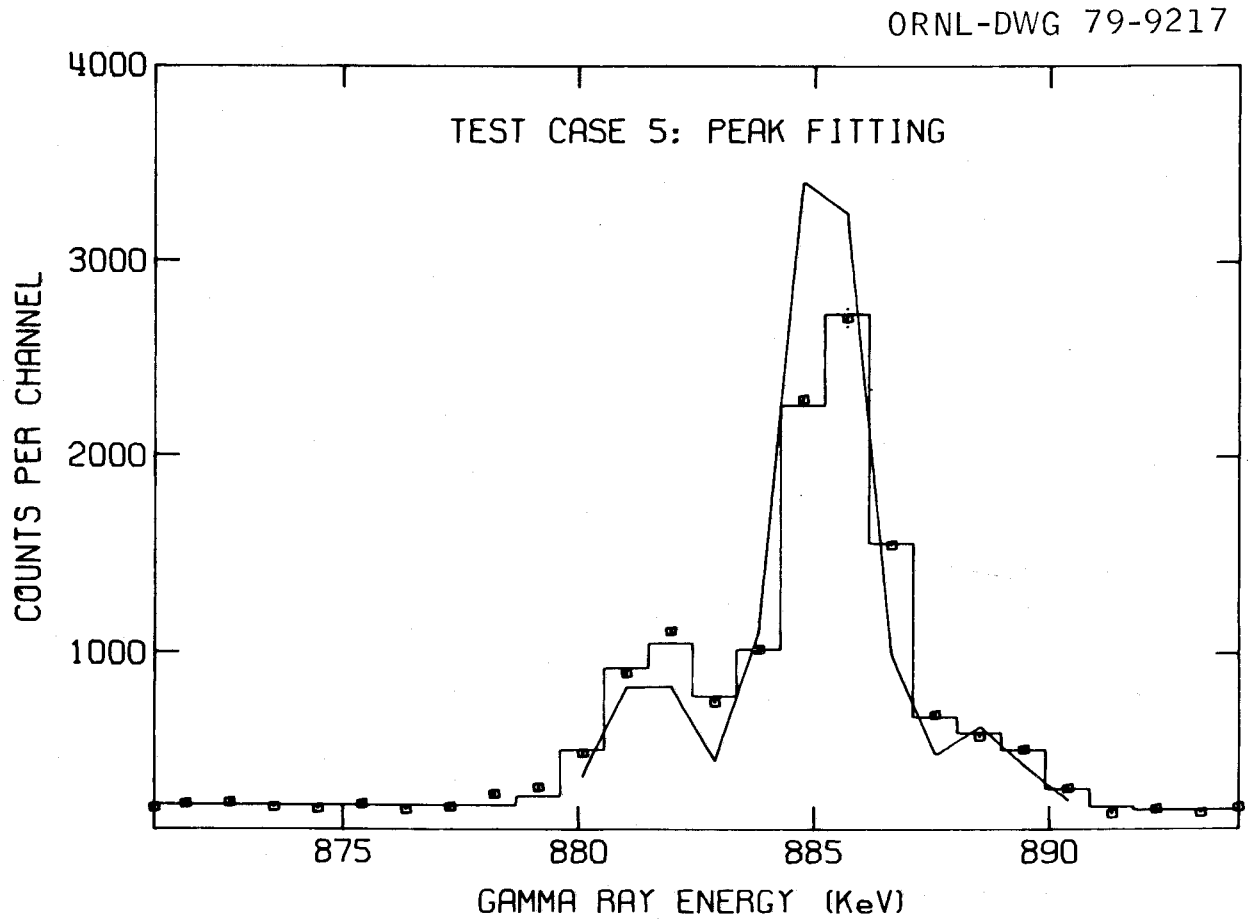

Fig. 10. LSFODF least-squares shape fit of three exponentials integrated over channel widths and a linear background to the ^{238}U 882.1, 885.9, and 888.9-keV triplet from 1.30-MeV incident neutrons. The histogram and other curve are the final fit and initial guess, respectively.

IV. MEASURED GAMMA-RAY PRODUCTION CROSS SECTIONS

A. $^{7}Li(n,n'\gamma)$ 478 keV Gamma-ray Production Cross Section

Figure 11 shows Ge(Li) spectra measured with the ^{7}Li sample for a 0.50-MeV wide bin from 4.96-MeV neutrons and a 0.06-MeV wide bin from 1.24-MeV neutrons, respectively. The inserts show the 478-keV line shape which, because of its short lifetime, Doppler broadens with increasing neutron energy. At low-neutron energies the spectra are very clean and the high-energy tails on the peaks are apparent. Upper Fig. 11 contains only three gamma-ray groups: the 478-keV ^{7}Li line, the 661.5-keV ^{137}Cs line, and the 197.1-keV ^{19}F line produced by neutron scattering in the detector. The remaining asymmetric wide groups are caused mainly by Ge inelastic scattering.[34] Neutrons on ^{7}Li produce only the 478-keV line. At higher energies shown in lower Fig. 11 the background and Ge lines are more intense and more lines appear. Nearly all of these lines have been identified to be from either Pb or Fe. Figure 12 shows the 478-keV cross section obtained from these spectra and compares it with those from other workers.[35,36] These cross sections are listed in Appendix A. Error estimates are discussed at the end of this section and the comparison will be discussed in the next section.

B. Gamma-ray Production Cross Sections and Branching Ratios for ^{238}U

In order to facilitate the identification of weak photon groups the thirty-three ^{238}U spectra, each 36-nsec wide, spanning neutron energies from 0.67 to 4.30 MeV were collapsed into five spectra. In particular, the collapsed spectra span incident neutron energies from 0.67 to 1.00, 1.00 to 1.21, 1.21 to 1.49, 1.49 to 2.00, and 2.00 to 4.30 MeV and are shown in detail in Appendix B.

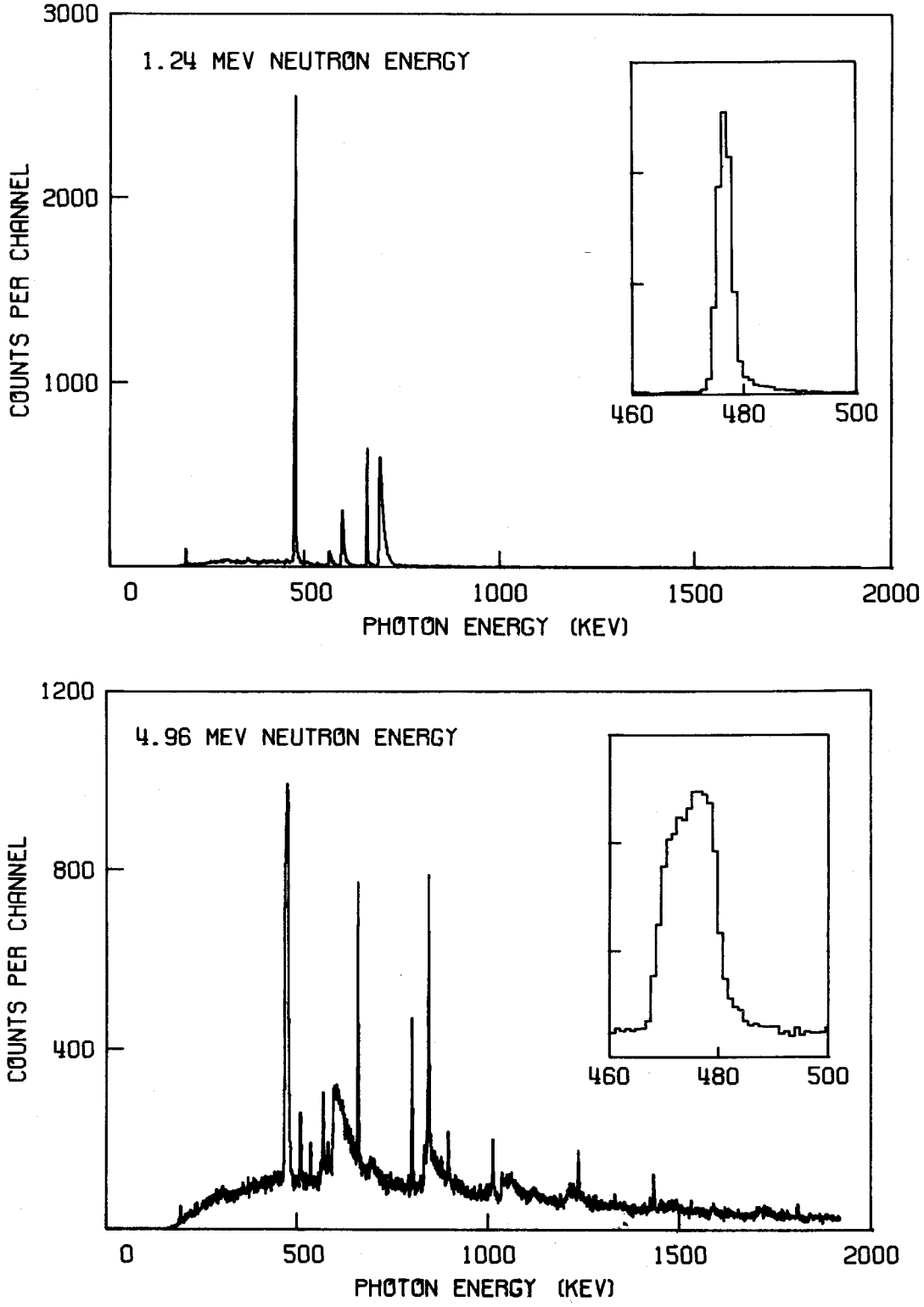

Fig. 11. Measured γ-ray spectra from neutron bombardment of ^{7}Li where the inserts show the 478-keV line which is Doppler broadened and has high-energy tail from pileup.

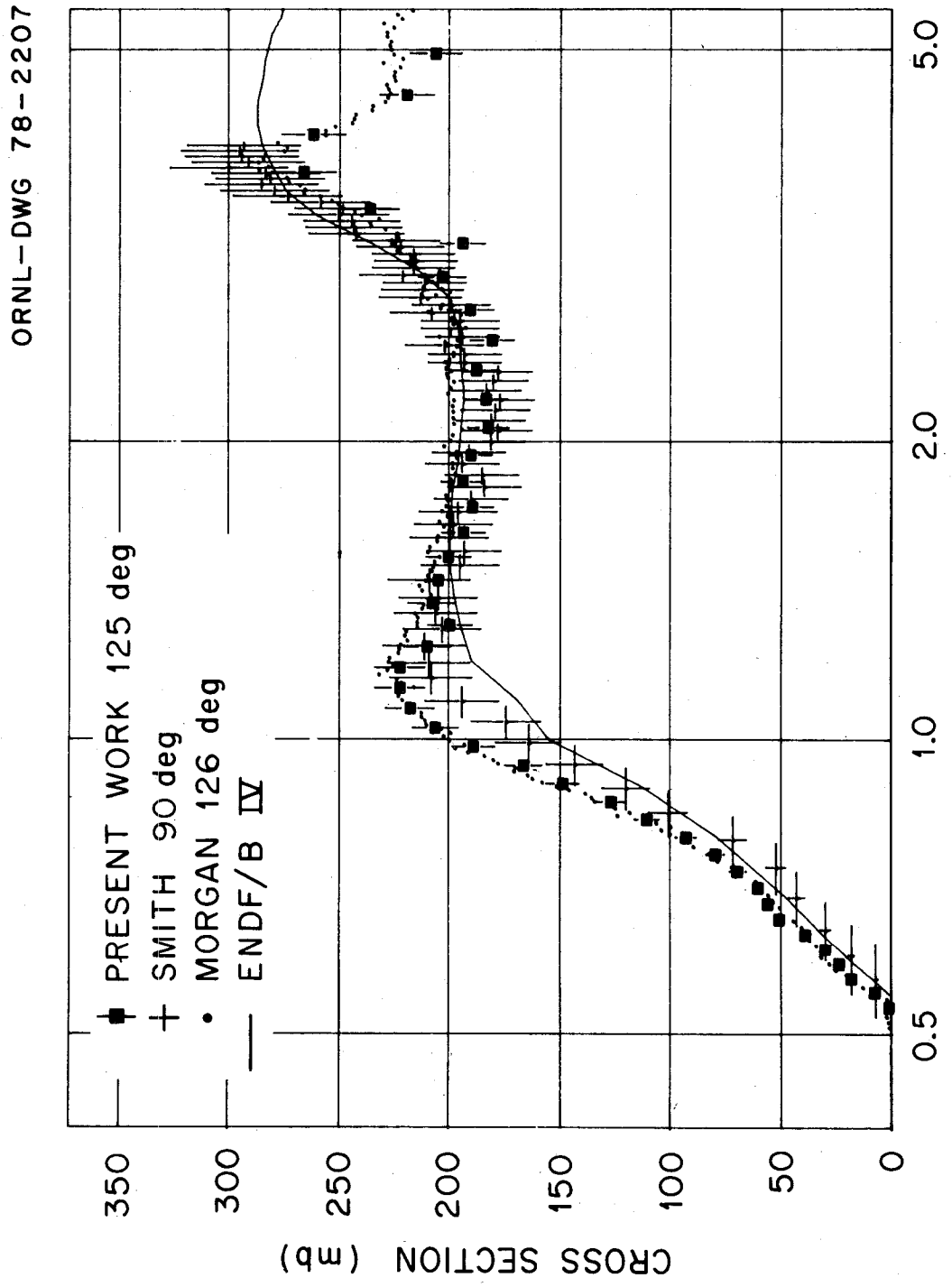

Fig. 12. Measured 4π cross sections for the production of the 478-keV γ-ray in ^{7}Li by neutron inelastic scattering.

Obtaining photopeak areas from the uncollapsed spectra and using Eq. (2) twenty-eight cross sections for ^{238}U photon production were calculated and are shown in Figs. 13 to 24. These cross sections are listed in Appendix A. In addition, seven branching ratios for weak or unresolved transitions were measured with respect to the above cross sections. These branching ratios were obtained mostly from the collapsed spectra and are listed in Table IV. These data represent all the experimental information extractable from this measurement for inelastic scattering on ^{238}U levels up to 1223.9 keV of excitation.

TABLE IV. Measured γ-ray Branching Ratios

All energies in keV

Level Energy	Branching Ratio	
930.8	$I_\gamma(930.8)/I_\gamma(885.9)$	$= .038 \pm .006$
930.8	$I_\gamma(250.7)/I_\gamma(885.9)$	$= .10 \pm .03$
950.0	$I_\gamma(269.9)/I_\gamma(905.1)$	$= .21 \pm .07$
997.5	$I_\gamma(849.1)/I_\gamma(952.6)$	$= .70 \pm .13$
997.5	$I_\gamma(317.4)/I_\gamma(952.6)$	$= .13 \pm .03$
1128.7	$I_\gamma(396.8)/I_\gamma(1083.8)$	$= .39 \pm .06$
1167.7 and 1169.1	$\dfrac{I_\gamma(435.8) + I_\gamma(437.2)}{I_\gamma(1019.3) + I_\gamma(1020.7)}$	$= .24 \pm .06$

In particular, Figs. 13 and 14 show measured cross section for the six possible photon decays from the 680.1-keV 1^-, 731.9-keV 3^-, and 827.1-keV 5^- rotational members of the K = 0 octuple band to the 0.0-keV 0^+, 44.9-keV 2^+, 148.4-keV 4^+, and 307.2-keV 6^+ rotational members of the GS band. These states are shown on the level diagram of Fig. 1 and

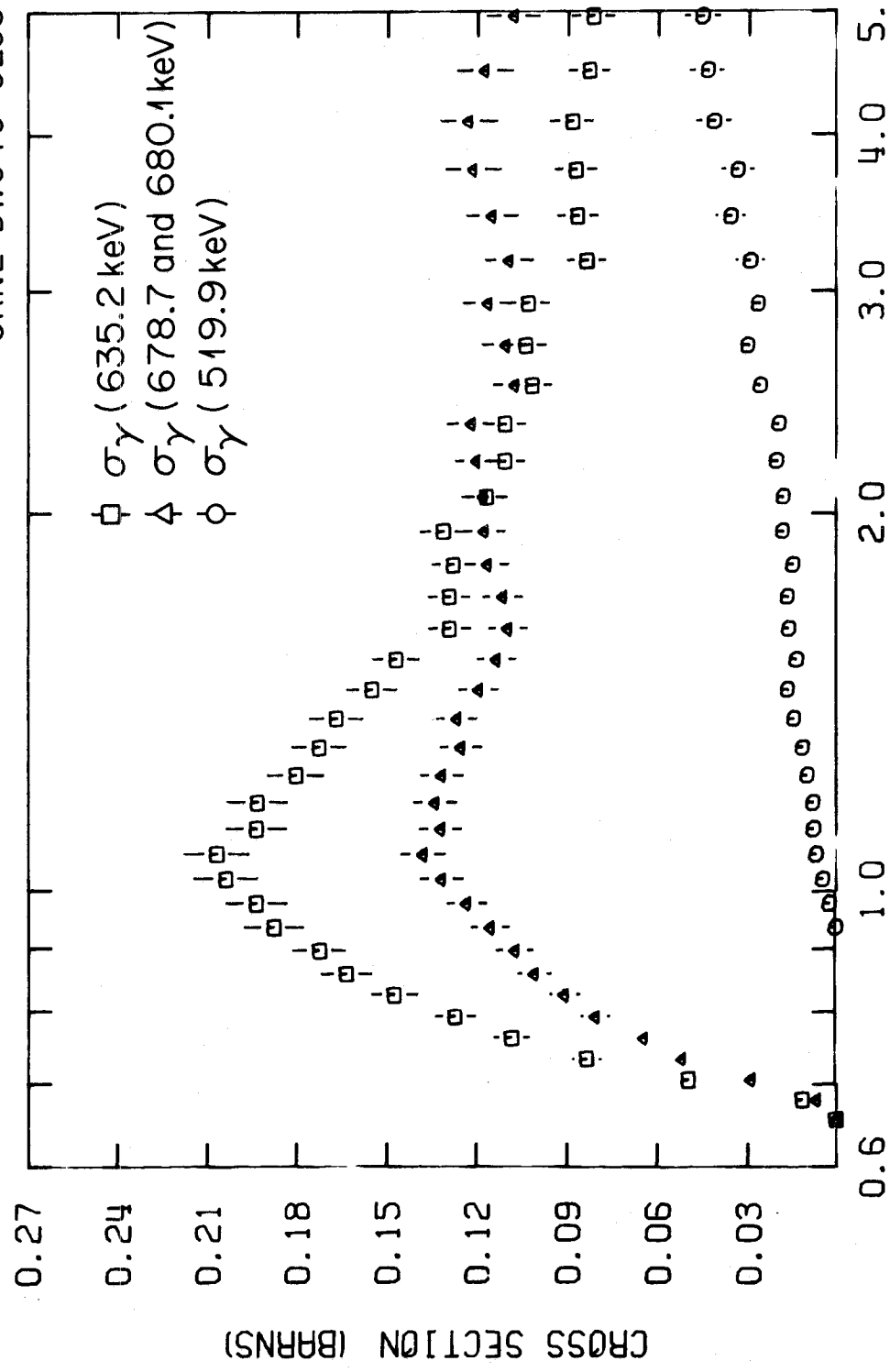

Fig. 13. Inferred 4π γ-ray production cross sections for octupole-band decays: the 680.1 and 635.2-keV transitions are from the 680.1-keV 1^- member to the 0^+ and 2^+ levels, respectively; and the 678.7 and 519.9-keV transitions are from the 827.1-keV 5^- member to the 4^+ and 6^+ levels, respectively.

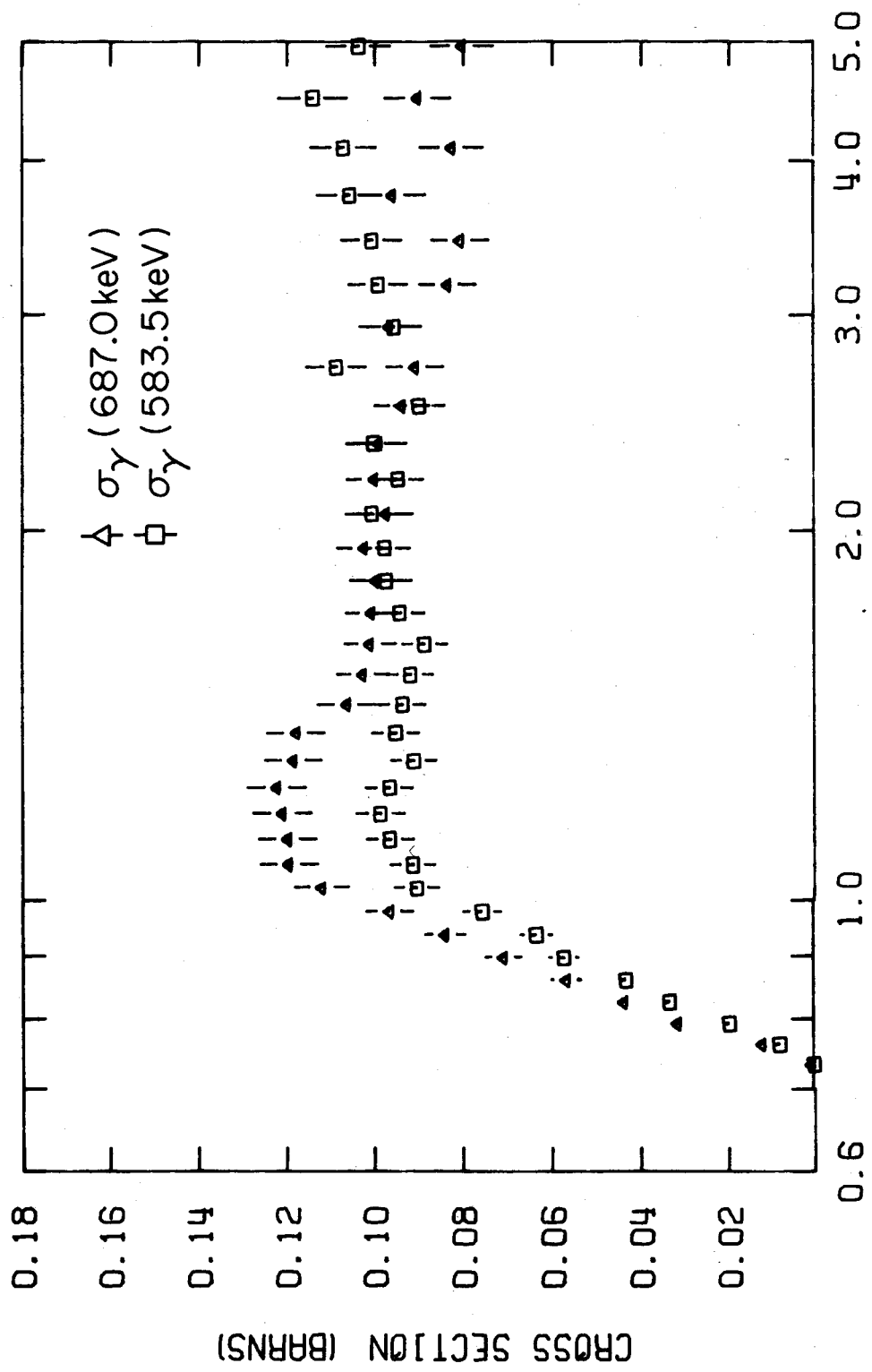

Fig. 14. Inferred 4π γ-ray production cross sections for the 687.0 and 583.5-keV transitions from the 731.9-keV 3^- member of the octupole band to the 2^+ and 4^+ levels, respectively.

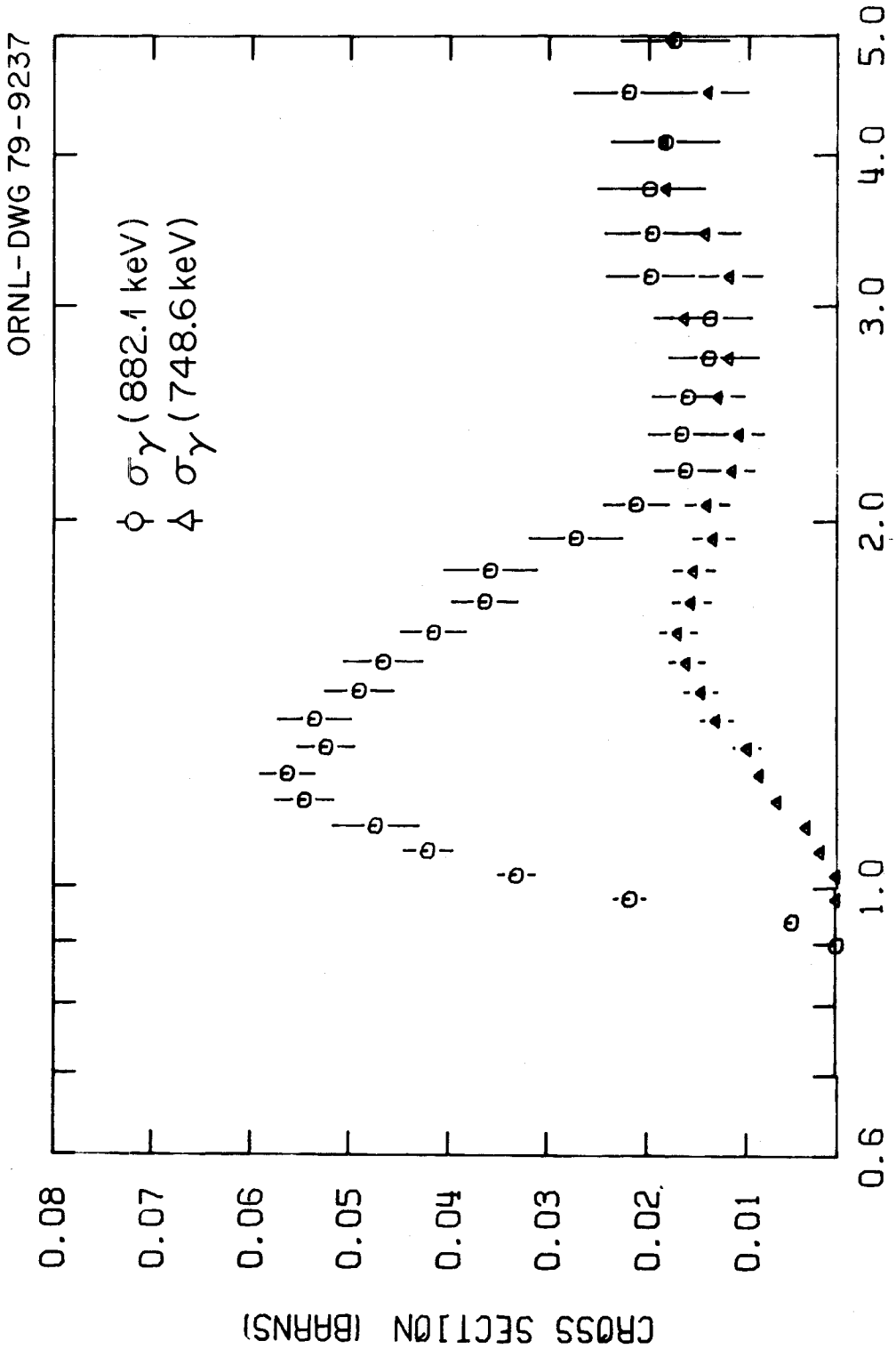

Fig. 15. Inferred 4π γ-ray production cross sections for decays from the proposed $K^\pi = 0^+$ first-excited band: the 882.1-keV transition is from the 927.0-keV (0^+) member to the 2^+ level and the 748.6-keV transition is from the 1055.8-keV (4^+) member to the 6^+ level.

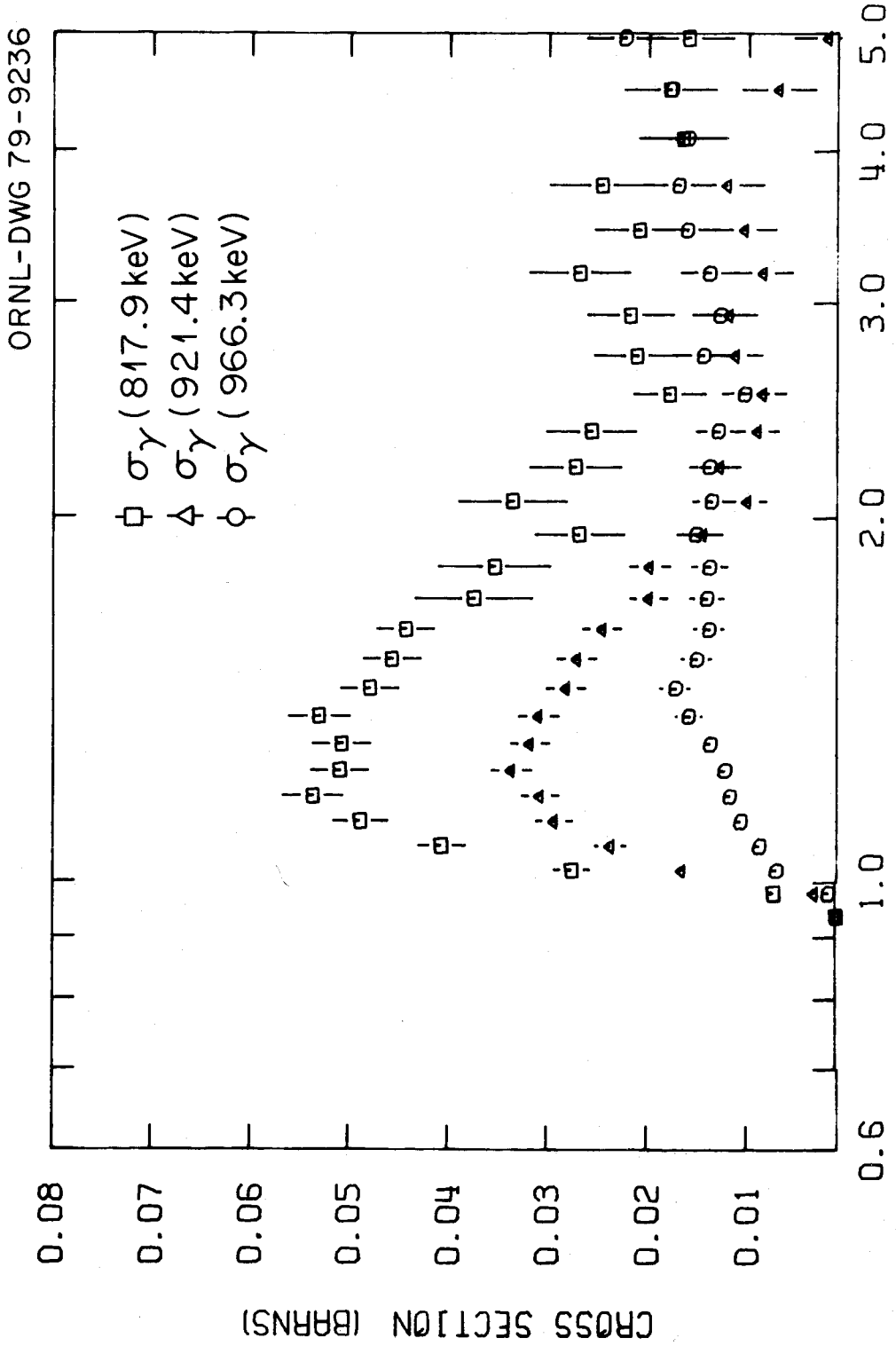

Fig. 16. Inferred 4π γ-ray production cross sections for the 817.9, 921.4, and 966.3-keV transitions from the 966.3-keV 2^+ member of the first-excited $K^\pi = 0^+$ band to the 4^+, 2^+, and 0^+ levels. This level may also decay by E0.

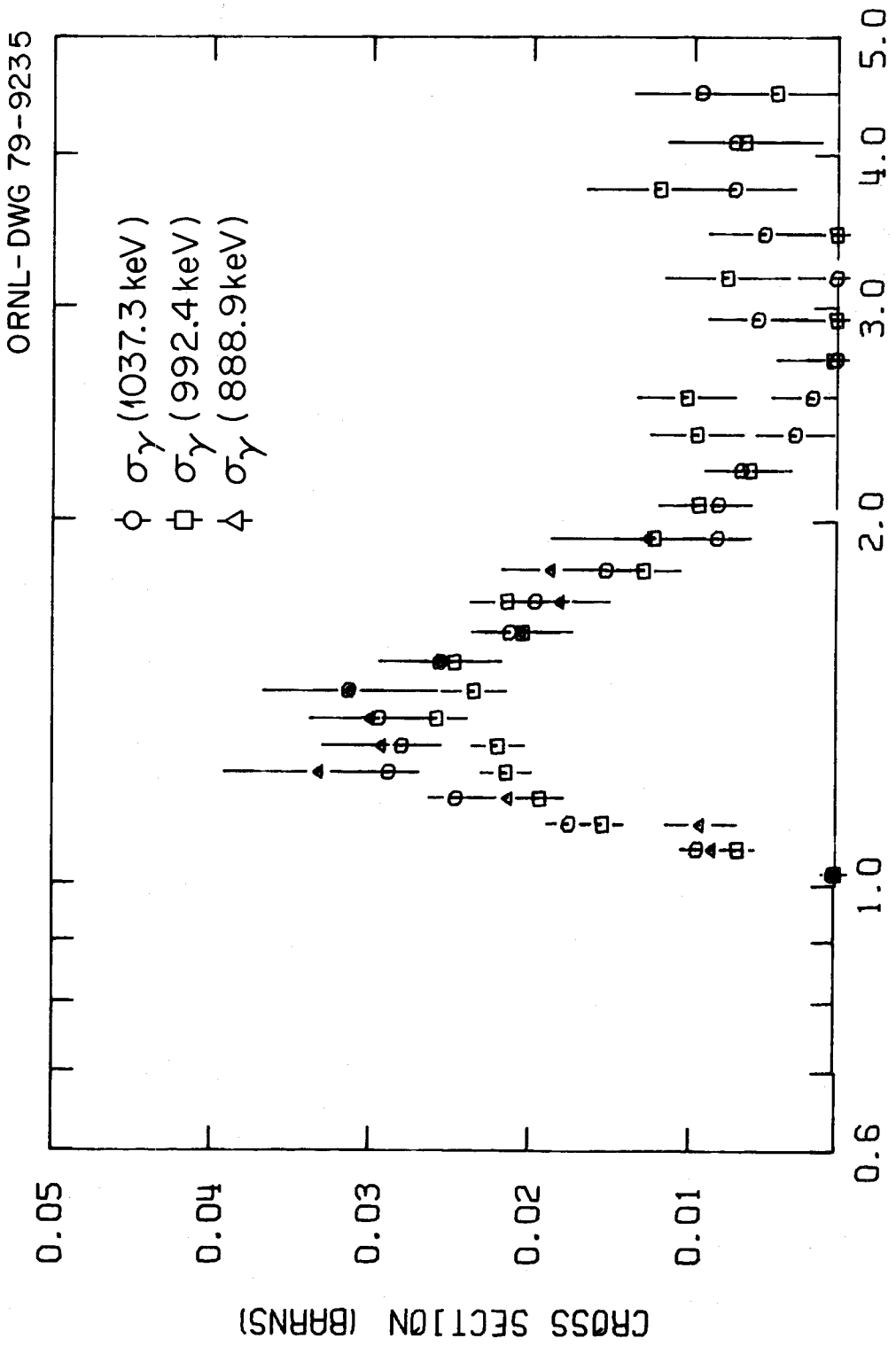

Fig. 17. Inferred 4π γ-ray production cross sections for 1037.3, 992.4, and 888.9-keV transitions from the 1037.3-keV 2^+ member of the beta band to 0^+, 2^+, and 4^+ levels, respectively. Photon decays from the 0^+ and 4^+ members of the beta band are not observed and the 2^+ member also decays by E0.

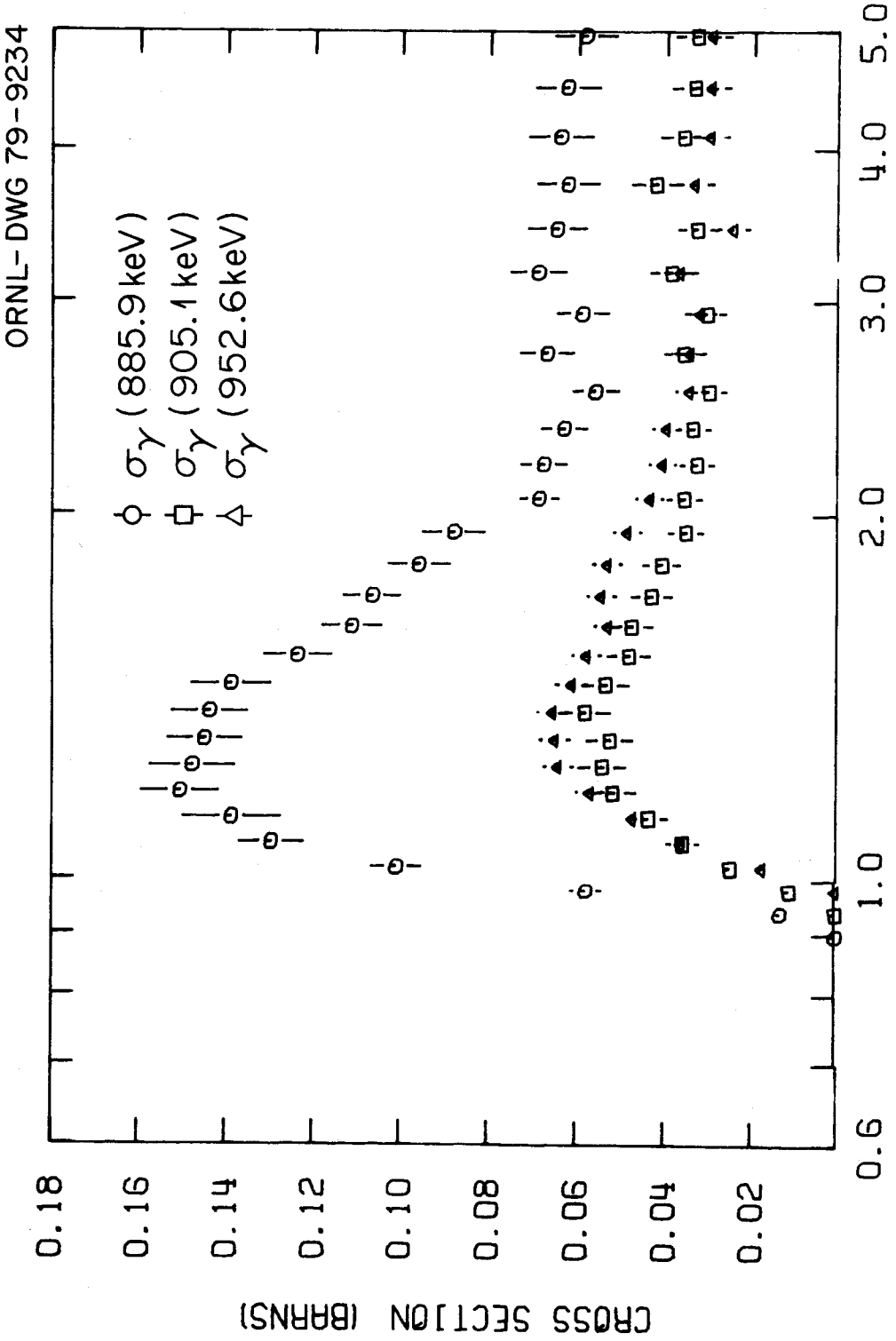

Fig. 18. Inferred 4π γ-ray production cross sections for 885.9, 905.1, and 952.6-keV transitions from the 930.8-keV (1^-), 950.0-keV (2^-), and 997.5-keV 3^- members of the proposed $K^\pi = 1^-$ band to the 2^+ level, respectively.

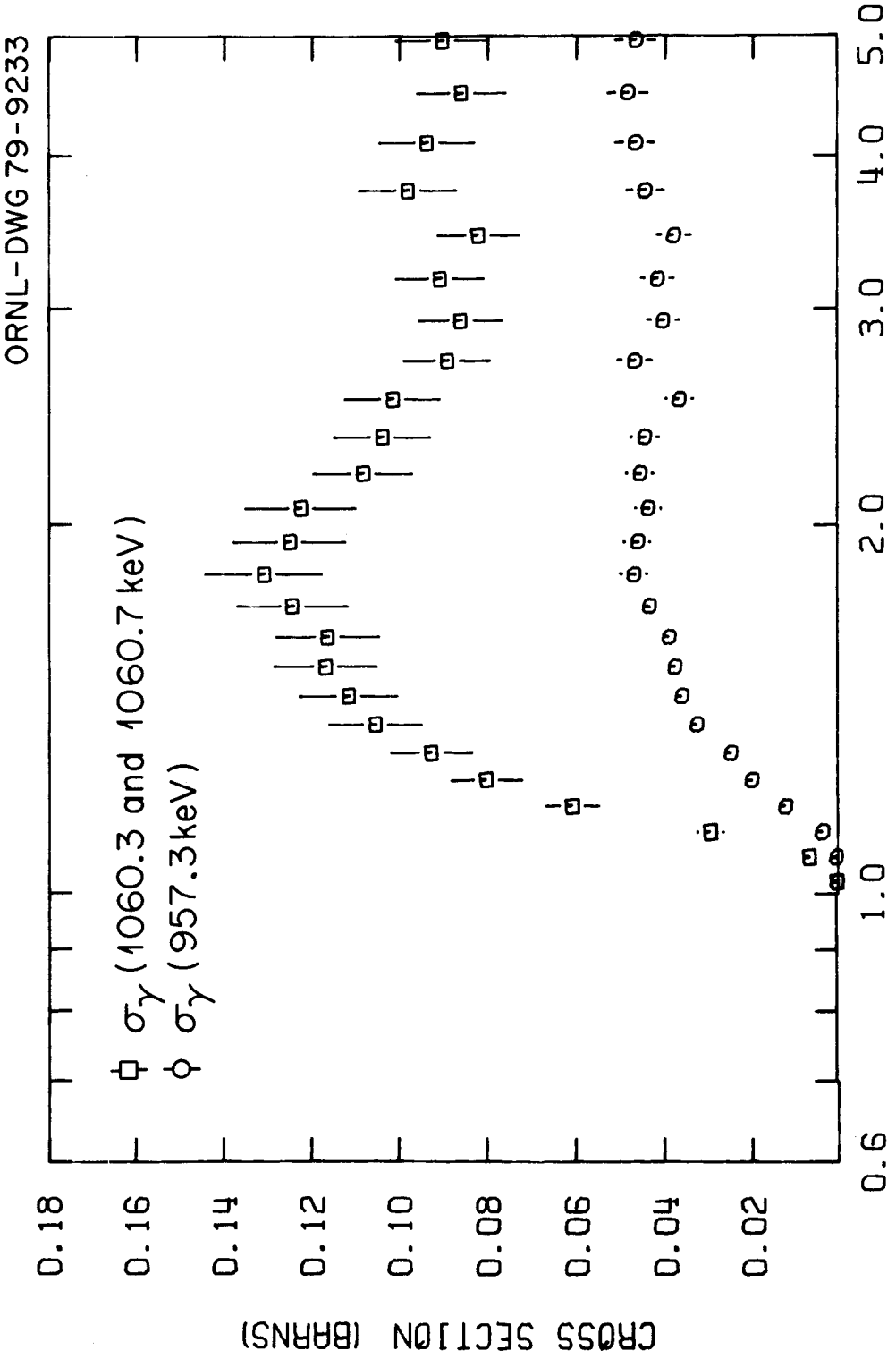

Fig. 19. Inferred 4π γ-ray production cross sections for decays from the gamma band: the 1060.7 and 957.3-keV transitions are from the 1105.6-keV (3^+) member to the 2^+ and 4^+ levels, respectively; and the 1060.3-keV transition is from the 1060.3-keV 2^+ member to the GS.

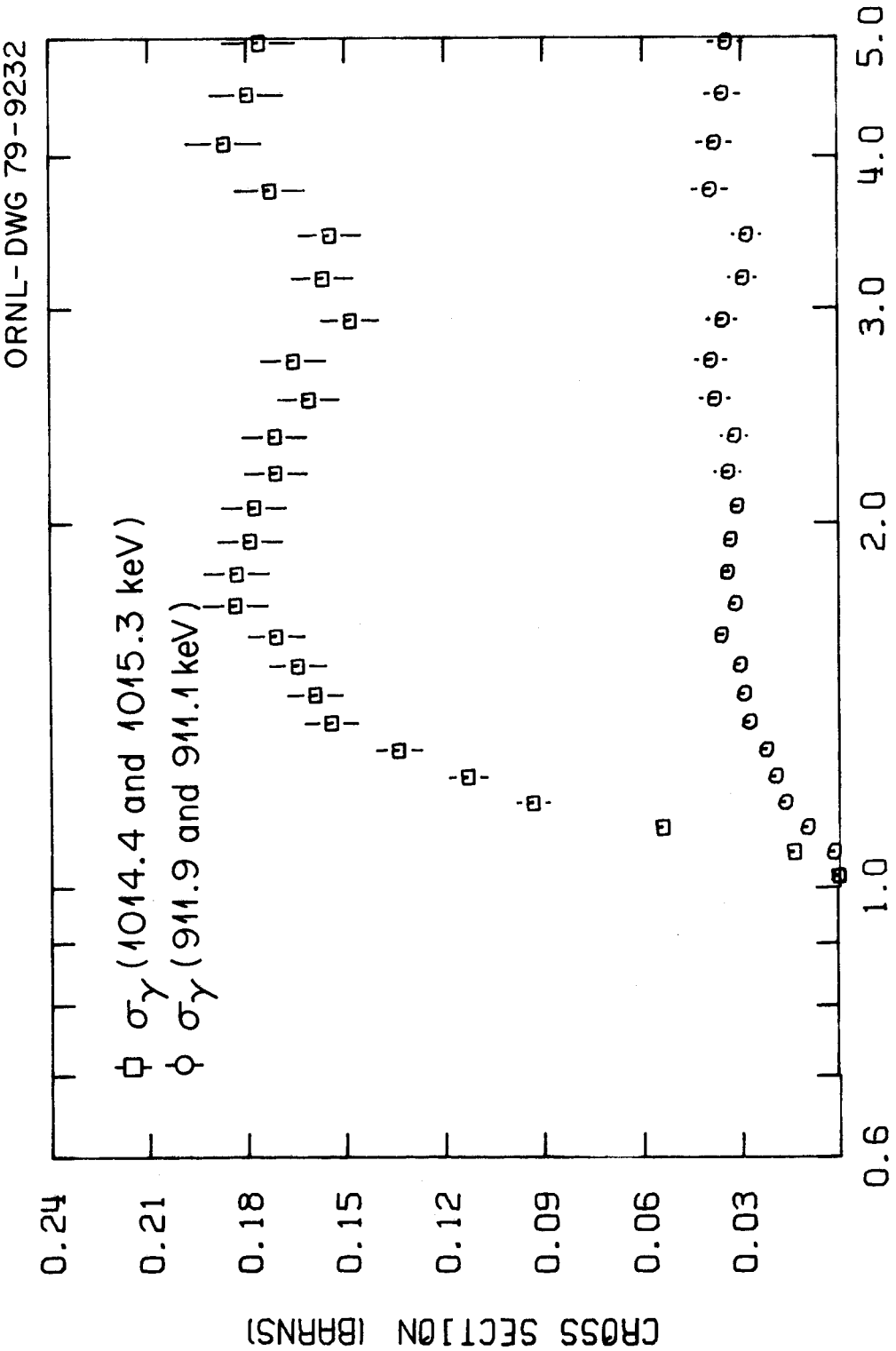

Fig. 20. Inferred 4π γ-ray production cross sections for the 1015.3 and 911.9-keV decays from the gamma-band, 1060.3-keV, 2^+ member to the 2^+ and 4^+ levels, respectively. These transitions are doublet with the corresponding 1014.4 and 911.1-keV transitions from the 1059.3-keV (3^+) level.

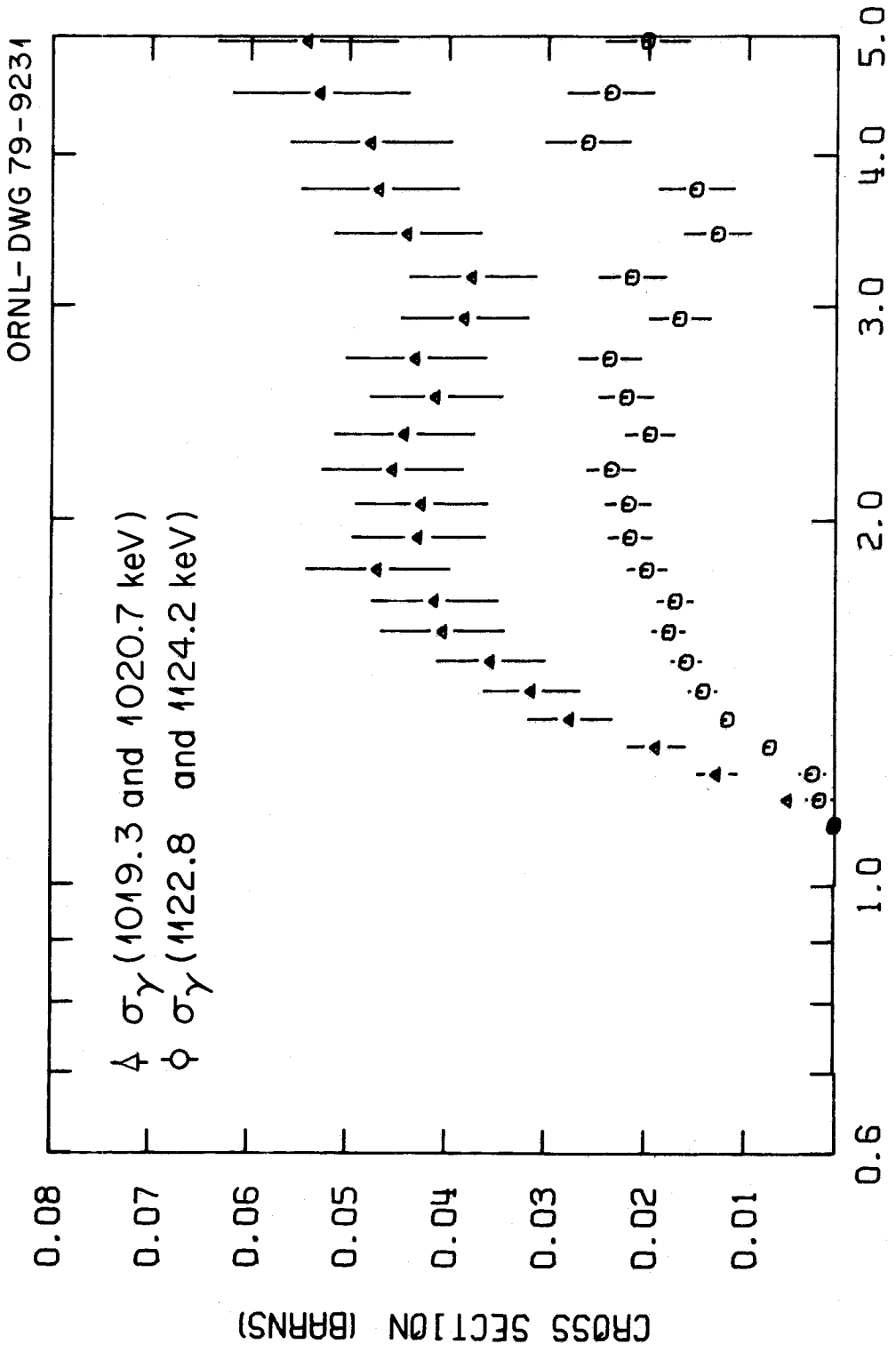

Fig. 21. Inferred 4π γ-ray production cross sections for the 1019.3 and 1122.8-keV transitions from the gamma-band, 1167.7-keV (4^+) member to the 4^+ and 2^+ levels, respectively. These transitions are doublet with the corresponding decays from the 1169.1-keV 3^- level.

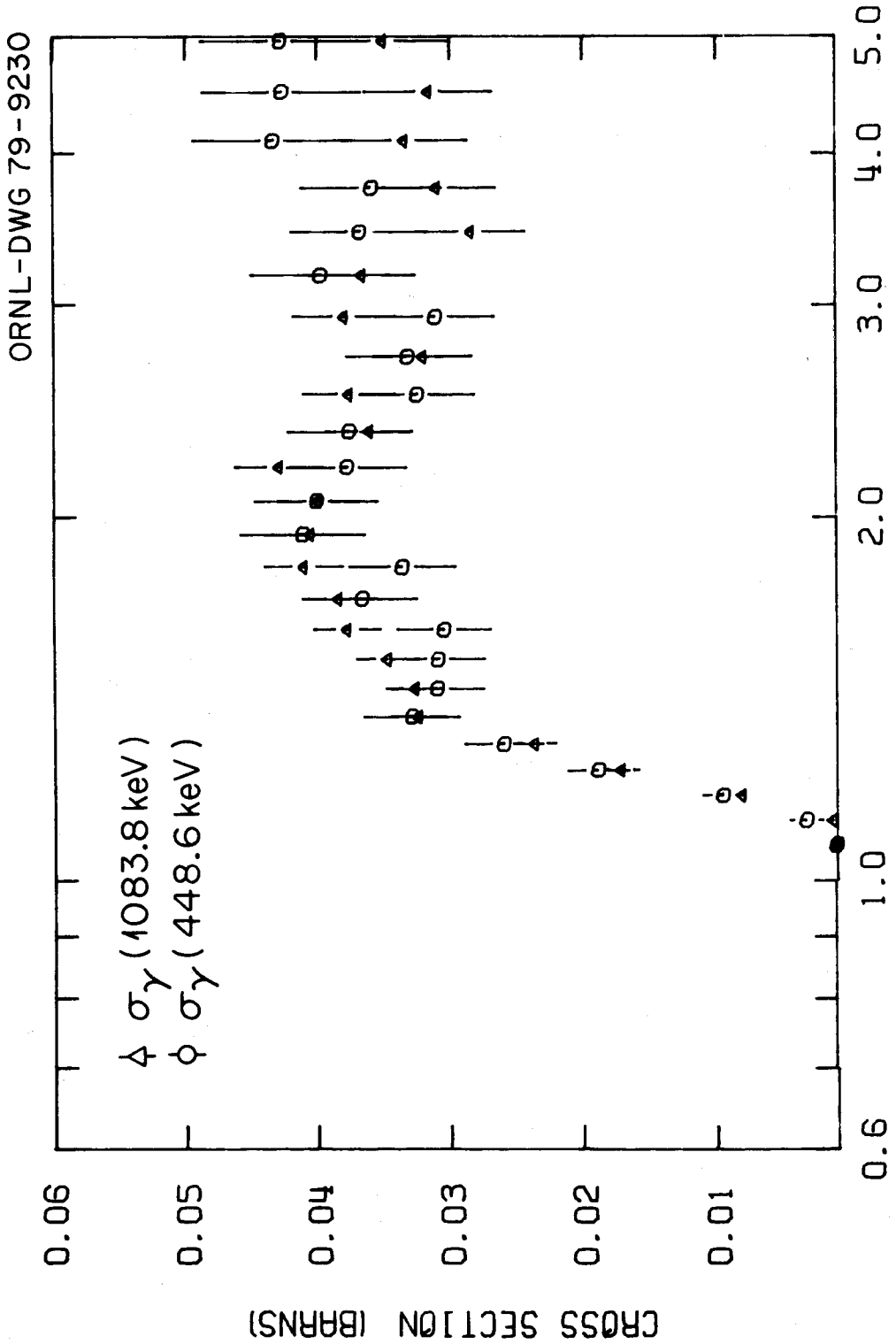

Fig. 22. Inferred 4π γ-ray production cross sections for the 1083.8 and 448.6-keV transitions from the 1128.7-keV (2^-) member of a proposed K = 2 band, to the 2^+ and 1^- levels.

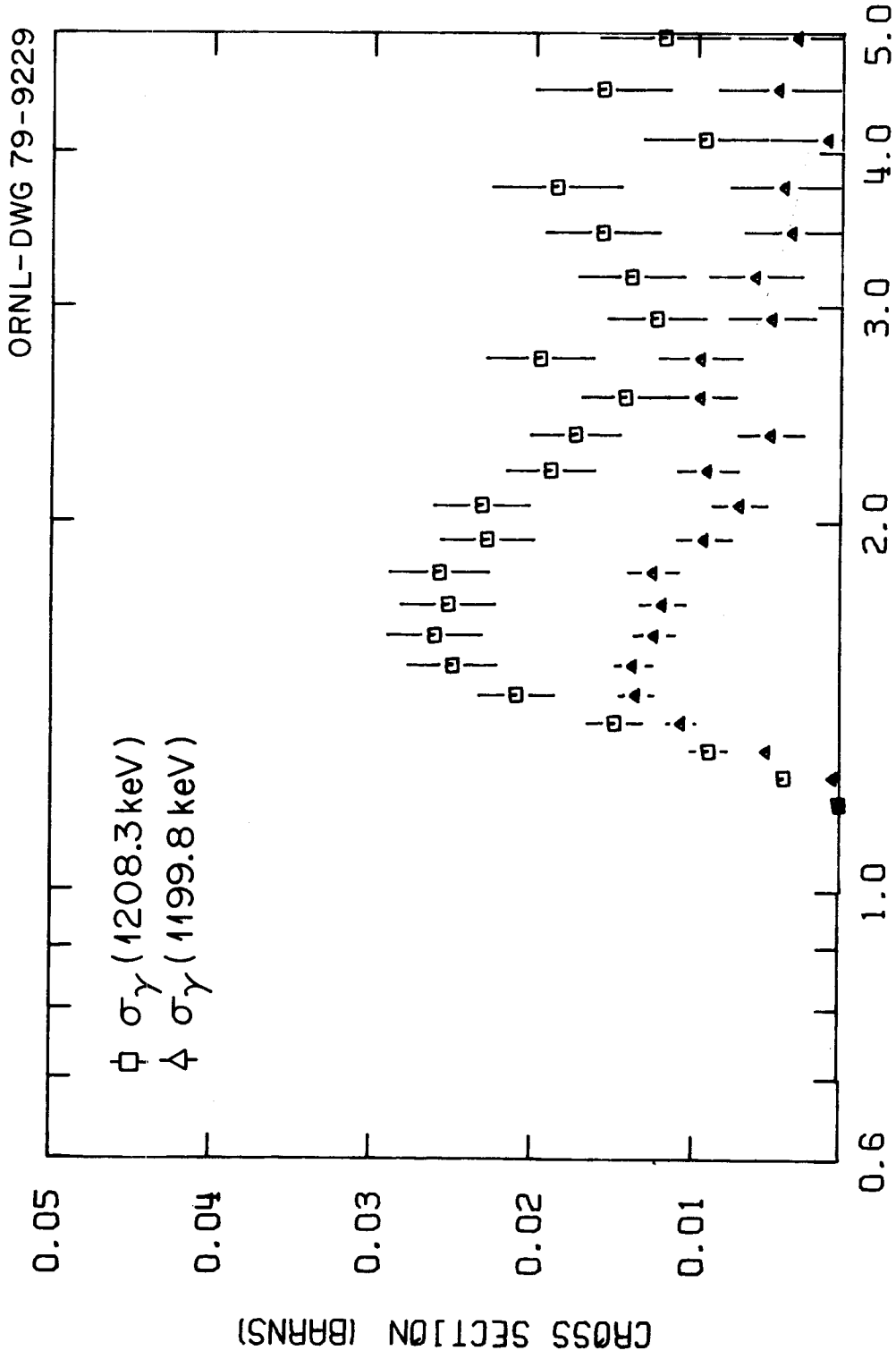

Fig. 23. Inferred 4π γ-ray production cross sections for a 1208.3-keV transition to the GS and a 1199.8-keV transition to either the GS or 2^+ level.

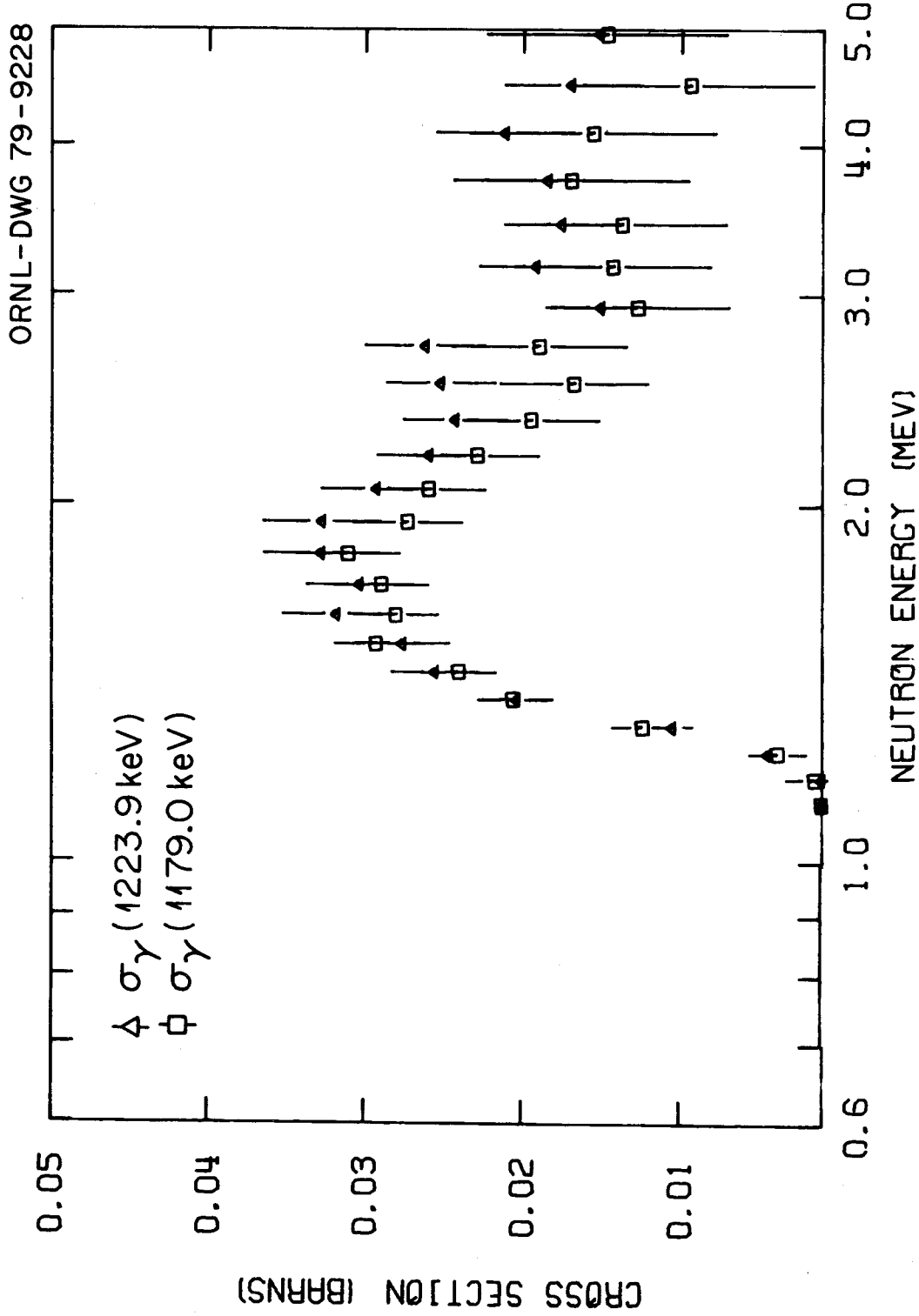

Fig. 24. Inferred 4π γ-ray production cross sections for the 1223.9 and 1179.0-keV transitions from the 1223.9-keV 2^+ level to the 0^+ and 2^+ levels, respectively.

throughout the remainder of this report will simply be designated as the 1^-, 3^-, 5^-, 0^+, 2^+, 4^+, and 6^+ levels, respectively. Figure 13 shows cross sections for the $1^-\rightarrow 2^+$ 635.2-keV decay, the $5^-\rightarrow 6^+$ 519.9-keV decay and the 680.1 and 678.7-keV doublet from the $1^-\rightarrow 0^+$ and $5^-\rightarrow 4^+$ decays, respectively. Figure 14 shows the 687.0 and 583.5-keV decay cross sections from the 3^- level to the 2^+ and 4^+ levels, respectively. Because these five cross sections measure all possible decay modes from the octupole band, assuming higher members are not populated their sum must be equal to the total inelastic scattering cross section of the octupole band plus all decay cross section from higher excited states into the band.

Figures 15 and 16 show cross sections for gamma decay from the 927.0-keV (0^+), 966.3-keV 2^+, and 1055-keV (4^+) members of the proposed first-excited K = 0 band. The spin and parity of only the 2^+ member of this band has been firmly established and only single decays from the (0^+) and (4^+) members of this band have been observed. Figure 15 shows 882.1 and 748.6-keV decay cross sections for the 927-keV $(0^+)\rightarrow 2^+$ and 1055-keV $(4^+)\rightarrow 6^+$ transitions, respectively. Figure 16 shows cross sections for 966.3, 921.4, and 817.9-keV transitions from the 966.3-keV 2^+ state to the 0^+, 2^+, and 4^+ levels, respectively.

Figure 17 shows cross sections for 1037.3, 992.4, and 888.9 keV decays from the 1037.3 keV 2^+ beta vibrational level to the 0^+, 2^+, and 4^+ levels, respectively. No photon decays from the 993-keV 0^+ or 1127-keV (4^+) members of the beta vibrational band are clearly observed although a small 1127-keV cross section may be doublet with the 1128.7-keV level.

Figure 18 shows 885.9, 905.1, and 952.6-keV decay cross sections from the 930.8-keV (1^-), 950.0-keV (2^-), and 997.5-keV 3^- members of the proposed K = 1 band to the 2^+ level. In addition, five BR with respect to these transitions were measured and are listed in Table IV. They are the 930.8 and 250.7-keV decays from the 930.8-keV (1^-) state to the 0^+ and 1^- levels, the 269.9-keV decay from the 950.0-keV (2^-) level to the 1^- level, and the 849.1 and 317.4-keV decays from the 997.5-keV 3^- level to the 4^+ and 1^- levels, respectively. The other decays into and from this band and the multipolarity of these decays are a major source of confusion in the comparison of these measured cross sections with the ENDF/B-V inelastic cross sections.

The decay cross sections from the K = 2 gamma vibrational band, shown in Figs. 19 to 21, are mixed through unresolved doublet transitions among themselves and with transitions from the proposed $K^\pi = 2^-$ band and the 1059.5-keV (3^+) level. Figure 19 shows decay cross sections from the gamma-vibrational band where the 1060.3-keV $2^+ \rightarrow 0^+$ and the 1105.6-keV $(3^+) \rightarrow 2^+$ transitions are measured as a 1060.3-1060.7-keV doublet, and the 1105.6-keV $(3^+) \rightarrow 4^+$ transition (957.3-keV) is resolved. Figure 20 shows cross sections from the other decays from the gamma vibrational 2^+ level; however, these cross sections are doublets with the 1014.4 and 911.1-keV transition from the 1059.5-keV level to the 2^+ and 4^+ levels. Figure 21 shows 1122.8 and 1019.3-keV decay cross sections from the gamma band 1167.7-keV (4^+) level to the 2^+ and 4^+ levels; however, these cross sections are with the 1124.2 and 1020.7-keV photons from the corresponding 1169.1-keV 3^- decays. Although the doublet structure complicates these cross sections, sums of these cross sections are a measure of the decay cross section of sums of levels.

Figure 22 shows 1083.8 and 448.6-keV decay cross sections for transitions from the 1128.7-keV (2^-) state to the 2^+ and 1^- levels. In addition, the branching ratio of the transition to the 3^- state was measured to be 0.39 ± .06 with respect to the 1083.8-keV cross section. The transitions from the 3^- state of this K = 2 band were shown in Fig. 21 and are doublets with transitions from the 1167.7 keV 4^+ level.

The above 24 gamma-ray production cross sections and 7 branching ratios are all the information available from this measurement on the proposed rotational bands of Ellis.[3] We find no conflict with the measured thresholds for production of these photons and their placement in the decay scheme of Ellis.[3] In addition, four other decay cross sections were calculated from the measured spectra. Figure 23 shows cross sections for 1208.3 and 1199.8-keV photons. Inspection of their thresholds indicates that the 1208.3-keV photon is a GS transition, whereas the very weak 1199.8-keV photon is either a GS transition or 2^+ transition. Figure 24 shows decay cross sections for 1223.9 and 1179.0-keV transitions from the 1223.9-keV 2^+ state to the 0^+ and 2^+ levels. These levels are not shown in Fig. 1.

The above 28 cross sections are listed in Appendix A.

C. Uncertainties

The listed errors with the Appendix A cross sections are uncorrelated and follow from the recoil proton and photopeak statistical uncertainties with an additional fraction of the photopeak areas added quadratically. For most lines this fraction is 5% and accounts for uncertainties in extracting areas from distorted line shapes and possible pile-up correction uncertainties. For a few lines this fraction was increased to include additional uncertainties from separating closely-spaced doublets and other confusions connected with the photopeak areas.

In addition to these uncorrelated uncertainties there is an overall normalization uncertainty, correlated over all energy bins of all cross sections, which arises mainly from the flux and detector efficiency measurements. The various systematic errors from the flux determination[19] are listed in Table V. For incident neutron energies above 0.70 MeV these errors quadratically sum to be less than 5%. Allowing a 3% uncertainty for the Ge(Li) efficiency measurement and a 2% uncertainty in the multiple scattering and attenuation correction gives a normalization error of 6% or less. This simple separation of error into correlated and uncorrelated components is ambiguous; however, the above estimates are believed to be realistic.

Two other possible sources of uncertainty, for which it is difficult to give numerical estimates, arise from the photon angular distributions and from the potential for unknown doublet structure. In particular, the photon angular distributions $\sigma_\gamma(\theta)$ for E1, M1, or E2 transitions between states of definite parity are of the form

$$\sigma_\gamma(\theta) = C_o + C_2 P_2(\cos\theta) + C_4 P_4(\cos\theta) \qquad (3)$$

TABLE V. Fluence Measurement Uncertainties

Source	Uncertainty	
Average Radiator Thickness (includes weight and uniformity of foil, but does not include uncertainties possibly due to impurities or stoichiometry of polyethylene)	1/2%	
Averaged Scattering Angle and Detector Solid Angle	1%	
Uncertainty in hydrogen angular distribution and uncertainty in computed cross section due to error in determining incident neutron energy	1%	
Analysis of pulse-height spectra for determination of number of proton recoil events	2%	$3.2<E_n<5.0$ MeV
	4%	$2.6<E_n<3.2$ MeV
	2%	$1.0<E_n<2.6$ MeV
	4%	$0.7<E_n<1.0$ MeV
	10%	$E_n<0.7$ MeV

where C_o, C_2, and C_4, are angle independent and P_2 and P_4 are the usual Legendre polynomials. The angle integrated cross section of $\sigma(\theta)$ is 4π C_o. This work measured $\sigma(\theta)$ at $\Theta = 125°$ for which $P_2 = 0$. Consequently, assuming $C_4 = 0$, C_o was measured directly and normalized to a 4π cross section though the efficiency calibration. If $C_4 \neq 0$ an error is introduced into the Appendix A cross sections. However, for E1 transitions C_4 must vanish and for the remaining transitions investigated in this work C_4 is believed to be small. This could be verified by satistical model calculations; see for example ref. 37.

The possibility that a measured and known ^{238}U transition is doublet with an unknown transition is another troublesome source of uncertainty. This is particularly true for neutron energies above 1.5 to 2.0 MeV where the spectra become very complicated because of the numerous weak photon groups which appear above the fission threshold. For example, the two E1 decays from the 3^- level to the GS band must have an energy independent cross-section ratio. Nevertheless, as indicated in Fig. 14, this ratio is constant only from threshold to $\sim$ 1.5 MeV. The unexplained increased cross section for the 583.5-keV transition above $\sim$ 1.5 MeV is probably due to another transition of unknown origin with energy near 583.5 keV. The cross section for the 966.3 keV line shown in Fig. 16 is another example of this problem.

Finally these cross sections have been measured with a timing resolution function width of 36-nsec FWHM. This width corresponds to the energy difference of adjacent data points in the Figs. 13 to 24 cross sections.

V. INELASTIC SCATTERING CROSS SECTIONS

A. ^{7}Li(n,n´) Li*(478 keV) Inelastic Cross Section

This cross section could provide a useful standard for other gamma-ray production measurements and is of interest to fusion work. As illustrated in Fig. 11, gamma-ray spectra from neutron bombardment of ^{7}Li contain only the 478-keV line whose production cross section has a relatively low threshold and is both isotropic with angle and smooth with energy. Because of these properties and also to verify the normalization of the ^{238}U(n,n´γ) cross sections, we have measured this ^{7}Li cross section simultaneously with those of ^{238}U.

Figure 12 compares our resulting cross sections with those of the ENDF/B-IV evaluation[38] and the recent measurements of Smith[35] and Morgan.[36] Earlier measurements are discussed in ref. 35. Our plotted errors are uncorrelated standard deviations from statistical errors and the 5% pileup-lineshape uncertainty. Quadratic addition of an estimated 6% correlated uncertainty in the normalization gives an 8% absolute error for each data point. The cross sections of Morgan[36] have small relative errors (not shown) and a 10% absolute error, whereas the data of Smith[35] have 5% and 9% for relative and absolute errors, respecitvely. The only serious discrepancy is from threshold to $\sim$ 1.3 MeV where both ORELA cross sections are in excellent agreement with one another and larger than either the Smith[35] or evaluated values. Above $\sim$ 2.0 MeV our cross sections are on average $\sim$ 6% smaller than the Morgan[36] values. From $\sim$ 1.3 to exactly 2.4 MeV our cross sections agree well with the Smith[35] data. Above 2.4 MeV they are smaller.

The two ORELA measurements used different beam lines, ^{7}Li samples, photon detectors, flux determinations and procedures and are consistent within their quoted uncertainties; consequently a suitable average of these results easily provides a $^{7}Li(n,n'\gamma)$ 478-keV gamma-ray production cross section accurate in both shape and magnitude to 7%.

B. ^{238}U Branching Ratios

In order to calculate the scattering cross section $\sigma(E^*)$ from level E^*, population cross sections $\sigma'(E^*)$ must be obtained from the γ-ray production or decay cross sections $\sigma_\gamma(E_\gamma)$ where E_γ is the transition energy and the dependence on the neutron energy is implicit. This procedure requires at least one $\sigma_\gamma(E_\gamma)$ for every level considered with a complete knowledge of its decay properties: gamma-ray branching ratios (BR), relative strength of possible E0 decay and for low energy photon decays its internal conversion coefficients which require knowledge of the transition multipolarities. From these population cross sections and decay information, the scattering cross sections can easily be obtained.

Table VI lists the level decay properties used in this preliminary analysis and depends heavily on the compilation of Ellis[3] who has recently organized level and decay information on ^{238}U. This compilation[3] results in the proposed level and band structure shown in Fig. 1 which our data does not contradict and we assume correct. The Fig. 1 level diagram and Table VI decay properties depend heavily on four measurements: the ^{238}Pa β-decay spectrum of Trautmann et al.,[14] the $^{238}U(n,n'\gamma)$ work of Demidov et al.[15] and McMurray et al.,[13,16] and the Coulomb excitation work of McGowan et al.[17] Not included in the compilation[3] are Coulomb excitation work in progress by McGowan[18] and J. G. Alessi et al.[20]

Table VI requires explanation on a level by level basis since there are both missing and conflicting data for which assumptions must be made. Column four to eight labeled β^-, DEY, MCM, MCG, and ORNL are the gamma-ray BR of Trautmann et al.,[14] Demidov et al.,[15] McMurray et al.,[16] McGowan,[18] and of the present measurement, respectively. The last column is the total intensity BR used in this analysis and was calculated using the total internal conversion coefficients of Hager and Seltzer[39] and whenever possible the gamma-ray BR from the present work.

The BR of the octupole intraband E2 transitions, shown in Fig. 1 and listed in Table VI, with respect to the crossover E1 transitions were calculated[17] assuming a GS intrinsic quadrupole moment with K a good quantum number. K appears to be conserved for both this and the GS band since the crossover E1 transitions obey Alaga's rule.[40] In particular, below 1.5 MeV $\sigma_\gamma(3^-\rightarrow 4^+)/\sigma_\gamma(3^-\rightarrow 2^+) = 0.78 \pm .02$ which agrees with other results and Alaga's rule of 0.81. Above 1.5 MeV, as shown in Fig. 14, $\sigma_\gamma(3^- - 4^+)$ seems doublet with an unknown γ-ray; consequently we use $\sigma'(731.9) = 1.92\ \sigma_\gamma(687.0)$ for all neutron energies. Likewise, below the 5^- threshold at $\sim$ 1.0 MeV $\sigma_\gamma(1^-\rightarrow 0^+)/\sigma_\gamma(1^-\rightarrow 2^+) = 0.62 \pm .02$ which also agrees with other results and Alaga's rule of 0.61. Above $\sim$ 1.0 MeV as shown in Fig. 13 the $\sigma_\gamma(5^-\rightarrow 4^+)$ component doublet with $\sigma_\gamma(1^-\rightarrow 0^+)$ is appreciable; hence we use $\sigma'(680.1) = 1.62\ \sigma_\gamma(635.2)$. Alaga's rule requires $\sigma_\gamma(5^-\rightarrow 6^+)/\sigma_\gamma(5^-\rightarrow 4^+) = 0.59$; consequently subtraction of 1.69 $\sigma_\gamma(5^-\rightarrow 6^+)$ from $\sigma_\gamma(1^-\rightarrow 2^+$ and $5^-\rightarrow 4^+)$ should yield a BR of 0.62 with respect to $\sigma_\gamma(635.2)$ for all incident neutron energies which it satisfyingly does within statistical uncertainty. Hence, the required assumption that $\sigma'(827.1) = 3.22\ \sigma_\gamma(519.9)$ is somewhat verified. In summary the octupole band BR of Table VI follows a simple rotational model and the intraband E2 BR were obtained employing a GS quadrupole moment.

Production cross sections for gamma-ray decay from the proposed first-excited $K^{\pi} = 0^{+}$ band are shown in Figs. 15 and 16. This band is not populated by ^{238}Pa beta decay.[14] Only single decays are observed from the proposed 927.0-keV (0^{+}) and 1055.8-keV (4^{+}) members giving $\sigma'(927.0) = \sigma_{\gamma}(882.1)$ and $\sigma'(1055.8) = \sigma_{\gamma}(748.6)$, respectively. There are at least five gamma branches from the 966.3-keV 2^{+} member and the suggestion[3] of an E0 decay to the 2^{+} level. Figure 16 shows measured cross sections for the E2 decays which give BR in reasonable agreement with those from other works. It is interesting to note that these BR are discrepant with Alaga's rule by a factor of 4. The 1^{-} and 3^{-} BR of McGowan[18] are used for the total transition BR used to calculate the inelastic scattering, whereas the suggested E0 strength of Ellis[3] is not. This level probably has some E0 decay; however, the conclusion that 67.5% of its population decays by E0 seems excessive and unwarranted from the data.[18] The resulting transition BR gives $\sigma'(966.3) = 2.02[\sigma_{\gamma}(921.4) + \sigma_{\gamma}(817.9)]$.

Decays from the proposed $K^{\pi} = 1^{-}$ band are a major source of confusion because of discrepant BR of unknown multipolarities which can transfer appreciable cross section from the $K^{\pi} = 0^{-}$ band into the $K^{\pi} = 1^{-}$ band. Fortunately, for each rotational member we measure one decay cross section which are shown in Fig. 18. Using the Table IV BR for the 930.8-keV (1^{-}) band head gives $\sigma'(930.8) = 1.17\ \sigma_{\gamma}(885.9)$ assuming E2 photons for the $1^{-} \rightarrow 1^{-}$ decay. This transition can proceed by both E2 and M1 photons with the mixing ratio unknown. We somewhat arbitrarily choose a pure E2 decay which results in a 13% BR, whereas a pure M1 decay would give a 27% BR. Decays from the 950.0-keV (2^{-}) member are more confused. Trautmann

et al.,[14] Demidov et al.,[15] and McGowan[18] all obtain nearly equal 1^- and 3^- branches; however, these branches with respect to the 2^+ decay are discrepant suggesting that the 905.1 keV gamma is a doublet. A 1055.8-keV $(4^+)\rightarrow 4^+$ decay would give a 907.4 ± 1.0 keV photon which could cause confusion. In addition, the 218.4-keV 3^- decay nearly coincides in energy with possible decays from the 1167.6 and 1169.1-keV levels to the 950.0-keV levels. We measure and use the smallest 1^- branch and assume a 3^- branch of 0.23. These two decays can be E2-M1 mixtures which we assume to be pure E2 resulting in $\sigma'(950.0) = 1.62\ \sigma_\gamma(905.1)$. The BR from the 3^- member are also confused as shown in Table VI. Perhaps some of the confusion is caused by the ^{56}Fe 847.2 keV line. McGowan et al.[17] suggest a 11% branch from population considerations which is ignored because of our discrepant E1 BR. Using our measured BR and the 5^- BR of Trautmann et al.[14] result in $\sigma'(997.5) = 2.19\ \sigma_\gamma(952.6)$.

Only transitions from the 1037.3-keV 2^+ member of the proposed $K^\pi = 0^+$ beta-vibrational band are clearly observed. Their production cross sections are shown in Fig. 17 and give BR in reasonable agreement with those from other workers. The small branches measured by McGowan[18] to the 1^- and 3^- levels are employed as well as the measured[17] E0 transition strength. The resulting transition BR give $\sigma'(1037.3) = 2.40[\sigma_\gamma(1037.3) + \sigma_\gamma(992.4) + \sigma_\gamma(888.9)]$.

Gamma rays from the $K^\pi = 2^+$ gamma-vibrational band are extremely mixed as doublets. Fortunately, these levels decay only to the ground state band and E0 transitions are probably hindered because of the K selection rule. The 2^+ and 4^+ branches from the 1060.3-keV 2^+ member are doublets with the corresponding decays from the 1059.5 (3^+) level. In addition,

the 0^+ branch from the 1060.3 keV 2^+ member is doublet with the 2^+ decay of the 1105.6-keV (3^+) member leaving only the $(3^+)\rightarrow 4^+$ branch resolved. Nevertheless, $\sigma'(1060.3) + \sigma'(1105.6) + \sigma'(1059.5) = \sigma_\gamma(1060.3\text{-}1059.5) + \sigma_\gamma(1014.4\text{-}1015.3) + \sigma_\gamma(911.1\text{-}911.9) + \sigma_\gamma(957.3)$ which is sufficient for our needs except that the $\sim$ 1060-keV doublet contributes to the 1048-keV pseudolevel and the 1105.6-keV level contributes to the 1170-keV pseudolevel. However, from threshold to $\sim$ 2.0 MeV these gamma-ray production cross sections have roughly the same shape and using the Table VI BR one can deduce that about 10% of $\sigma_\gamma(1060.3\text{-}1060.7)$ is from the (3^+) level. Consequently, $\sigma'(1105.6) = \sigma_\gamma(957.3) + 0.10\ \sigma_\gamma(1060.3\text{-}1060.7)$ and $\sigma'(1060.3) + \sigma'(1059.5) = 0.90\ \sigma_\gamma(1060.3\text{-}1060.7) + \sigma_\gamma(1014.4\text{-}1015.3) + \sigma_\gamma(911.1\text{-}911.9)$.

Figures 21 and 22 show gamma-ray production cross sections for the proposed 1128.7-keV (2^-) and 1169.1-keV 3^- members of the $K^\pi = 2^-$ band. We measure cross sections for two decays from the 2^- member whose BR is in qualitative agreement with those from other works. The discrepancy could be from confusion with a possible beta band $(4^+)\rightarrow 2^+$ decay. The other three branches of Trautmann et al.,[14] normalized to the summed 1083.3, 448.6, and 396.8-keV branches, result in the intensity BR as shown; however, four decays have been assumed E2 where M1 is also possible. These intensity BR give $\sigma(1128.7) = 1.62[\sigma_\gamma(1083.3) + \sigma_\gamma(448.6)]$. Our measured decays from the (4^-) member shown in Fig. 21 are doublet with the corresponding transitions from the gamma-band (4^+) level confusing the BR. We simply do not see a 489.6-keV branch as intense as McGowan[18] or Trautmann et al.,[14] and assume it to be zero, resulting in intensity BR which give $\sigma'(1167.7) + \sigma'(1169.1) = 1.253[\sigma_\gamma(1019.3\text{-}1020.7) + \sigma_\gamma(1122.8\text{-}1124.2)]$.

TABLE VI. ^{238}U Level-Decay Branching Ratios Where Columns Labeled β^-, DEY, MCM, and MCG are Those From Ref. 14, 15, 16, and 18, Respectively

Level	Transition	Energy	Gamma-Ray BR β^-	DEY	MCM	MCG	ORNL	Total BR
K = 0 Octupole Band								
680.1	$1^-\rightarrow 0^+$	680.1 E1	73	66	40		.62	.383
	$\rightarrow 2^+$	635.2 E1	88	100	60		1.00	.617
731.9	$3^-\rightarrow 2^+$	687.0 E1	54	90	56	1.00	1.00	.522
	$\rightarrow 4^+$	583.5 E1	41	59	44	.81	.78	.406
	$\rightarrow 1^-$	51.8 E2						.072[b]
827.1	$5^-\rightarrow 4^+$	678.7 E1					1.00	.576
	$\rightarrow 6^+$	519.9 E1	yes[c]	yes			.59	.310
	$\rightarrow 3^-$	95.2 E2						.114[b]
K = 0 Band								
927.0	$(0^+)\rightarrow 2^+$	882.1 E2			yes	yes	yes	1.000
966.3	$2^+\rightarrow 0^+$	966.3 E2			9	.088	.126	.071
	$\rightarrow 2^+$	921.4 E2		7.9	31	.285	.328	.186
	$\rightarrow 2^+$	921.4 E0						0.000[a]
	$\rightarrow 4^+$	817.9 E2		21	60	.484	.546	.309
	$\rightarrow 1^-$	286.2 E1				.068		.047
	$\rightarrow 3^-$	234.4 E1				.075		.053
1055.8	$(4^+)\rightarrow 6^+$	748.6 E2					yes	1.000
K = 1 Band								
930.8	$(1^-)\rightarrow 0^+$	930.8 E1	yes	5.9	2	.257	.04	.034
	$\rightarrow 2^+$	885.9 E1	45	80	98	1.000	1.00	.852
	$\rightarrow 1^-$	250.7 E2[a]	7			.109	.10	.114
950.0	$(2^-)\rightarrow 2^+$	905.1 E1	23	16	1.00	.552	1.00	.616
	$\rightarrow 1^-$	269.9 E2[a]	12	15		.207	0.21	.164
	$\rightarrow 3^-$	218.1 E2[a]	14	16		.241		.220[a]
997.5	$3^-\rightarrow 2^+$	952.6 E1	21	35	53	1.00	1.00	.456
	$\rightarrow 4^+$	849.1 E1	14	47	47	1.67	0.70	.319
	$\rightarrow 1^-$	317.4 E2				0.13	0.13	.067
	$\rightarrow 5^-$	170.4 E2	3					.157
K = 0 Beta Band								
1037.3	$2^+\rightarrow 0^+$	1037.3 E2		4.2	55	.371	.360	.150
	$\rightarrow 2^+$	992.4 E2		6.8	45	.274	.301	.125
	$\rightarrow 2^+$	992.4 E0		I(E0)/I(E2) = 4.4 ± 1.2				.552
	$\rightarrow 4^+$	888.9 E2				.283	.339	.140
	$\rightarrow 1^-$	357.2 E1				.034		.015
	$\rightarrow 3^-$	305.4 E1				.038		.017
K = 3 Band								
1059.5	$(3^+)\rightarrow 2^+$	1014.4 E2	yes	12	yes			doublet
	$\rightarrow 4^+$	911.1 E2	yes	20	yes			doublet
K = 2 Gamma Band								
1060.3	$2^+\rightarrow 0^+$	1060.3 E2	45	48	yes	.398	.33	doublet
	$\rightarrow 2^+$	1015.3 E2	100	70	yes	.581	.48	doublet
	$\rightarrow 4^+$	911.9 E2	19	2	yes	.019	.09	doublet
1105.6	$(3^+)\rightarrow 2^+$	1060.7 E2	yes	?	yes	doublet		0.29
	$\rightarrow 4^+$	957.5 E2	18	?	yes	.0022	.11	1.00
1167.7	$(4^+)\rightarrow 2^+$	1122.8 E2	yes					doublet
	$\rightarrow 4^+$	1019.3 E2	yes					doublet
K = 2 Band								
1128.7	$(2^-)\rightarrow 2^+$	1083.3 E2	56	8.5	53	.39	.436	.316
	$\rightarrow 1^-$	448.6 E2[a]	76	12	47	.49	.393	.302
	$\rightarrow 3^-$	396.8 E2[a]	18			.12	.171	.134
	$\rightarrow 2^-$	197.9 E2[a]	9					.081
	$\rightarrow 1^-$	178.7 E2[a]	11					.120
	$\rightarrow 3^+$	69.2 E1	7					.047
1169.1	$3^-\rightarrow 2^+$	1124.2 E1	yes		yes	.220	0.43	.558
	$\rightarrow 4^+$	1020.7 E1	yes	3.9		0.586	1.00	.240
	$\rightarrow 1^-$	489.6 E1	20			.193	.00	.000
	$\rightarrow 3^-$	437.2 E2[a]	16			?	.24	.143
	$\rightarrow 3^-$	171.3 E2[a]	3	36				.059

[a] Assumed to be correct.

[b] Calculated from simple rotational model, ref. 17.

C. Summed Inelastic Cross Sections

Figure 25 compares the summed ENDF/B-V cross section[2] for the 1^-, 3^-, and 5^- members of the octupole band to the corresponding summed gamma-ray production cross sections for GS-band decays; that is, $\sigma_\gamma(635.2) + \sigma_\gamma(678.7\text{-}680.1) + \sigma_\gamma(519.9) + 1.78\ \sigma_\gamma(687.0)$. Because E0 decays from this band are strictly forbidden, the summed σ_γ's must equal the inelastic scattering into the band up to 0.93 MeV, the threshold of the next populated level. For neutron energies above 0.93 MeV the summed σ_γ's must be less than the inelastic scattering since feeding from higher levels can only increase the measured cross sections. The summed σ_γ's do not include intraband E2 decays, but these can only transfer cross section from one rotational member to another. For example, inclusion of the $3^-\rightarrow1^-$ decay transfers, at 1.24 MeV, 0.017 b of cross section from the 1^- level to the 3^- level.

Figure 25 shows that the ENDF/B-V octupole-band cross section is $\sim$ 15% larger than our measured value at 0.94 MeV and $\sim$ 10% larger at its maximum near 1.2 MeV. The errors shown in Fig. 25 have been propagated from the uncorrelated uncertainties and do not include the 6% normalization error. We conclude that the ENDF/B-V octupole-band cross section[2] is perhaps 10% too large. This conclusion is strengthened by the fact that our ^{7}Li cross section over the same neutron energies is larger than or equal to other measured and evaluated values.

Figure 26 compares the measured inelastic cross section summed for all levels from 680.1 to 1169.1 keV of excitation to the corresponding summed ENDF/B-V cross sections. In particular, from the population cross sections $\sigma'(E^*)$ and BR of the previous subsection, inelastic scattering

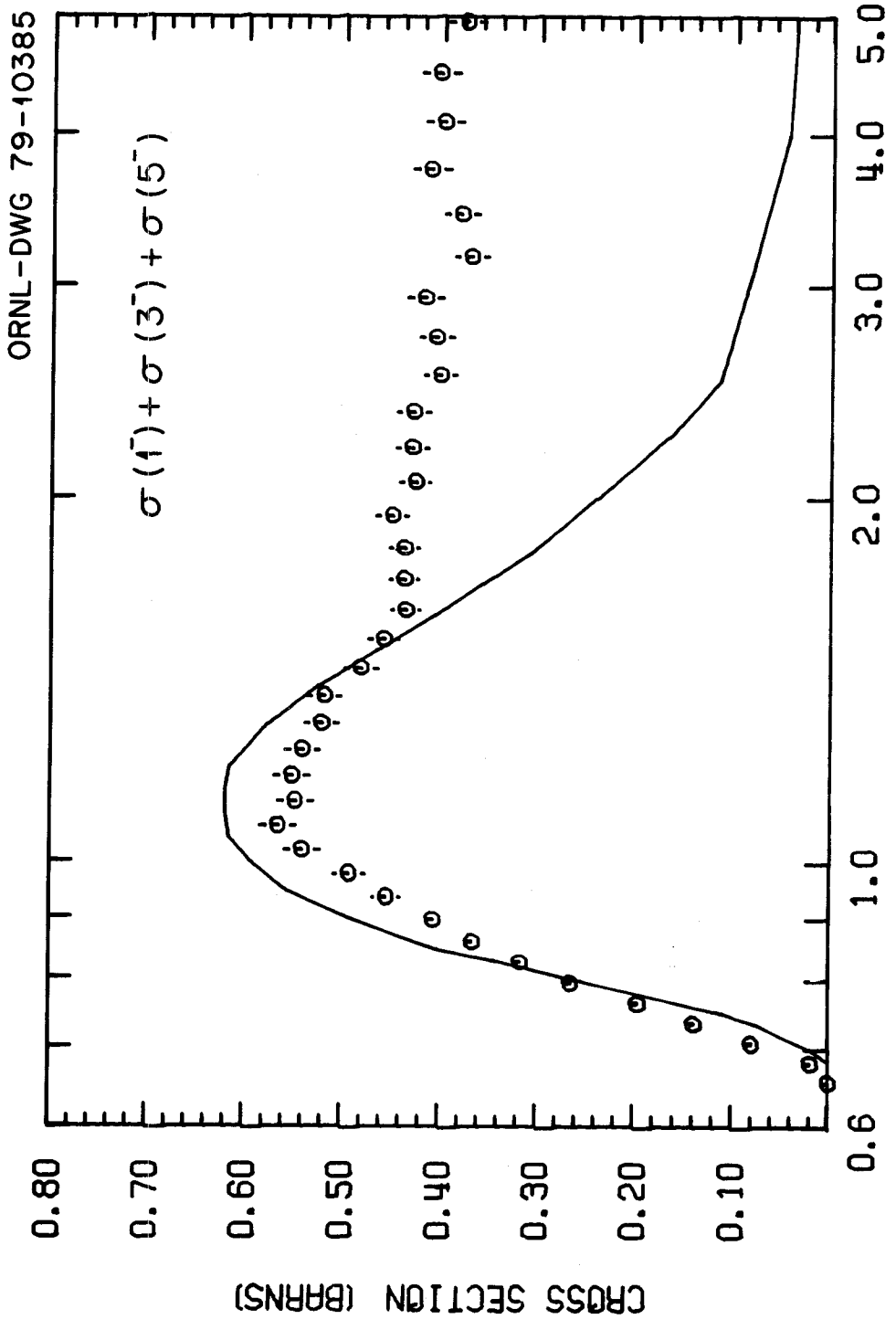

Fig. 25. Comparison between the summed 1^-, 3^-, and 5^- ENDF/B-V inelastic scattering cross sections and the corresponding summed γ-ray production cross sections for octupole-GS rotational band transitions.

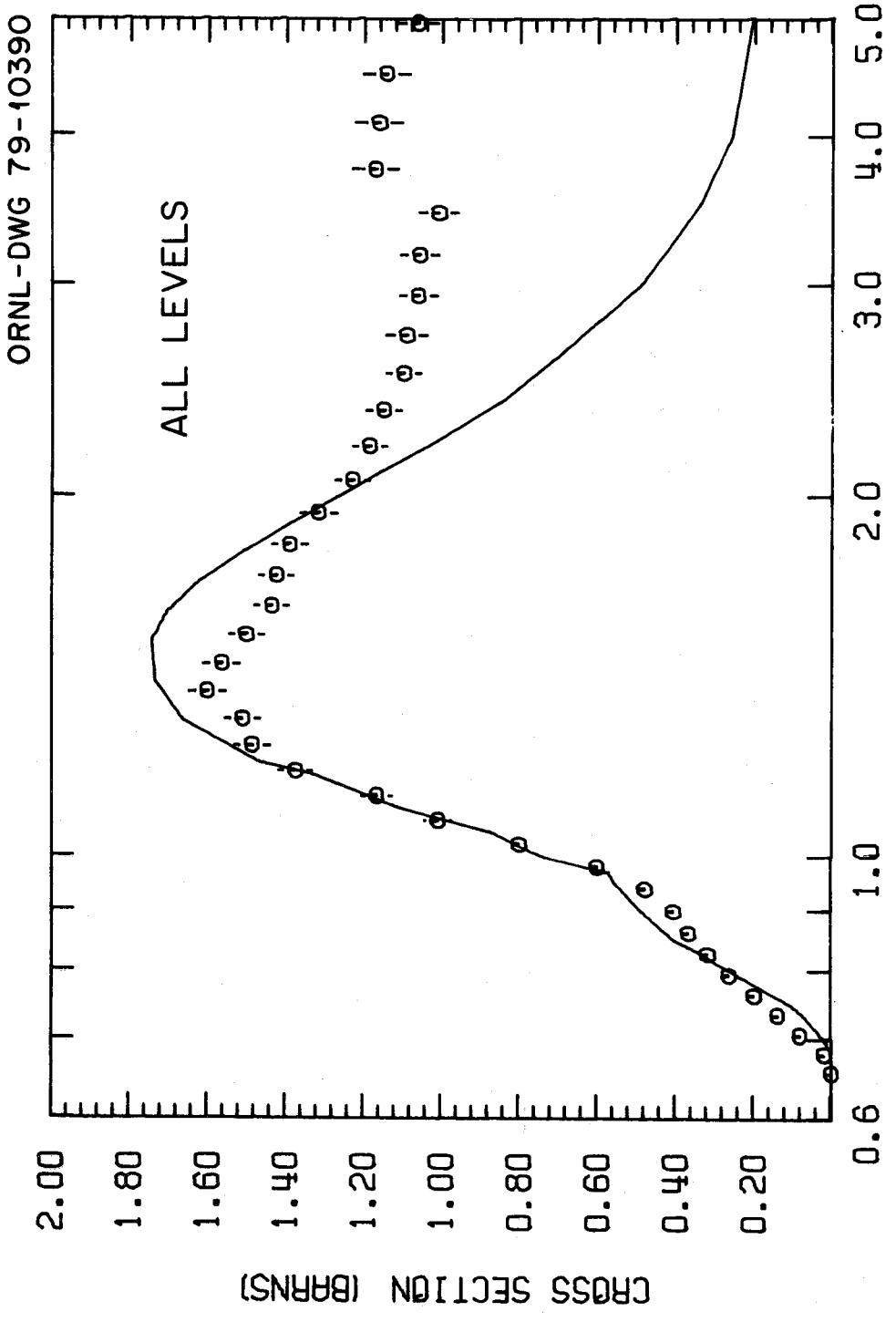

Fig. 26. Comparison between summed ENDF/B-V inelastic scattering cross sections and the corresponding GS-transition γ-ray production and E0 cross sections for all levels from 680.1 to 1169.1-keV of excitation.

cross sections were obtained by subtracting the feeding from higher levels. For example, the 930.8-keV level is only fed by the 1128.7 keV level; consequently, $\sigma(930.8) = \sigma'(930.8) - 0.081\ \sigma'(1128.7)$. Such inelastic cross sections were calculated for all levels from 680.1 to 1169.1 keV of excitation and their sum is shown as the data points in Fig. 26. This sum should and is also equal to the sum of the GS-band transition cross sections from these levels corrected for E0 transitions since the intralevel transitions only transfer cross section. For 1.2 MeV neutrons our summed measured cross section is in excellent agreement with the ENDF/B-V evaluated value, whereas at the ENDF/B-V maximum value of 1.75 barns we are approximately 10% low.

D. Level Inelastic Cross Sections

Figures 27 to 29 compare ENDF/B-V evaluation inelastic cross sections[2] from the individual rotational members of the octupole band to our measured values. The data points without error bars are population cross sections and the data points with error bars are inelastic scattering cross sections, corrected for feeding from all levels up to $\sim$ 1.2 MeV. The measured cross section for the 1^- level is $\sim$ 10% smaller at the maximum than the ENDF/B-V value. In addition, we accurately measure a steeper threshold below $\sim$ 0.8 MeV and a flatter threshold above 0.8 MeV than is evaluated.

Figure 28 shows a similar comparison for the 3^- member where the measured value is a surprising 20% lower than the evaluated value at its maximum. Before subtracting the contributions from feeding the measured cross section is 10% or 30 mb lower than the evaluated value. Subtracting the contributions from feeding reduces the cross section another 10% or

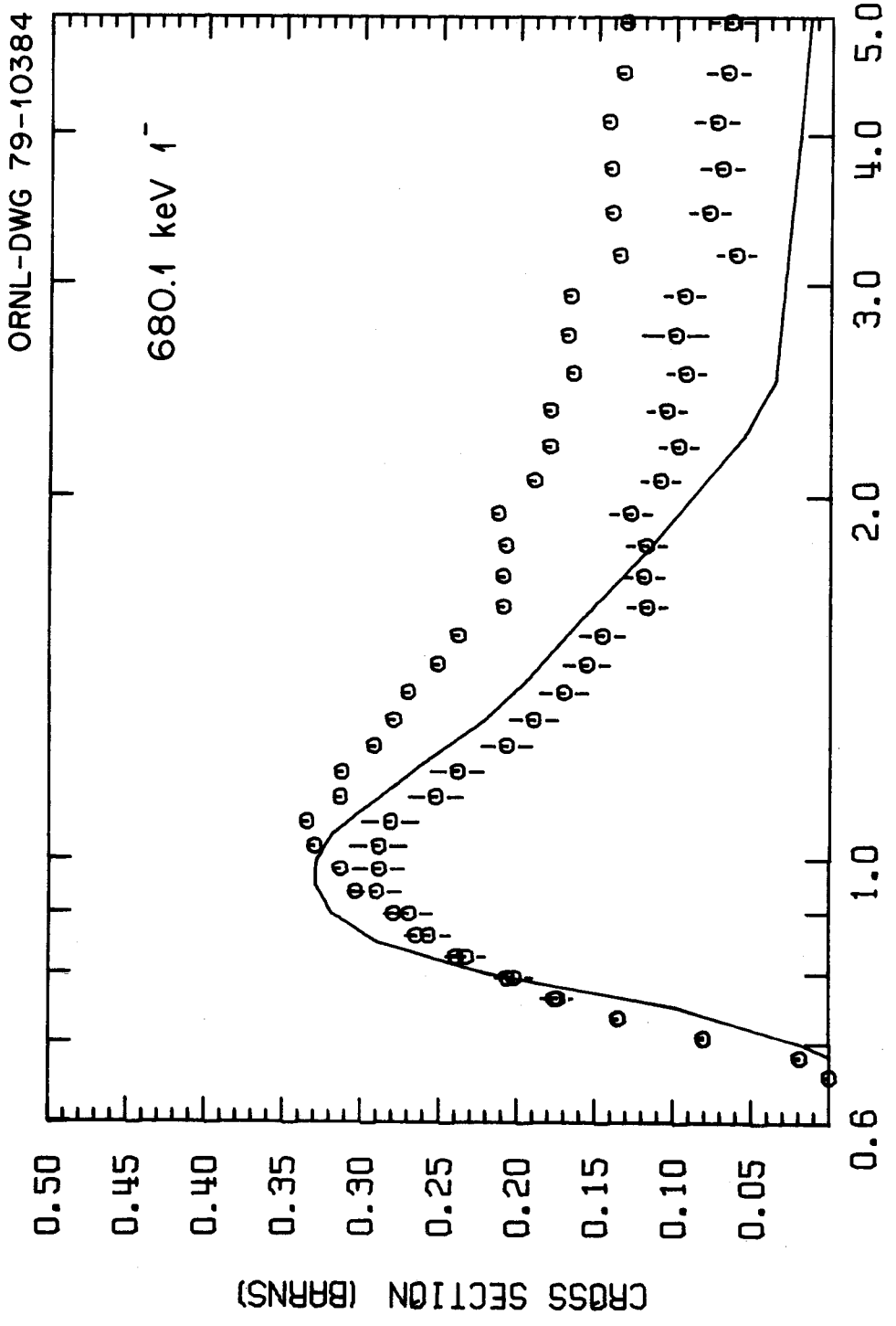

Fig. 27. Comparison between the ENDF/B-V and measured 680.1-keV 1^- inelastic scattering cross sections including (with error bars) and not including (without error bar) the feeding-correction for higher-energy excited levels.

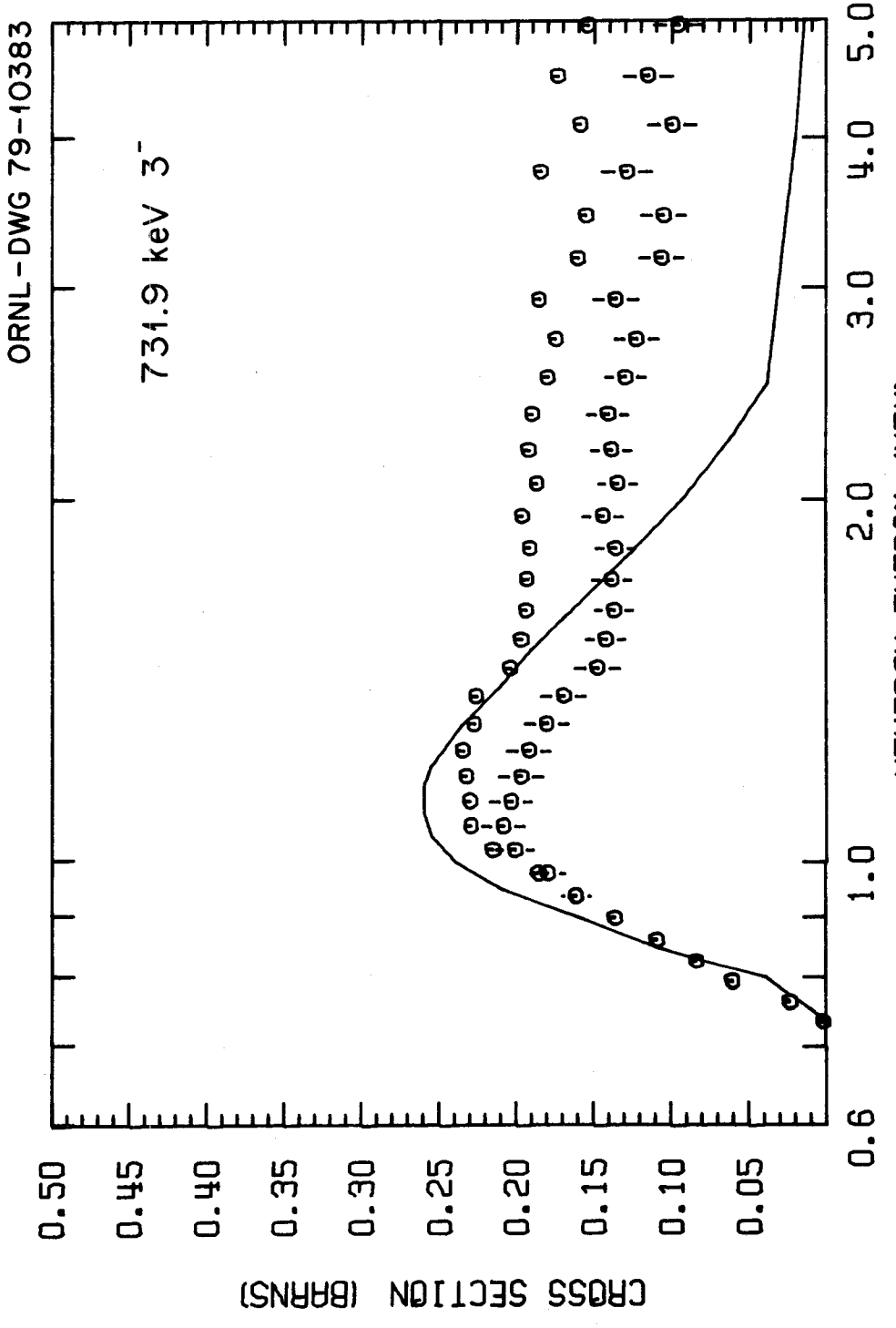

Fig. 28. Comparison between the ENDF/B-V and measured 731.9-keV 3^- inelastic scattering cross section including (with error bars) and not including (without error bars) the feeding correction for higher-energy excited levels.

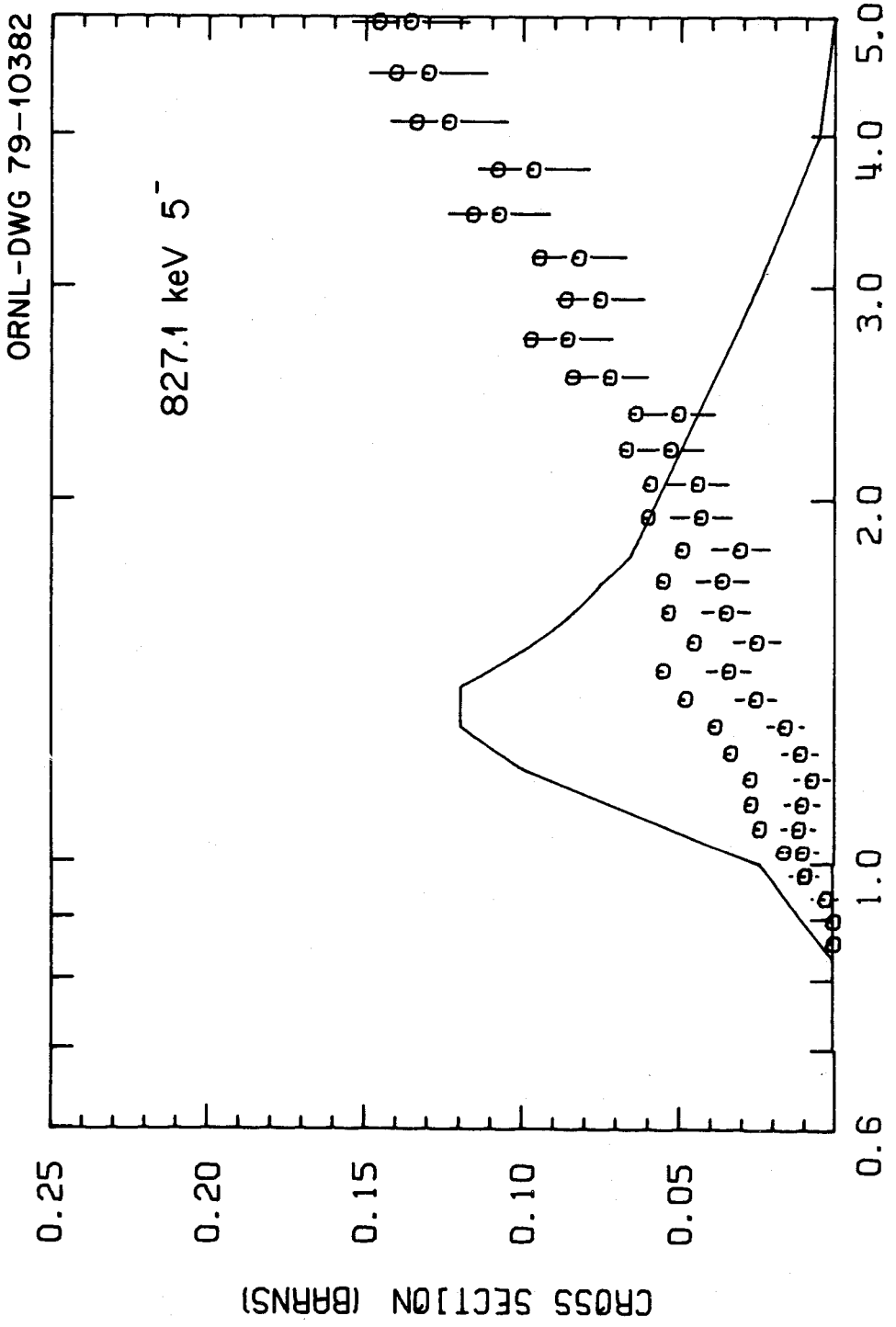

Fig. 29. Comparison between the ENDF/B-V and measured 827.1-keV 5^- inelastic scattering cross sections including (with error bars) and not including (without error bars) the feeding correction from the 997.5-keV level.

30 mb. Six levels feed the 3^- state of which the 950.0 (2^-) level subtracts 15 mb with a 218.4 keV branch. Conversely, the measured 3^- cross section is increased by its 0.072 BR to the 1^- level. This branch was calculated using a simple rotational model and a larger $3^-\rightarrow1^-$ BR would increase the 3^- cross section; however, the 1^- cross section would be reduced by an equal amount.

Figure 29 compares the measured and evaluated 5^- cross sections which are strikingly discrepant. Only the 997.5-keV 3^- level feeds this 5^- rotational member. A larger $5^-\rightarrow3^-$ BR than the calculated value of 11.4% would increase the 5^- cross section, but would further reduce the 3^- cross section.

Figures 30 to 33 show scattering cross sections for the remaining levels required to construct the ENDF/B-V 965, 1048, and 1170-keV cross sections shown in Figs. 34 to 36. In particular, Fig. 30 shows inelastic cross sections to the (0^+), 2^+, and (4^+) rotational members of the proposed first excited $K^\pi = 0^+$ band and Fig. 31 shows inelastic cross sections to the (1^-), (2^-), and 3^- members of the proposed $K^\pi = 0^-$ band. Figure 32 shows cross sections to the beta-band 1037.3-keV 2^+ member and the strongly excited gamma-band-head 2^+ state at 1060.3 keV which is doublet with a 1059.5-keV (3^+) state. Figure 33 shows cross sections for the 1105.6-keV (3^+) member of the gamma-band, a proposed 1128.7-keV (2^-) band head, and a 1167.7-1169.1-keV doublet of the gamma-band (4^+) member and 3^- level, respectively.

Figure 34 compares the ENDF/B-V 965-keV cross section[2] with the measured values employing the Table I correspondence. The cross section maxima are in good agreement with the measured value a few percent high;

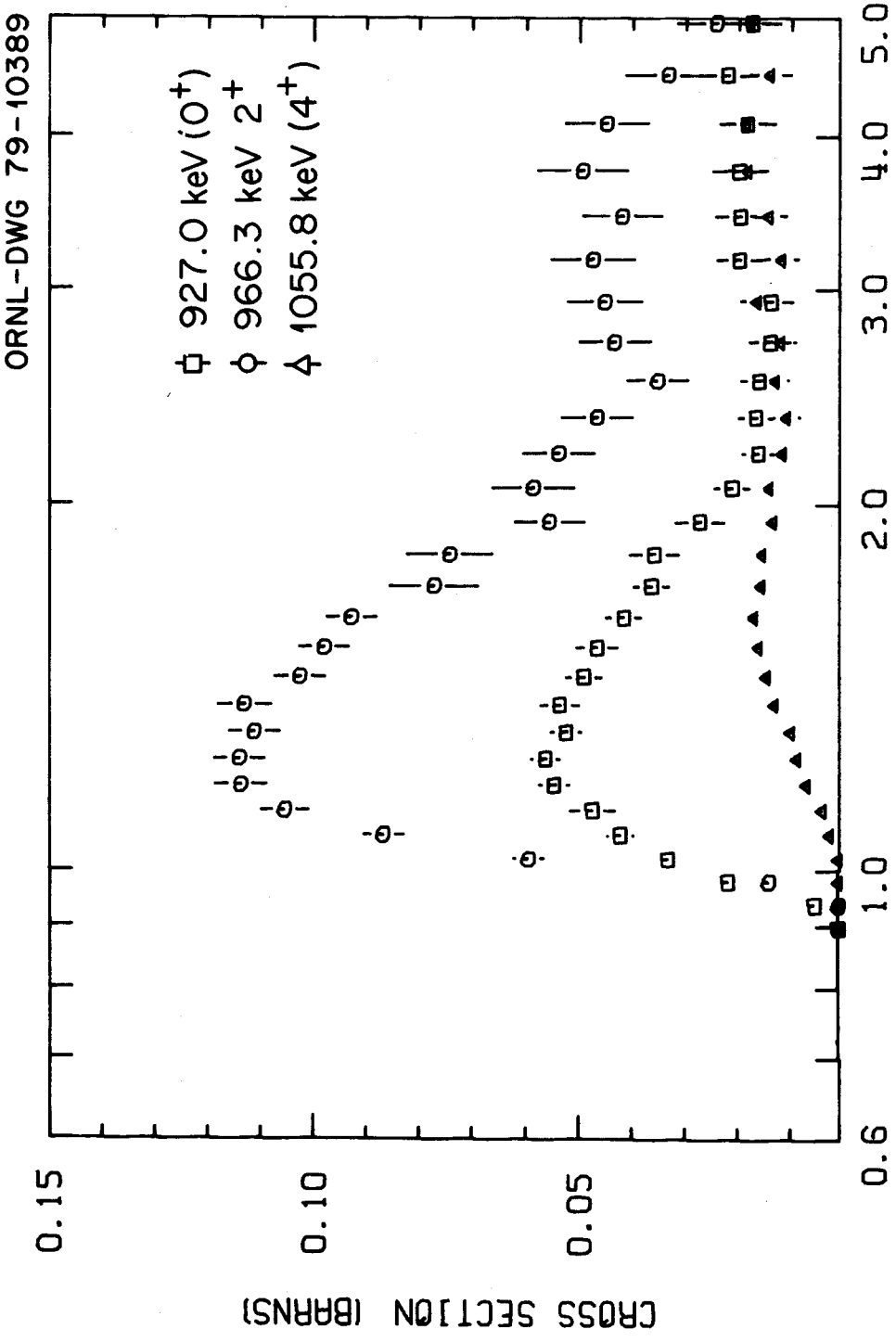

Fig. 30. Measured inelastic scattering cross sections to the (0^+), 2^+, and (4^+) rotational members of the proposed first-excited $K^\pi = 0^+$ band.

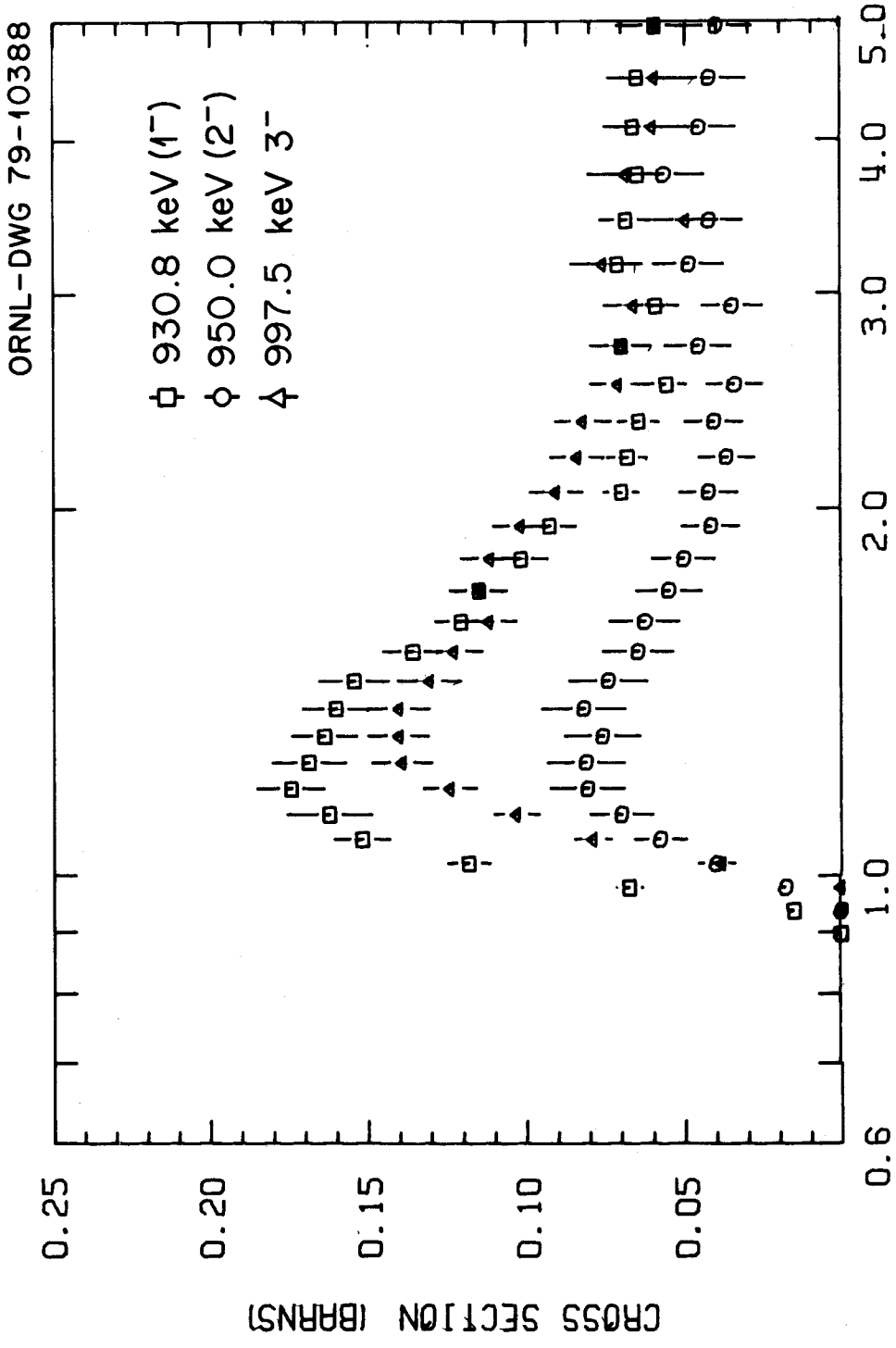

Fig. 31. Measured inelastic scattering cross sections to the (1^-), (2^-), and 3^- rotational members of the proposed second-excited $K^\pi = 1^-$ band.

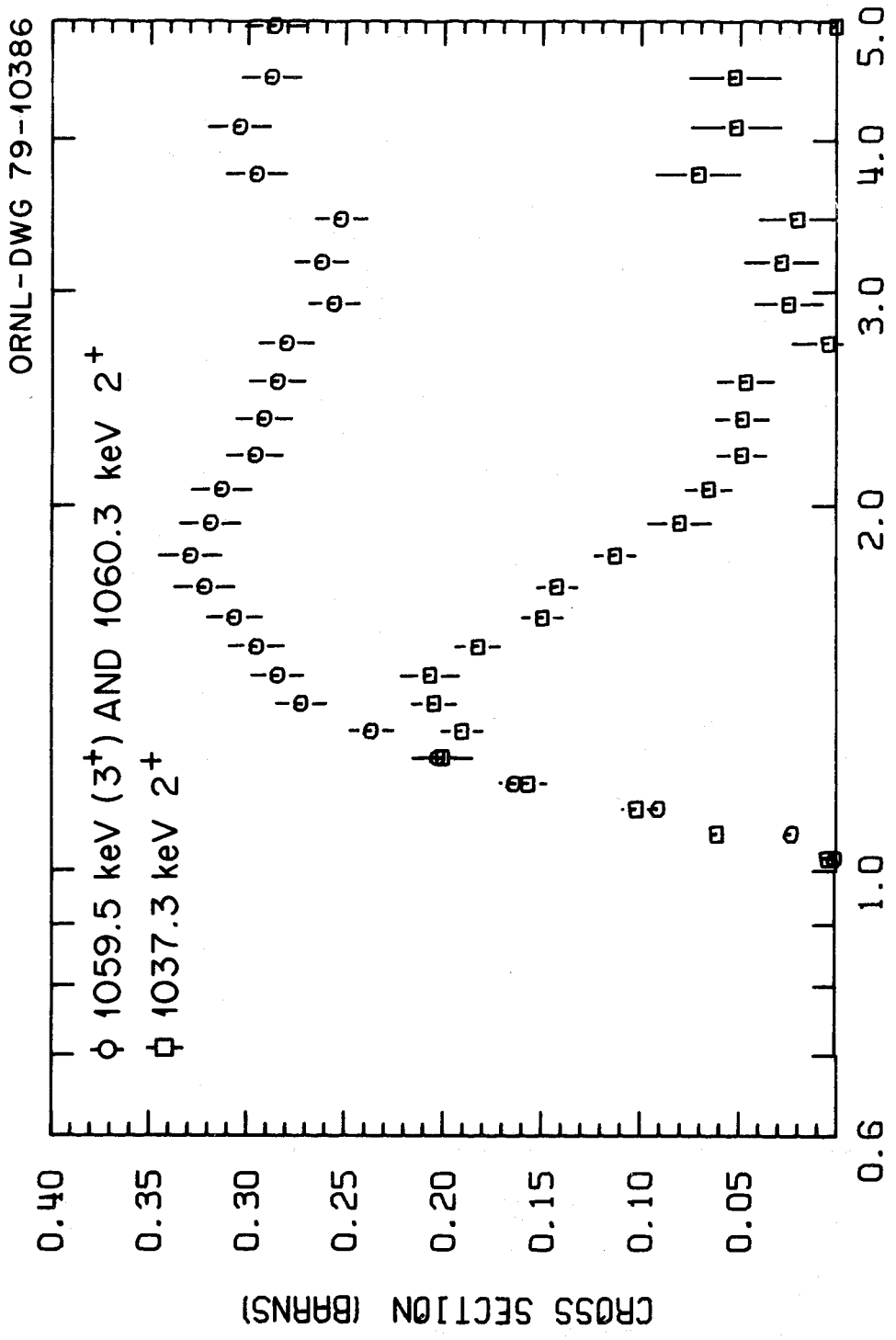

Fig. 32. Measured inelastic scattering cross sections to the 1037.3-keV beta-band 2^+ member and 1060.3-keV gamma-band 2^+ member which is doublet with the 1059.5-keV (3^+) level.

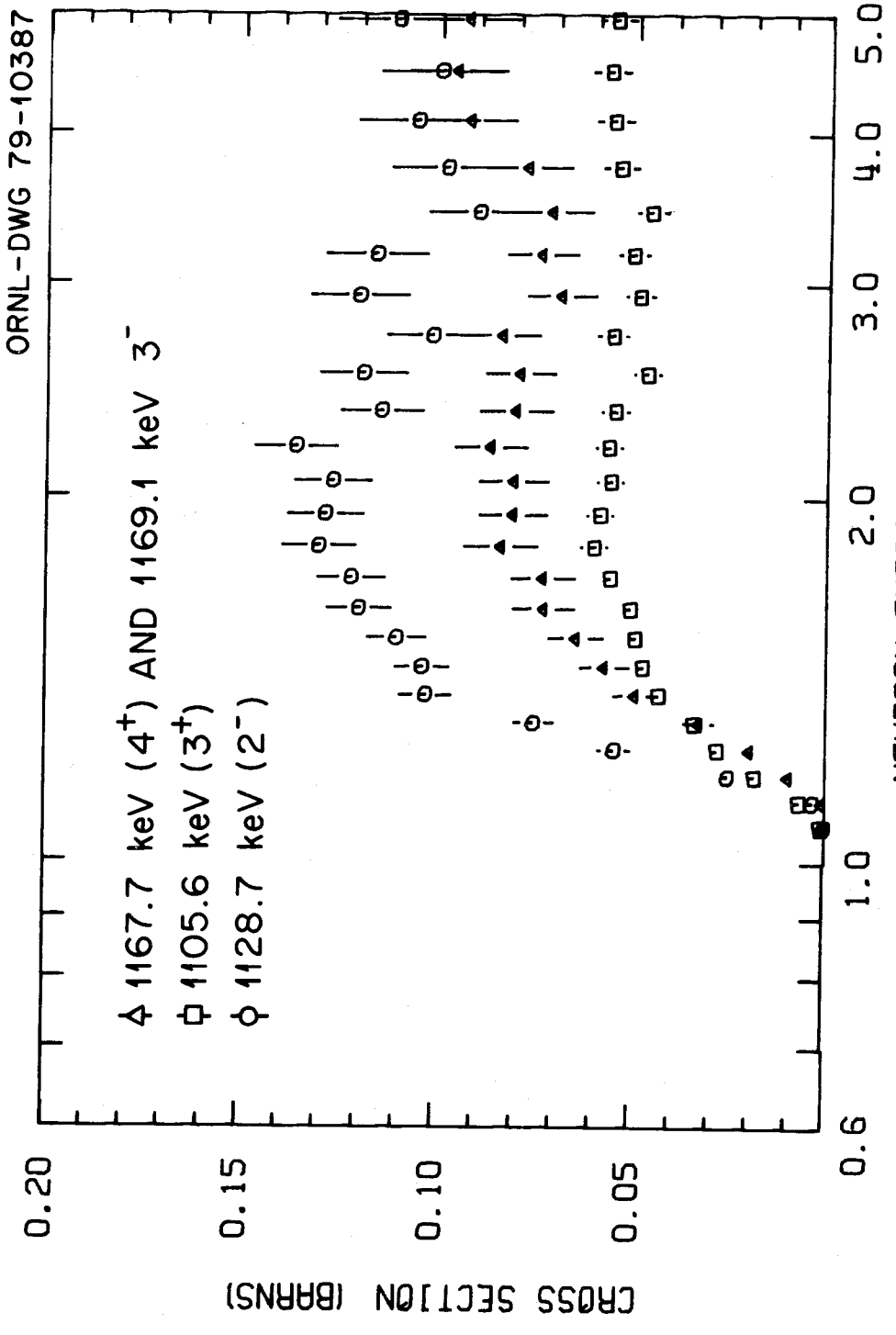

Fig. 33. Measured inelastic scattering cross sections to the 1105.6-keV (3^+) and 1167.7-keV (4^+) gamma-band members and the 1128.7-keV (2^-) and 1169.1-keV 3^- members of a suggested $K^\pi = 2^-$ rotational band.

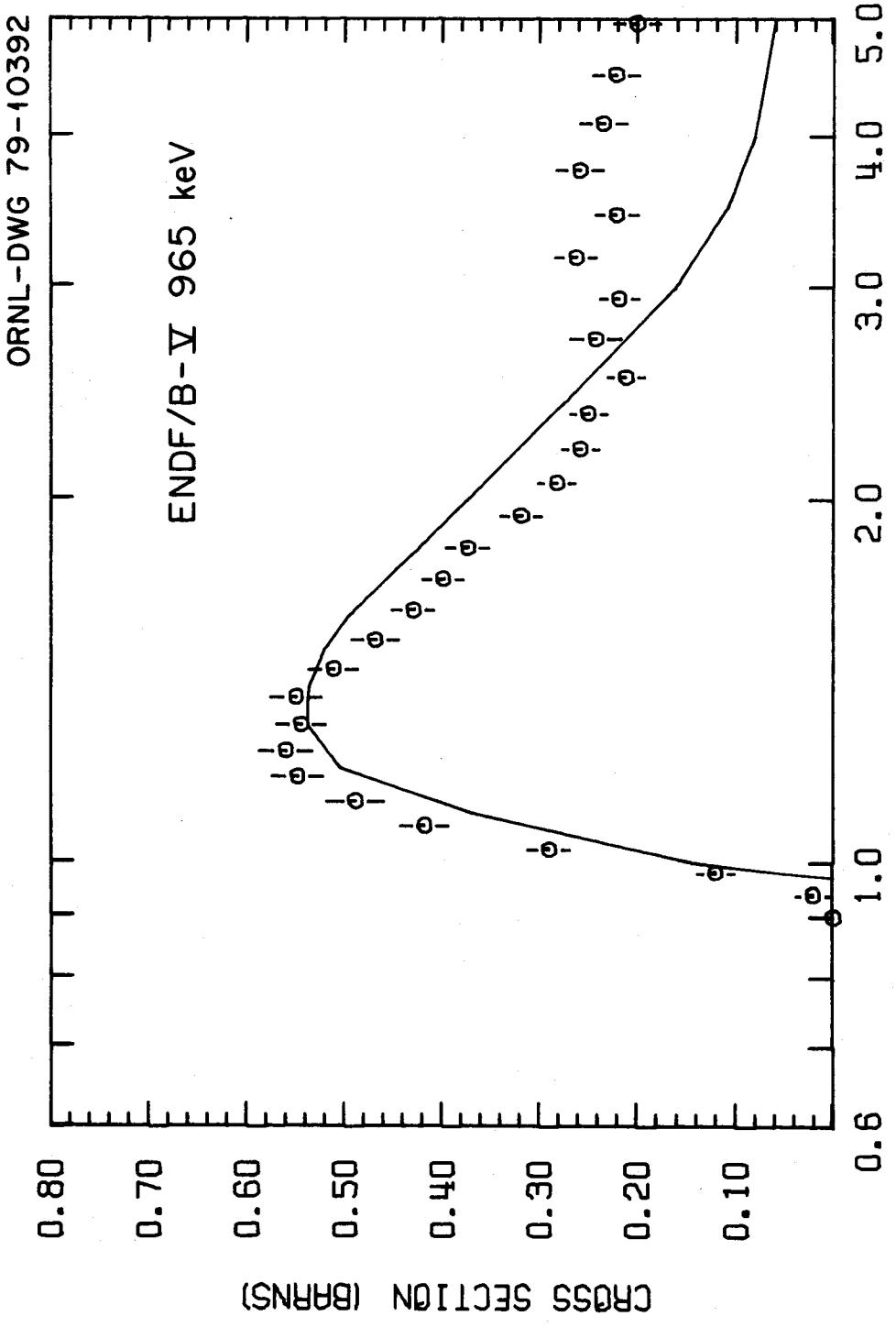

Fig. 34. Comparison between the ENDF/B-V 965-keV pseudolevel inelastic scattering cross section and the corresponding measured values obtained by summing the cross section to the 927.0, 930.8, 950.0, 966.3, and 997.5-keV levels.

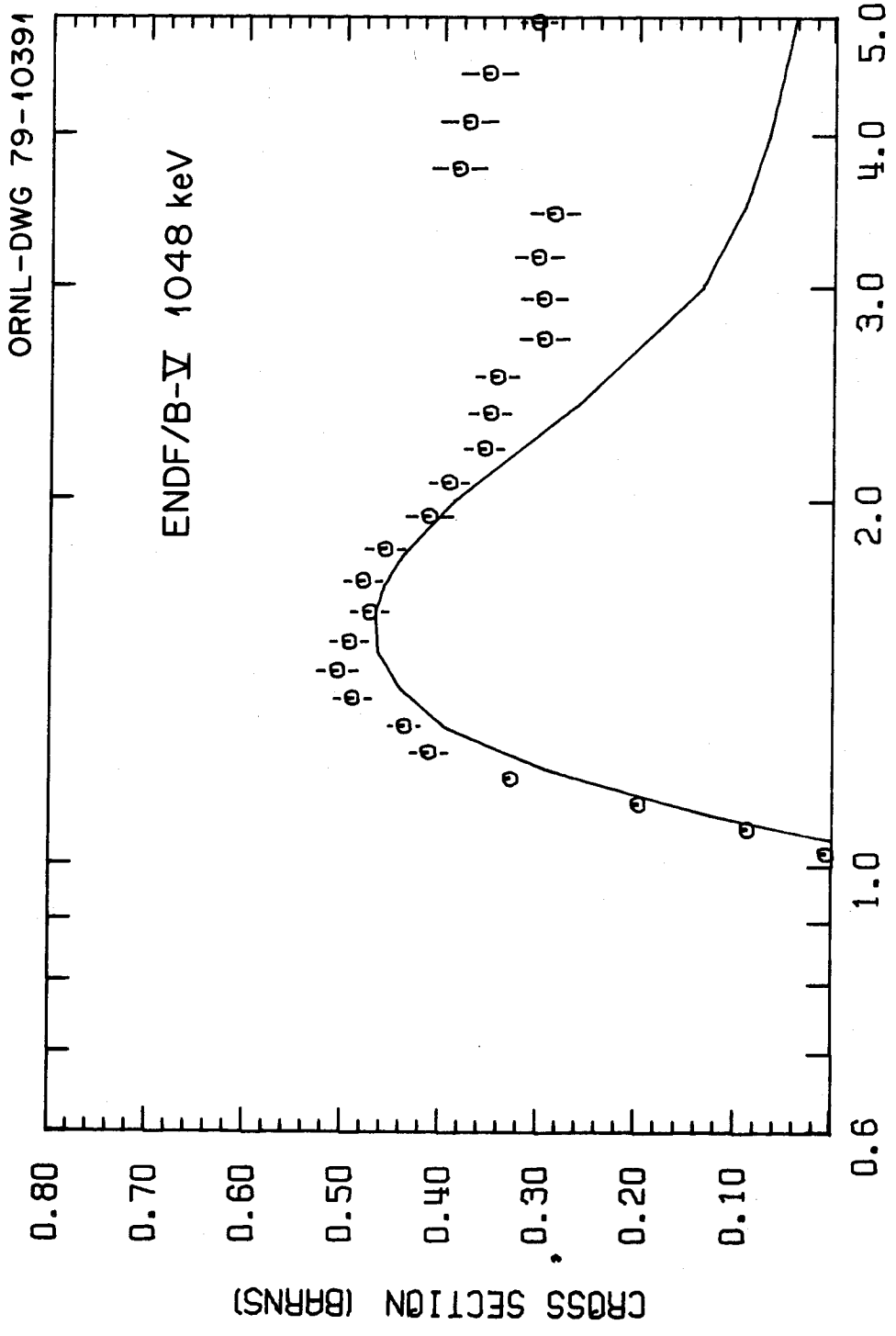

Fig. 35. Comparison between the ENDF/B-V 1048-keV pseudolevel inelastic scattering cross section and the corresponding measured values obtained by summing the cross sections to the 1037.3, 1055.8, 1059.5, and 1060.3-keV levels.

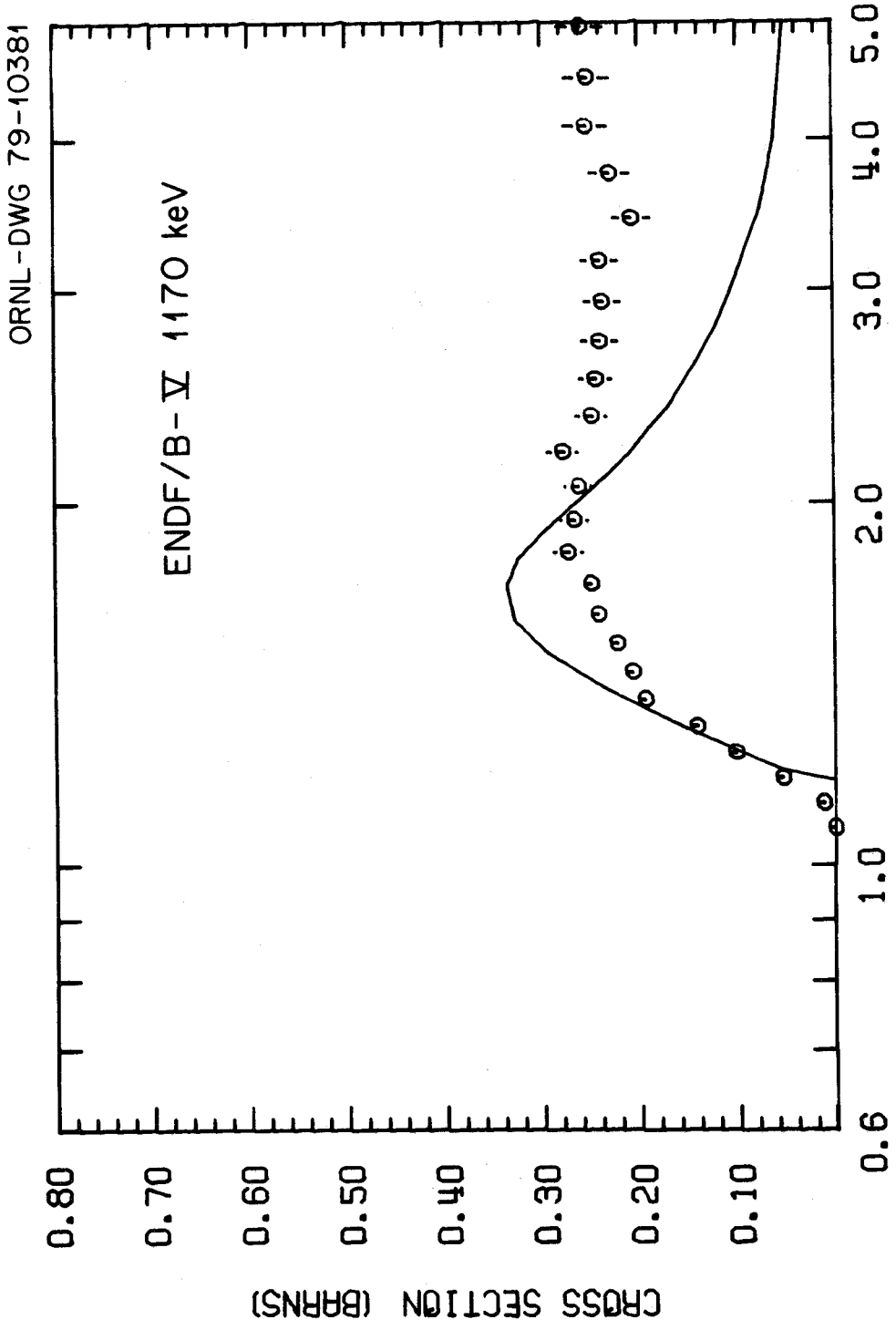

Fig. 36. Comparison between the ENDF/B-V 1170-keV pseudolevel inelastic scattering cross section and the corresponding measured values obtained by summing the cross sections to the 1105.6, 1128.7, 1167.7, and 1169.1-keV levels.

however, the pseudolevel cannot reproduce the threshold correctly. The suggested E0 decay of Ellis[3] from the 966.3-keV 2^+ level would increase the measured cross section by about 0.22 b at the maximum.

Figure 35 shows a similar comparison for the 1048-keV pseudolevel. Again the agreement is good, with the ENDF/B-V evaluation[2] about 5% lower than the maximum measured cross section. The measured E0 decay of McGowan et al.[17] for the 1037.3-keV 2^+ level accounts for about .11 b of the maximum cross section. The 25% error on this cross section is not contained in the plotted error bars.

Figure 36 compares the ENDF/B-V 1170-keV cross section[2] with the corresponding measured values which are the sum of those in Fig. 33. None of these cross sections were corrected for feeding and at the evaluated maximum near 1.5 MeV they are 25% smaller than the evaluated value. Appendix A lists cross sections for higher-energy levels, but our understanding is that the 1170-keV pseudolevel does not contain these levels. A few weakly populated levels, each with many branches, could easily not be detected in this measurement and would account for the Fig. 36 discrepancy which is also Fig. 31 discrepancy.

VI. CONCLUSIONS

The main results of this work are the 28 gamma-ray production cross sections shown in Figs. 13 to 24 and listed in Appendix A. Their neutron-energy thresholds are consistent with their placement in the Fig. 1 energy-level diagram of Ellis.[3] In addition, Table IV lists seven BR for weak transitions whose threshold energies could not be determined. These measured cross sections are on average smaller than those of McMurray et al.[13] The present cross sections for the intense 583.5, 635.2, 680.1, and 687.0-keV lines are $\sim$ 15% smaller than those of McMurray et al.,[13] whereas those of the other lines seem more consistent. The excellent result for the somewhat simultaneously-measured $^{7}Li(n,n'\gamma)$ $^{7}Li^{*}$(478 keV) cross section shown in Fig. 11 gives confidence to the present ^{238}U cross sections since many potential sources of error including the fluence measurement are common to both results.

The sum of GS-band-transition, gamma-ray production cross sections provides an upper limit to summed inelastic cross sections independent of non-GS transitions if possible E0 decays are accounted for correctly. Figure 25 shows that the proposed ENDF/B-V summed 1^{-}, 3^{-}, and 5^{-} cross section is at least 10% too large. Figure 26 indicates that the summed ENDF/B-V cross sections for all levels from 680.1 to 1169.1 keV of excitation is correct at $\sim$ 1.2 MeV neutron energy and $\sim$ 10% too small at the maximum cross near 1.5 MeV.

Section V of this report is the first time to our knowledge that actinide inelastic cross sections have been extracted from gamma-ray production cross sections. The procedure is straightforward. From the present data and other decay information, the total intensity BR of

Table VI were calculated which allowed the gamma-ray production cross sections to determine population cross sections. These with the BR allowed feeding corrections to be made resulting in the Figs. 27 to 33 inelastic cross sections. The weak link is inadequate knowledge of the ^{238}U decay scheme. In particular:

(1) E0 transitions are allowed between levels of the same J^{π} and K and can be appreciable for actinide nuclei. Over 50% of the 1037.3-keV 2^+ decay is by a measured[17] E0 strength and it has been suggested[3] that 62.5% of the 966.3-keV 2^+ decay is by E0; however this latter E0 strength seems excessive, unwarranted by the data, and has been ignored. This E0 and the possible other E0's require clarification, either by direct measurement, microscopic calculations, or from updated systematics.

(2) Internal conversion coefficients for low-energy decays in actinide nuclei are large which necessitates knowledge of the transition multipolarities or mixing ratios. For ^{238}U the E2-M1 mixing ratio for low-energy transitions between initial and final negative parity states are unknown. Throughout these have been assumed to be pure E2 decays which results in the minimum cross section for the initial level and the maximum cross section for the final level. This is a significant assumption which requires clarification. Whether a 250-keV transition is E2 or M1 gives a factor of two in its total intensity BR. For high energy transitions the internal conversion coefficients are $\lesssim$ 1% and have been ignored.

(3) There are many conflicting BR caused by suspected gamma-ray multiplets whose members are produced with different intensities in different measurements. This confuses the comparison and incorporation of other measured BR. The 1059.5-1060.3, 1127-1128.7 and 1167.7-1169.1-keV level pairs are nearly degenerate in energy giving many doublet gamma-rays. Moreover, some gamma rays may be doublet with other ^{238}U lines and background lines; for example, the 905.1, 218.1, and 849.1-keV transitions. The transitions from the higher bands do not follow Alaga's rule,[40] so these confusions require experimental clarification. Unfortunately, the required good timing resolution for the Ge(Li) detector reduced its efficiency for low energy transitions so that most could not be observed and none have threshold determinations to verify their origins.

Nevertheless, there is general agreement on ^{238}U BR which results in the Figs. 27 to 29 and 34 to 35 comparisons with the proposed ENDF/B-V evaluated cross sections. This comparison indicates that the evaluated 1^-, 3^-, and 5^- cross sections are respectively 10%, 20%, and at least 50% too large at their maximum values, whereas the 965 and 1048-keV pseudolevels have about the correct strength. The present measurement of the threshold shape for these cross sections is very good and disagree with their evaluated values. This comparison is considered preliminary and does not contain uncertainty estimates for the BR. It is hoped that the new Coulomb excitation measurements of McGowan[18] and the Coulomb-excitation, gamma-gamma coincidence work of Alessi et al.[20] will further clarify the ^{238}U level structure and decay scheme.

ACKNOWLEDGMENTS

The authors are indebted to the entire ORELA staff for the excellent Linac operation. J. G. Craven wrote the computer program for data acquisition. Many helpful discussions and advice from J. K. Dickens are gratefully acknowledged. F. K. McGowan is thanked for use of his gamma-ray branching ratios prior to publication and, with Y. A. Ellis, is thanked for valuable discussions on the ^{238}U level scheme. P. R. Kuehn is thanked for fabricating the ^{7}Li sample and R. H. Ward is thanked for his help in the design and fabrication of the telescope.

REFERENCES

1. J. H. Marable, J. L. Lucius, and C. R. Weisbin, "Compilation of Sensitivity Profiles for Several CSEWG Fast Reactor Benchmarks," ORNL-5262 (1977).
2. W. Poenitz, E. Pennington, A. B. Smith, and R. Howerton, "Evaluated Fast Neutron Cross Sections of ^{238}U," ANL/NDM-32 (1977).
3. Y. A. Ellis, *Nuclear Data Sheets* 21, 549 (1977).
4. L. Cranberg and J. Levin, *Phys. Rev.* 109, 2063 (1956).
5. A. Smith, *Nucl. Phys.* 47, 633 (1963).
6. L. Stromberg and S. Schwartz, *Nucl. Phys.* 71, 511 (1965).
7. E. Barnard, A. T. G. Ferguson, W. R. McMurray, and I. J. Van Heerden, *Nucl. Phys.* 80, 46 (1966).
8. E. Barnard, J. A. M. DeVilliers, and D. Reitmann, "Proc. Second Inter. Conf. on Nuclear Data for Reactors," Helsinki; IAEA Press (1970) Vol. 2, page 103.
9. P. Guenther and A. Smith, "Proc, Conf. on Nuclear Cross Sections and Technology," Washington D.C., *NBS Special Publication* 425 (1975) Vol. 2, p. 862.
10. G. Haouat, J. Sigaud, J. Lachkar, Ch. Lagrange, B. Duchemin, and Y. Patin, Proc. Inter. Conf. on the Interaction of Neutrons with Nuclei, Lowell, Massachusetts, CONF-760715-P2 (1976), Vol. 2, P. 1330.
11. L. E. Beghian, G. H. R. Kegel, T. V. Marcella, B. K. Barnes, G. P. Couchell, J. J. Egan, A. Mittler, D. J. Pullen, and W. A. Schier, *Nuc. Sci. Eng.* 69, 191 (1979).
12. P. Guenther et al. private communication to Ref. 2.

13. W. R. McMurray et al., Southern Universities Annual Reports and private communication (1978).

14. N. Trautmann, R. Denig, N. Kaffrell, and G. Hermann, *Z. Naturforsh* 23a, 2127 (1968).

15. A. M. Demidov, L. I. Gover, Y. K. Cherepantsev, M. R. Ahmed, C. Al-Nadzhar, and M. A. Al-Amili, Proc. 25th Ann. Conf. Nucl. Specrosc. Struct. At. Nuclei, Leningrad, P. 159 (1975).

16. W. R. McMurray and I. J. Van Heerden, *Z. Phys.* 253, 289 (1972); W. R. McMurray and I. J. Van Heerden, SUNI-23, p. 12 (1973).

17. F. K. McGowan, C. E. Bemis, Jr., W. T. Milner, J. L. C. Ford, Jr., M. L. Robinson, and P. H. Stelson, *Phys. Rev.* C 10, 1146 (1974); F. K. McGowan, private communication to Y. A. Ellis (1976); F. K. McGowan, private communication (1978).

18. F. K. McGowan, private communication (1979).

19. G. L. Morgan, D. K. Olsen, and J. W. McConnell, *Nucl. Inst. and Meth.* 157, 525 (1978).

20. J. G. Alessi, J. X. Saladin, C. Baktash, and T. J. Humanic, *BAPS* 23, 614 (1978).

21. N. C. Pering and T. A. Lewis, *IEEE Transactions on Nuclear Science*, NS-18, 929 (1971).

22. Beam line designed and constructed by R. W. Peelle, private communication.

23. R. L. Macklin, *Nucl. Inst. Meth.* 91, 79 (1971).

24. J. H. Todd, "Instrument and Controls Division Annual Progress Report for Period Ending September 1, 1970," ORNL-4620, p. 36, Oak Ridge National Laboratory (1970).

25. N. A. Betz, J. W. Reynolds, and G. G. Slaughter, USAEC Division of Technical Information Report No. OCNF 690301, 1969 (unpublished).

26. G. D. James, Proc. of Symposium on Neutron Standards and Applications, Gaithersburg, Maryland, *NBS Special Publication* 493 (1977), p. 319.

27. C. M. Lederer, J. M. Hollander, and I. Perlman, "Table of Isotopes," Sixth Edition (John Wiley & Sons, New York, 1967).

28. J. L. Gammel, in *Fast Neutron Physics*, Part II, edited by J. B. Marion and J. L. Fowler (Interscience, New York, 1963).

29. Hans Bichsel, in *American Institute of Physics Handbook*, 3rd edition, edited by D. E. Gray (McGraw-Hill Book Company, New York, 1972).

30. J. G. Craven, "OPRODF, A Decsystem-10 Data Manipulation Program for ORELA Data Formated Files," ORNL/CSD/TM-45 (1978).

31. Written by J. K. Dickens; described in J. K. Dickens "Fission Yields for Thermal-Neutron Fission of ^{241}Pu," accepted for publication in *Nucl. Sci. Eng.*

32. D. M. Wharton and D. K. Olsen, "LSFODF: A Generalized Nonlinear Least-Squares Fitting Program for Use With ORELA ODF Files," ORNL/TM-6545 (1978).

33. E. Storm and H. I. Israel, *Nucl. Data Tables* A7, 565 (1970).

34. J. L. Rodda, R. L. Macklin, and J. H. Gibbons, *Nucl. Inst. and Meth.* 74, 224 (1969).

35. D. L. Smith, *Nucl. Sci. Eng.* 61, 540 (1976).

36. G. L. Morgan, "Cross Sections for the ^{7}Li(n,xn) and ^{7}Li(n,n$\hat{}\gamma$) Reactions Between 1 and 20 MeV," ORNL/TM-6247 (1978).

37. P. T. Karatzas, G. P. Couchell, B. K. Barnes, L. E. Beghian, P. Harihar, A. Mittler, D. J. Pullen, E. Sheldon, and N. B. Sullivan, *Nucl. Sci. Eng.* 67, 34 (1978).

38. R. T. LaBauve, L. Stewart, and M. Battat, ENDF/B-IV MAT 1272, Los Alamos Scientific Laboratory (May 1974).

39. R. S. Hager and E. C. Seltzer, *Nucl. Data* A4, 1 (1968).

40. G. Alaga, K. Alder, A. Bohr, and B. R. Mattelson, *Dan. Mat.-Fys Medd.* 29, No. 9 (1955).

APPENDIX A

This appendix lists the 125° angle-differential γ-ray production cross sections measured in this work multiplied by 4π. Page 83 lists the ^{7}Li 478-keV cross section and pages 84 to 88 list 28 cross sections for ^{238}U transitions. On each page the first column, E_n, gives the incident-neutron-bin center energy in MeV and the remaining columns, σ_γ, list pairwise the corresponding cross sections and absolute errors in barns. On the top of each column pair in parenthesis the γ-ray transition energy is given in keV. The listed errors are uncorrelated between energy bins and γ-ray transitions. Not listed is a ∿ 6% normalization uncertainty which is correlated over all energy bins and all γ-ray transitions. The ratio of the ^{238}U cross sections to that of ^{7}Li can be obtained by division in which case the normalization uncertainty cancels. In addition, division of the listed cross sections by 4π gives the angle differential cross sections at 125°.

^{7}Li γ-ray Production Cross Section

E_n	σ_γ(478 keV)	
5.496	0.2143	0.0126
4.958	0.2060	0.0119
4.496	0.2192	0.0127
4.095	0.2613	0.0149
3.746	0.2658	0.0150
3.440	0.2356	0.0132
3.170	0.1937	0.0107
2.930	0.2029	0.0112
2.717	0.1903	0.0109
2.526	0.1804	0.0102
2.355	0.1875	0.0104
2.200	0.1831	0.0100
2.060	0.1821	0.0098
1.934	0.1901	0.0102
1.818	0.1938	0.0103
1.713	0.1895	0.0100
1.616	0.1933	0.0102
1.528	0.2002	0.0105
1.446	0.2049	0.0107
1.371	0.2078	0.0109
1.302	0.1996	0.0104
1.237	0.2097	0.0110
1.178	0.2221	0.0116
1.122	0.2220	0.0116
1.071	0.2174	0.0114
1.023	0.2060	0.0108
0.978	0.1887	0.0099
0.936	0.1661	0.0087
0.896	0.1483	0.0078
0.859	0.1266	0.0067
0.825	0.1105	0.0059
0.792	0.0928	0.0050
0.761	0.0796	0.0043
0.732	0.0694	0.0038
0.705	0.0603	0.0033
0.679	0.0558	0.0031
0.655	0.0506	0.0029
0.632	0.0388	0.0023
0.610	0.0297	0.0018
0.589	0.0237	0.0015
0.569	0.0179	0.0013
0.550	0.0074	0.0007
0.532	0.0008	0.0004
0.515	-0.0001	0.0004

^{238}U γ-ray Production Cross Sections and Absolute Errors

E_n	σ_γ(678.7-80.1)		σ_γ(635.2)		σ_γ(687.0)		σ_γ(583.5)		σ_γ(519.9)		σ_γ(882.1)	
4.958	0.1078	0.0092	0.0815	0.0072	0.0802	0.0073	0.1037	0.0076	0.0453	0.0058	0.0173	0.0055
4.496	0.1174	0.0096	0.0827	0.0071	0.0903	0.0077	0.1140	0.0081	0.0435	0.0059	0.0219	0.0056
4.095	0.1229	0.0098	0.0885	0.0075	0.0826	0.0074	0.1071	0.0077	0.0415	0.0058	0.0183	0.0055
3.746	0.1213	0.0095	0.0874	0.0072	0.0960	0.0078	0.1058	0.0076	0.0335	0.0056	0.0198	0.0053
3.440	0.1151	0.0088	0.0867	0.0070	0.0807	0.0068	0.1006	0.0070	0.0360	0.0051	0.0196	0.0048
3.170	0.1095	0.0083	0.0837	0.0064	0.0835	0.0067	0.0993	0.0069	0.0294	0.0047	0.0198	0.0045
2.930	0.1165	0.0083	0.1032	0.0074	0.0967	0.0070	0.0957	0.0066	0.0268	0.0044	0.0137	0.0043
2.717	0.1105	0.0082	0.1041	0.0072	0.0909	0.0067	0.1087	0.0071	0.0303	0.0045	0.0139	0.0041
2.526	0.1074	0.0076	0.1019	0.0068	0.0938	0.0065	0.0900	0.0060	0.0261	0.0038	0.0160	0.0037
2.355	0.1221	0.0081	0.1110	0.0071	0.0991	0.0066	0.1004	0.0064	0.0198	0.0036	0.0166	0.0034
2.200	0.1203	0.0077	0.1110	0.0069	0.1002	0.0065	0.0949	0.0060	0.0208	0.0033	0.0162	0.0032
2.060	0.1179	0.0074	0.1172	0.0070	0.0974	0.0062	0.1007	0.0062	0.0184	0.0031	0.0212	0.0034
1.934	0.1177	0.0073	0.1316	0.0077	0.1025	0.0064	0.0979	0.0060	0.0187	0.0031	0.0272	0.0048
1.818	0.1166	0.0072	0.1283	0.0074	0.0997	0.0062	0.0974	0.0060	0.0152	0.0030	0.0358	0.0048
1.713	0.1116	0.0068	0.1295	0.0074	0.1008	0.0062	0.0944	0.0057	0.0172	0.0027	0.0364	0.0035
1.616	0.1099	0.0066	0.1295	0.0073	0.1012	0.0061	0.0889	0.0054	0.0166	0.0025	0.0415	0.0034
1.528	0.1136	0.0067	0.1474	0.0081	0.1028	0.0061	0.0921	0.0055	0.0141	0.0024	0.0466	0.0041
1.446	0.1195	0.0069	0.1555	0.0085	0.1065	0.0069	0.0940	0.0056	0.0172	0.0023	0.0490	0.0036
1.371	0.1269	0.0072	0.1672	0.0091	0.1179	0.0068	0.0954	0.0056	0.0149	0.0021	0.0535	0.0039
1.302	0.1256	0.0070	0.1730	0.0093	0.1186	0.0068	0.0913	0.0053	0.0120	0.0018	0.0524	0.0030
1.237	0.1320	0.0073	0.1808	0.0097	0.1223	0.0069	0.0968	0.0056	0.0104	0.0018	0.0563	0.0029
1.178	0.1342	0.0074	0.1935	0.0103	0.1211	0.0069	0.0989	0.0057	0.0085	0.0018	0.0546	0.0031
1.122	0.1323	0.0073	0.1940	0.0104	0.1199	0.0068	0.0967	0.0056	0.0084	0.0018	0.0474	0.0045
1.071	0.1382	0.0076	0.2072	0.0111	0.1196	0.0068	0.0916	0.0053	0.0076	0.0017	0.0421	0.0025
1.023	0.1321	0.0073	0.2041	0.0109	0.1121	0.0064	0.0907	0.0053	0.0052	0.0017	0.0332	0.0020
0.978	0.1237	0.0069	0.1939	0.0104	0.0968	0.0056	0.0759	0.0045	0.0031	0.0015	0.0218	0.0016
0.936	0.1157	0.0064	0.1880	0.0100	0.0843	0.0049	0.0637	0.0038	0.0011	0.0013	0.0055	0.0013
0.896	0.1075	0.0060	0.1727	0.0092	0.0711	0.0042	0.0575	0.0035			-0.0011	0.0005
0.859	0.1010	0.0057	0.1638	0.0088	0.0571	0.0035	0.0436	0.0028				
0.825	0.0910	0.0052	0.1478	0.0080	0.0440	0.0028	0.0337	0.0023				
0.792	0.0809	0.0047	0.1276	0.0070	0.0319	0.0022	0.0202	0.0017				
0.761	0.0648	0.0038	0.1088	0.0060	0.0128	0.0012	0.0088	0.0013				
0.732	0.0522	0.0032	0.0837	0.0048	0.0017	0.0006	-0.0011	0.0011				
0.705	0.0292	0.0020	0.0501	0.0031	0.0003	0.0011						
0.679	0.0073	0.0013	0.0122	0.0014								
0.655	-0.0017	0.0011	-0.0003	0.0011								

^{238}U γ-ray Production Cross Sections and Absolute Errors

E_n	σ_γ(885.9)		σ_γ(905.1)		σ_γ(966.3)		σ_γ(921.4)		σ_γ(817.9)		σ_γ(952.6)	
4.958	0.0584	0.0074	0.0329	0.0053	0.0224	0.0040	0.0019	0.0035	0.0159	0.0046	0.0295	0.0045
4.496	0.0624	0.0076	0.0334	0.0054	0.0176	0.0039	0.0068	0.0038	0.0178	0.0048	0.0296	0.0045
4.095	0.0639	0.0076	0.0359	0.0054	0.0159	0.0038	0.0167	0.0038	0.0165	0.0046	0.0298	0.0044
3.746	0.0622	0.0073	0.0421	0.0059	0.0169	0.0037	0.0119	0.0037	0.0246	0.0053	0.0333	0.0046
3.440	0.0647	0.0069	0.0326	0.0049	0.0160	0.0033	0.0102	0.0032	0.0208	0.0046	0.0245	0.0038
3.170	0.0689	0.0067	0.0386	0.0052	0.0138	0.0030	0.0083	0.0030	0.0268	0.0052	0.0365	0.0039
2.930	0.0588	0.0061	0.0304	0.0044	0.0127	0.0029	0.0118	0.0029	0.0217	0.0045	0.0319	0.0037
2.717	0.0669	0.0064	0.0357	0.0048	0.0144	0.0028	0.0111	0.0028	0.0210	0.0044	0.0342	0.0037
2.526	0.0558	0.0054	0.0299	0.0040	0.0101	0.0024	0.0083	0.0024	0.0178	0.0038	0.0344	0.0034
2.355	0.0629	0.0055	0.0336	0.0043	0.0128	0.0023	0.0089	0.0023	0.0256	0.0046	0.0396	0.0034
2.200	0.0676	0.0055	0.0327	0.0041	0.0138	0.0022	0.0127	0.0022	0.0272	0.0047	0.0405	0.0032
2.060	0.0686	0.0047	0.0356	0.0042	0.0136	0.0020	0.0099	0.0020	0.0335	0.0055	0.0434	0.0032
1.934	0.0880	0.0073	0.0353	0.0042	0.0151	0.0020	0.0144	0.0021	0.0268	0.0046	0.0486	0.0034
1.818	0.0960	0.0074	0.0408	0.0046	0.0138	0.0019	0.0198	0.0021	0.0354	0.0058	0.0531	0.0035
1.713	0.1066	0.0068	0.0430	0.0048	0.0140	0.0018	0.0199	0.0020	0.0375	0.0060	0.0544	0.0035
1.616	0.1113	0.0071	0.0475	0.0051	0.0138	0.0016	0.0246	0.0021	0.0443	0.0030	0.0529	0.0033
1.528	0.1237	0.0081	0.0481	0.0052	0.0151	0.0016	0.0270	0.0021	0.0457	0.0030	0.0578	0.0035
1.446	0.1390	0.0093	0.0534	0.0057	0.0172	0.0016	0.0282	0.0021	0.0479	0.0031	0.0612	0.0039
1.371	0.1439	0.0090	0.0581	0.0061	0.0158	0.0014	0.0309	0.0021	0.0530	0.0032	0.0654	0.0038
1.302	0.1451	0.0088	0.0524	0.0055	0.0137	0.0011	0.0318	0.0021	0.0507	0.0031	0.0649	0.0037
1.237	0.1479	0.0100	0.0541	0.0056	0.0122	0.0011	0.0337	0.0021	0.0510	0.0030	0.0641	0.0036
1.178	0.1507	0.0091	0.0516	0.0054	0.0117	0.0011	0.0307	0.0020	0.0537	0.0032	0.0569	0.0033
1.122	0.1388	0.0114	0.0435	0.0046	0.0106	0.0010	0.0294	0.0019	0.0489	0.0029	0.0471	0.0028
1.071	0.1297	0.0076	0.0357	0.0038	0.0087	0.0009	0.0237	0.0016	0.0407	0.0025	0.0360	0.0022
1.023	0.1009	0.0059	0.0248	0.0027	0.0070	0.0009	0.0165	0.0013	0.0276	0.0018	0.0176	0.0014
0.978	0.0578	0.0037	0.0114	0.0015	0.0018	0.0007	0.0032	0.0007	0.0073	0.0009	-0.0008	0.0007
0.936	0.0136	0.0018	-0.0002	0.0007	0.0000	0.0006	0.0005	0.0006	-0.0001	0.0007		
0.896	0.0003	0.0009										

^{238}U γ-ray Production Cross Sections and Absolute Errors

E_n	σ_γ(1037.3)	σ_γ(992.4)	σ_γ(888.9)	σ_γ(748.6)	σ_γ(1060.3-60.7)	σ_γ(1014.4-15.3)
4.958				0.0177 0.0041	0.0903 0.0107	0.1760 0.0112
4.496	0.0095 0.0042	0.0048 0.0049		0.0139 0.0041	0.0860 0.0104	0.1795 0.0115
4.095	0.0074 0.0041	0.0068 0.0049		0.0184 0.0041	0.0938 0.0110	0.1868 0.0118
3.746	0.0074 0.0039	0.0121 0.0046		0.0181 0.0040	0.0981 0.0113	0.1725 0.0108
3.440	0.0056 0.0036	0.0000 0.0042		0.0141 0.0035	0.0821 0.0096	0.1545 0.0097
3.170	0.0000 0.0035	0.0079 0.0039		0.0117 0.0033	0.0908 0.0103	0.1567 0.0096
2.930	0.0059 0.0032	0.0009 0.0038		0.0163 0.0032	0.0862 0.0098	0.1483 0.0090
2.717	0.0000 0.0030	0.0013 0.0036		0.0118 0.0030	0.0892 0.0101	0.1657 0.0103
2.526	0.0025 0.0026	0.0104 0.0031		0.0129 0.0027	0.1017 0.0111	0.1610 0.0097
2.355	0.0036 0.0025	0.0097 0.0030		0.0108 0.0025	0.1040 0.0112	0.1714 0.0100
2.200	0.0070 0.0023	0.0064 0.0027		0.0115 0.0024	0.1084 0.0116	0.1711 0.0098
2.060	0.0084 0.0022	0.0096 0.0025		0.0140 0.0023	0.1226 0.0129	0.1777 0.0100
1.934	0.0084 0.0022	0.0124 0.0025	0.0127 0.0061	0.0134 0.0022	0.1251 0.0131	0.1790 0.0100
1.818	0.0154 0.0022	0.0130 0.0024	0.0187 0.0032	0.0153 0.0022	0.1310 0.0136	0.1832 0.0101
1.713	0.0197 0.0022	0.0215 0.0024	0.0181 0.0031	0.0156 0.0020	0.1244 0.0129	0.1836 0.0100
1.616	0.0214 0.0021	0.0205 0.0024	0.0205 0.0032	0.0169 0.0020	0.1164 0.0120	0.1711 0.0089
1.528	0.0257 0.0022	0.0248 0.0023	0.0256 0.0039	0.0160 0.0019	0.1169 0.0121	0.1647 0.0089
1.446	0.0314 0.0023	0.0235 0.0021	0.0313 0.0055	0.0146 0.0017	0.1117 0.0115	0.1594 0.0086
1.371	0.0295 0.0021	0.0259 0.0020	0.0300 0.0039	0.0130 0.0017	0.1056 0.0109	0.1545 0.0083
1.302	0.0280 0.0020	0.0220 0.0017	0.0293 0.0038	0.0099 0.0014	0.0928 0.0095	0.1340 0.0072
1.237	0.0289 0.0020	0.0215 0.0016	0.0332 0.0060	0.0087 0.0013	0.0803 0.0083	0.1131 0.0061
1.178	0.0246 0.0018	0.0194 0.0015	0.0213 0.0034	0.0069 0.0012	0.0609 0.0063	0.0935 0.0051
1.122	0.0176 0.0015	0.0155 0.0014	0.0094 0.0023	0.0040 0.0011	0.0297 0.0032	0.0543 0.0031
1.071	0.0097 0.0011	0.0071 0.0011	0.0087 0.0020	0.0025 0.0010	0.0073 0.0012	0.0145 0.0013
1.023	0.0011 0.0008	0.0010 0.0009	0.0000 0.0016	0.0006 0.0009	0.0005 0.0008	0.0003 0.0008

^{238}U γ-ray Production Cross Sections and Absolute Errors

E_n	σ_γ(911.1-11.9)	σ_γ(957.3)	σ_γ(1083.8)	σ_γ(448.6)	σ_γ(1122.8-24.2)	σ_γ(1019.3-20.7)
4.958	0.0344 0.0054	0.0465 0.0048	0.0350 0.0051	0.0428 0.0061	0.0200 0.0043	0.0542 0.0092
4.496	0.0356 0.0055	0.0483 0.0049	0.0316 0.0049	0.0427 0.0061	0.0237 0.0044	0.0529 0.0090
4.095	0.0380 0.0056	0.0466 0.0047	0.0334 0.0049	0.0434 0.0061	0.0260 0.0044	0.0478 0.0083
3.746	0.0394 0.0056	0.0444 0.0045	0.0310 0.0046	0.0359 0.0054	0.0150 0.0039	0.0469 0.0081
3.440	0.0282 0.0045	0.0379 0.0040	0.0284 0.0042	0.0368 0.0053	0.0130 0.0035	0.0440 0.0075
3.170	0.0295 0.0044	0.0417 0.0039	0.0366 0.0042	0.0398 0.0054	0.0215 0.0035	0.0375 0.0065
2.930	0.0357 0.0048	0.0404 0.0038	0.0380 0.0040	0.0311 0.0046	0.0167 0.0032	0.0383 0.0065
2.717	0.0392 0.0051	0.0469 0.0040	0.0320 0.0038	0.0332 0.0047	0.0237 0.0032	0.0432 0.0072
2.526	0.0380 0.0047	0.0366 0.0033	0.0376 0.0036	0.0325 0.0044	0.0220 0.0029	0.0411 0.0068
2.355	0.0321 0.0041	0.0445 0.0035	0.0361 0.0034	0.0376 0.0047	0.0196 0.0025	0.0443 0.0071
2.200	0.0341 0.0042	0.0456 0.0034	0.0430 0.0034	0.0378 0.0046	0.0235 0.0025	0.0455 0.0072
2.060	0.0313 0.0038	0.0437 0.0032	0.0400 0.0032	0.0401 0.0048	0.0218 0.0024	0.0425 0.0068
1.934	0.0336 0.0040	0.0461 0.0032	0.0406 0.0031	0.0412 0.0048	0.0216 0.0023	0.0429 0.0068
1.818	0.0344 0.0040	0.0469 0.0032	0.0411 0.0031	0.0336 0.0041	0.0199 0.0021	0.0469 0.0074
1.713	0.0321 0.0037	0.0434 0.0029	0.0385 0.0028	0.0367 0.0043	0.0170 0.0019	0.0412 0.0065
1.616	0.0363 0.0041	0.0390 0.0025	0.0378 0.0026	0.0305 0.0036	0.0177 0.0017	0.0404 0.0063
1.528	0.0307 0.0035	0.0377 0.0025	0.0348 0.0024	0.0310 0.0036	0.0159 0.0016	0.0355 0.0056
1.446	0.0295 0.0033	0.0361 0.0024	0.0327 0.0023	0.0310 0.0036	0.0142 0.0015	0.0314 0.0049
1.371	0.0279 0.0031	0.0327 0.0021	0.0324 0.0022	0.0329 0.0037	0.0118 0.0013	0.0276 0.0043
1.302	0.0227 0.0026	0.0250 0.0017	0.0237 0.0017	0.0260 0.0030	0.0075 0.0011	0.0189 0.0030
1.237	0.0199 0.0023	0.0203 0.0015	0.0172 0.0014	0.0189 0.0024	0.0032 0.0014	0.0128 0.0021
1.178	0.0171 0.0020	0.0127 0.0011	0.0081 0.0010	0.0095 0.0017	0.0025 0.0014	0.0056 0.0011
1.122	0.0104 0.0014	0.0043 0.0008	0.0012 0.0008	0.0033 0.0013	0.0009 0.0007	0.0003 0.0007
1.071	0.0024 0.0009	0.0011 0.0007		-0.0013 0.0011		
1.023	0.0007 0.0008					

^{238}U γ-ray Production Cross Sections and Absolute Errors

E_n	σ_γ(1199.8)		σ_γ(1208.3)		σ_γ(1223.9)		σ_γ(1179.0)	
4.958	0.0037	0.0038	0.0120	0.0041	0.0151	0.0042	0.0147	0.0077
4.496	0.0049	0.0039	0.0158	0.0043	0.0169	0.0043	0.0094	0.0079
4.095	0.0018	0.0037	0.0095	0.0039	0.0211	0.0045	0.0156	0.0079
3.746	0.0045	0.0035	0.0187	0.0041	0.0184	0.0041	0.0169	0.0075
3.440	0.0040	0.0031	0.0158	0.0036	0.0175	0.0037	0.0137	0.0067
3.170	0.0063	0.0030	0.0140	0.0034	0.0191	0.0037	0.0143	0.0063
2.930	0.0053	0.0028	0.0124	0.0031	0.0150	0.0032	0.0127	0.0059
2.717	0.0097	0.0026	0.0196	0.0034	0.0261	0.0039	0.0189	0.0056
2.526	0.0097	0.0023	0.0143	0.0028	0.0251	0.0035	0.0167	0.0047
2.355	0.0053	0.0021	0.0174	0.0029	0.0242	0.0034	0.0194	0.0044
2.200	0.0092	0.0020	0.0189	0.0028	0.0259	0.0034	0.0228	0.0040
2.060	0.0072	0.0018	0.0232	0.0030	0.0292	0.0036	0.0260	0.0037
1.934	0.0094	0.0018	0.0228	0.0030	0.0327	0.0038	0.0273	0.0036
1.818	0.0126	0.0016	0.0258	0.0031	0.0327	0.0038	0.0311	0.0034
1.713	0.0120	0.0015	0.0253	0.0030	0.0303	0.0035	0.0289	0.0031
1.616	0.0125	0.0013	0.0261	0.0030	0.0318	0.0035	0.0280	0.0028
1.528	0.0138	0.0012	0.0250	0.0028	0.0276	0.0031	0.0293	0.0027
1.446	0.0136	0.0011	0.0210	0.0024	0.0255	0.0028	0.0240	0.0025
1.371	0.0108	0.0010	0.0149	0.0018	0.0203	0.0023	0.0205	0.0023
1.302	0.0055	0.0008	0.0091	0.0012	0.0105	0.0013	0.0123	0.0020
1.237	0.0013	0.0006	0.0044	0.0008	0.0044	0.0008	0.0038	0.0019
1.178	0.0002	0.0006	0.0005	0.0006	0.0004	0.0006	0.0014	0.0019

APPENDIX B

This appendix contains figures of the measured gamma-ray pulse-height spectra collapsed over several 36-nsec wide, incident-neutron energy bins. Figures B1 to B5 show spectra produced by incident neutrons from 0.67 to 1.00, 1.00 to 1.21, 1.21 to 1.49, 1.49 to 2.00, and 2.00 to 4.30 MeV, which are the sums of 10, 4, 4, 5, and 10 data collection bins, respectively. In addition, to allow plotting, the pulse-height channels which span gamma-ray energies from 0.20 to 1.80 MeV have been averaged by a factor of two. Figures B6 to B25 show Figs. B1 to B5 expanded by at least four with unaveraged pulse-height channels. In particular, Figs. B6 to B10 show spectra for 0.2 to 0.6 MeV gamma rays, Figs. B11 to B15 for 0.6 to 1.0 MeV gamma rays, etc. No gamma-ray energies are shown but can be obtained from the energy scales where each small tick mark spans 5.0 keV which is $\sim$ 5 channels.

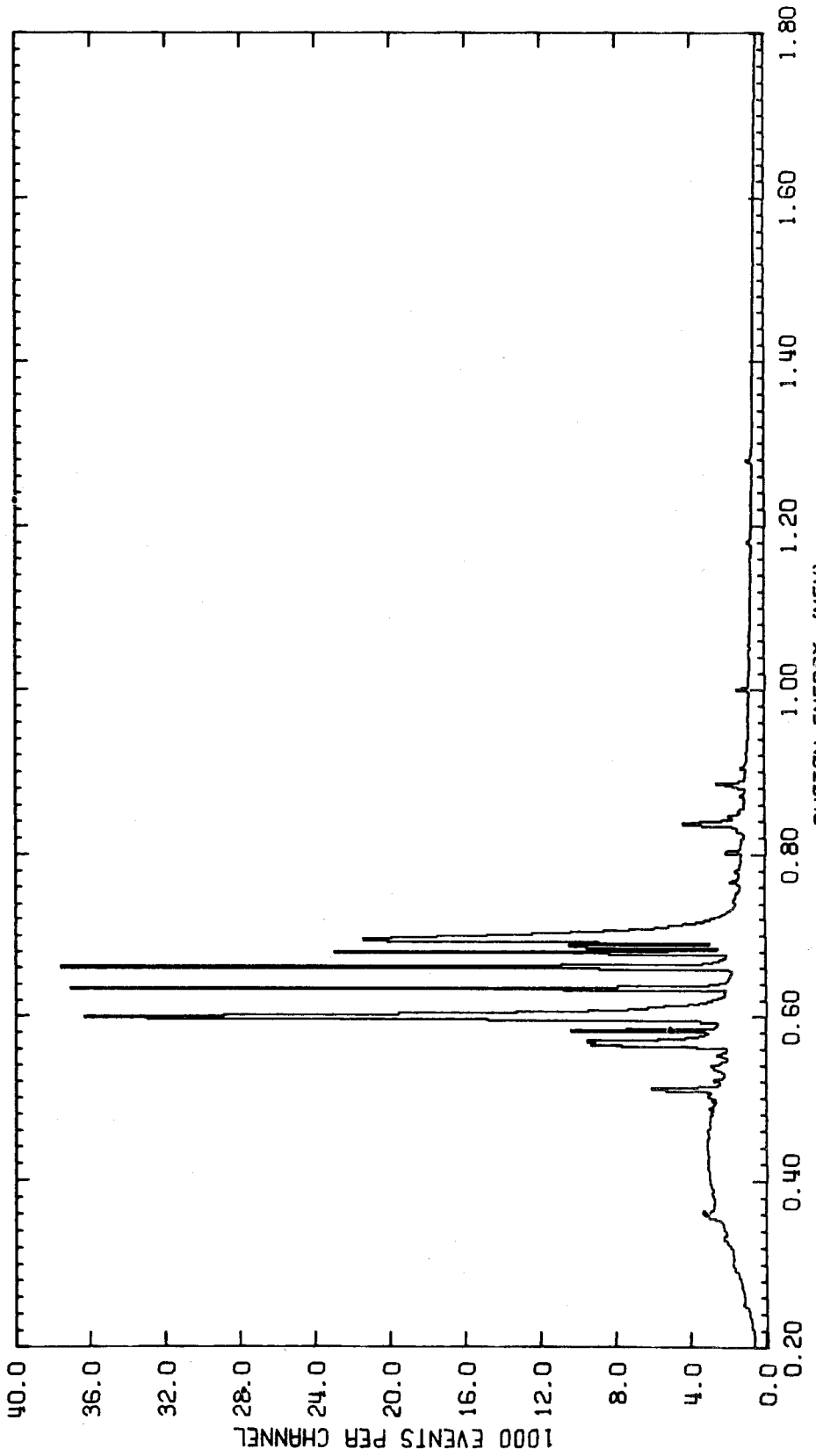

Fig. B1. Gamma-ray spectrum from 0.67 to 1.00-MeV incident neutrons.

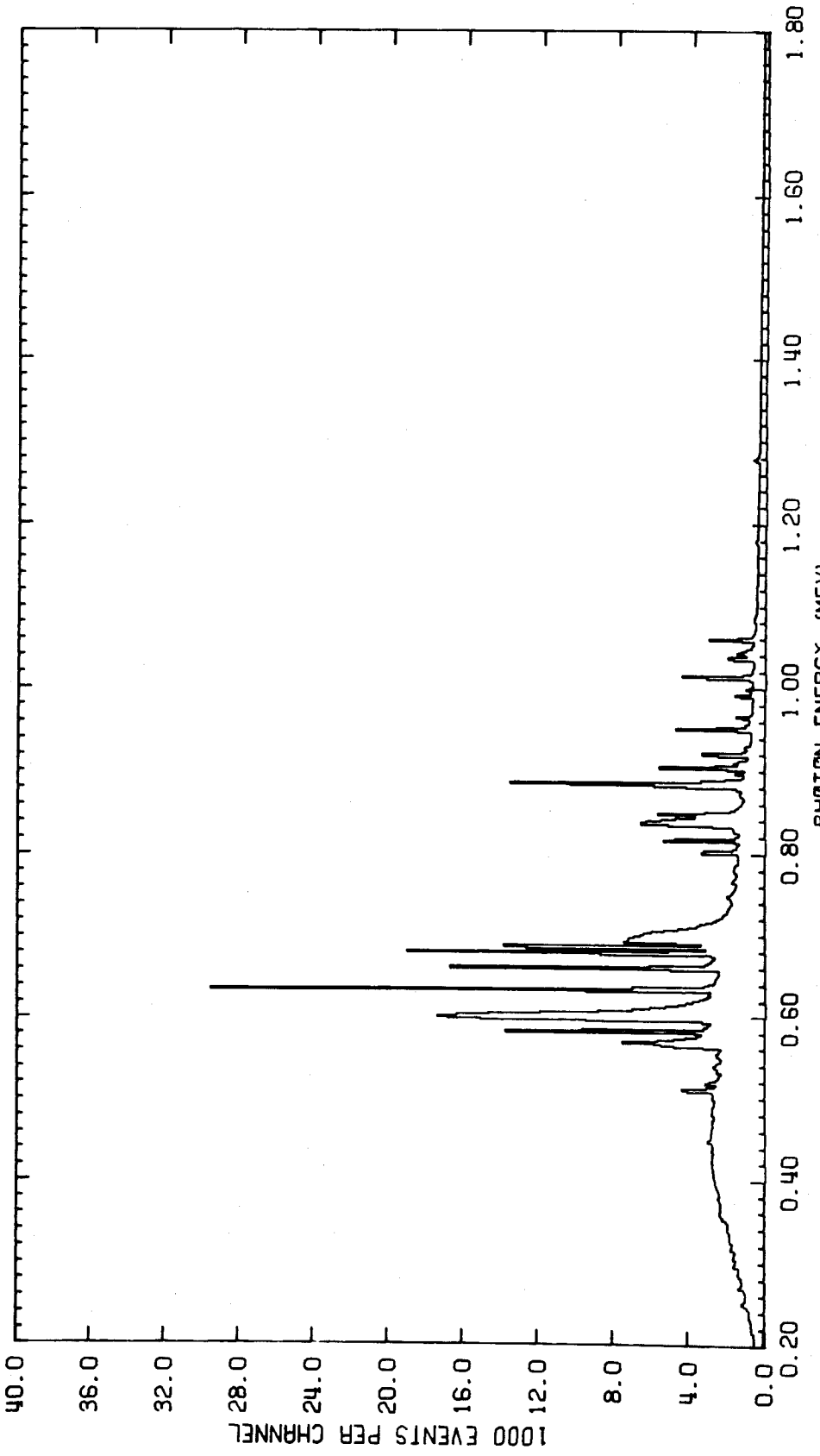

Fig. B2. Gamma-ray spectrum from 1.00 to 1.21-MeV incident neutrons.

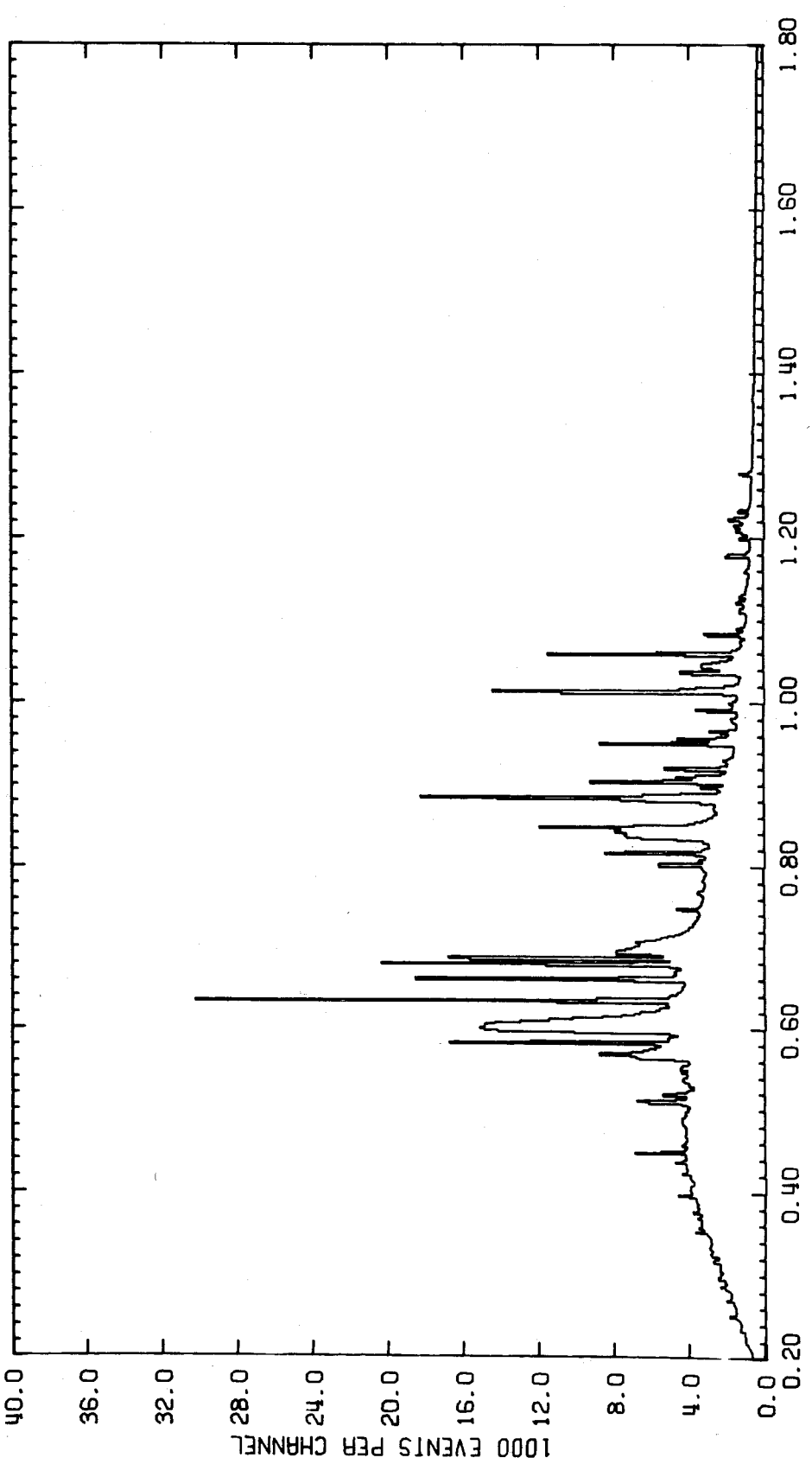

Fig. B3. Gamma-ray spectrum from 1.21 to 1.49-MeV incident neutrons.

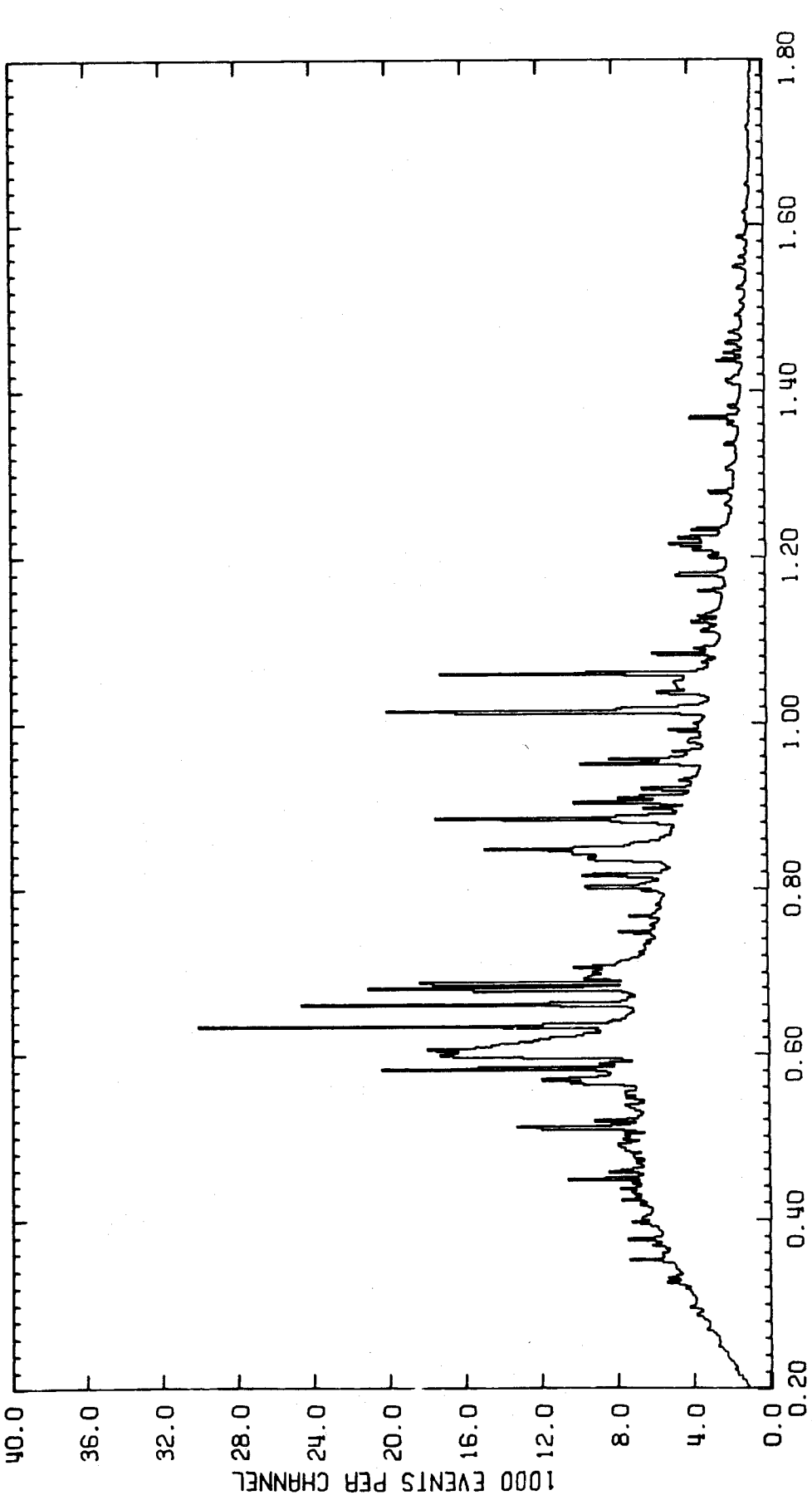

Fig. B4. Gamma-ray spectrum from 1.49 to 2.00-MeV incident neutrons.

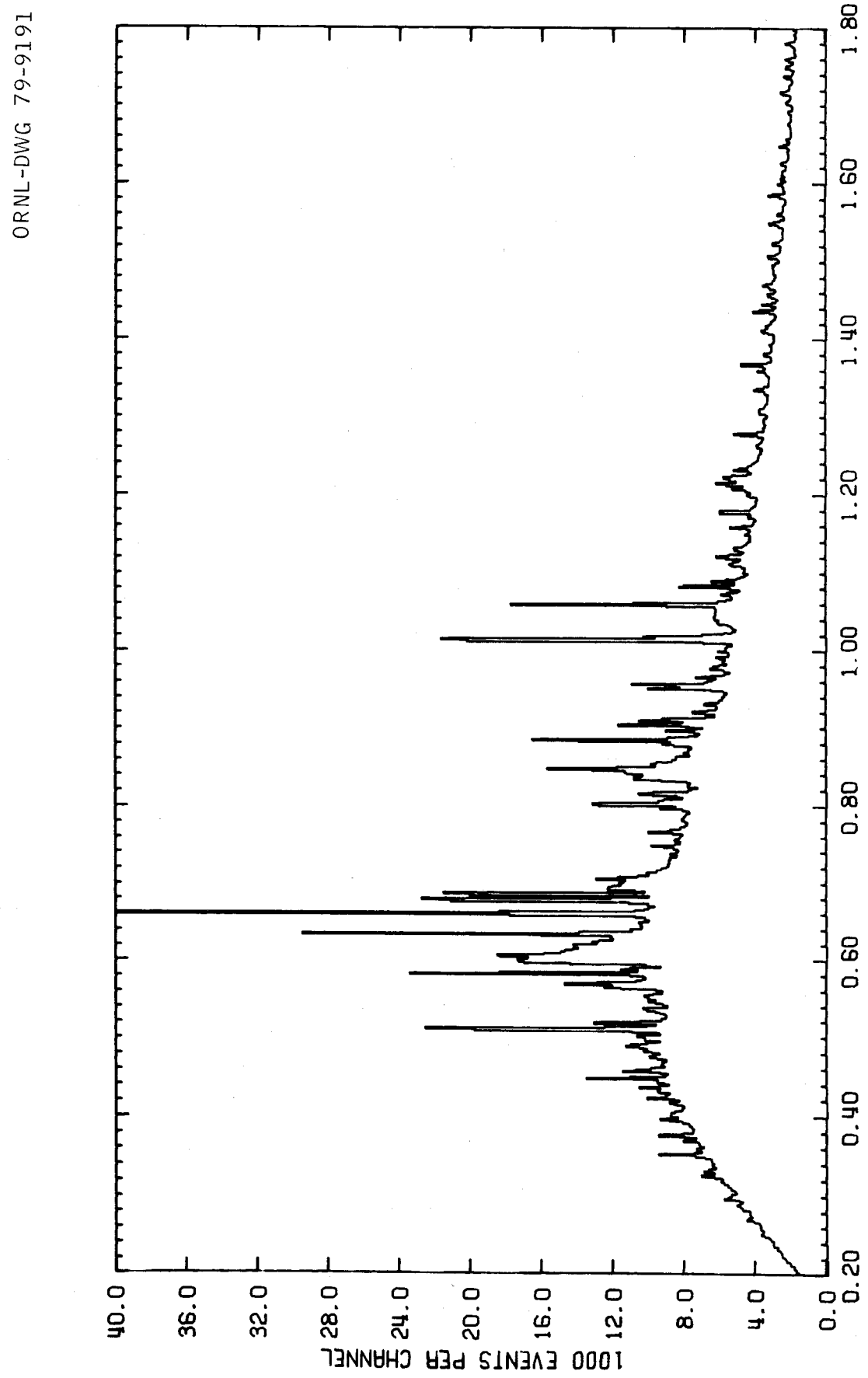

Fig. B5. Gamma-ray spectrum from 2.00 to 4.30-MeV incident neutrons.

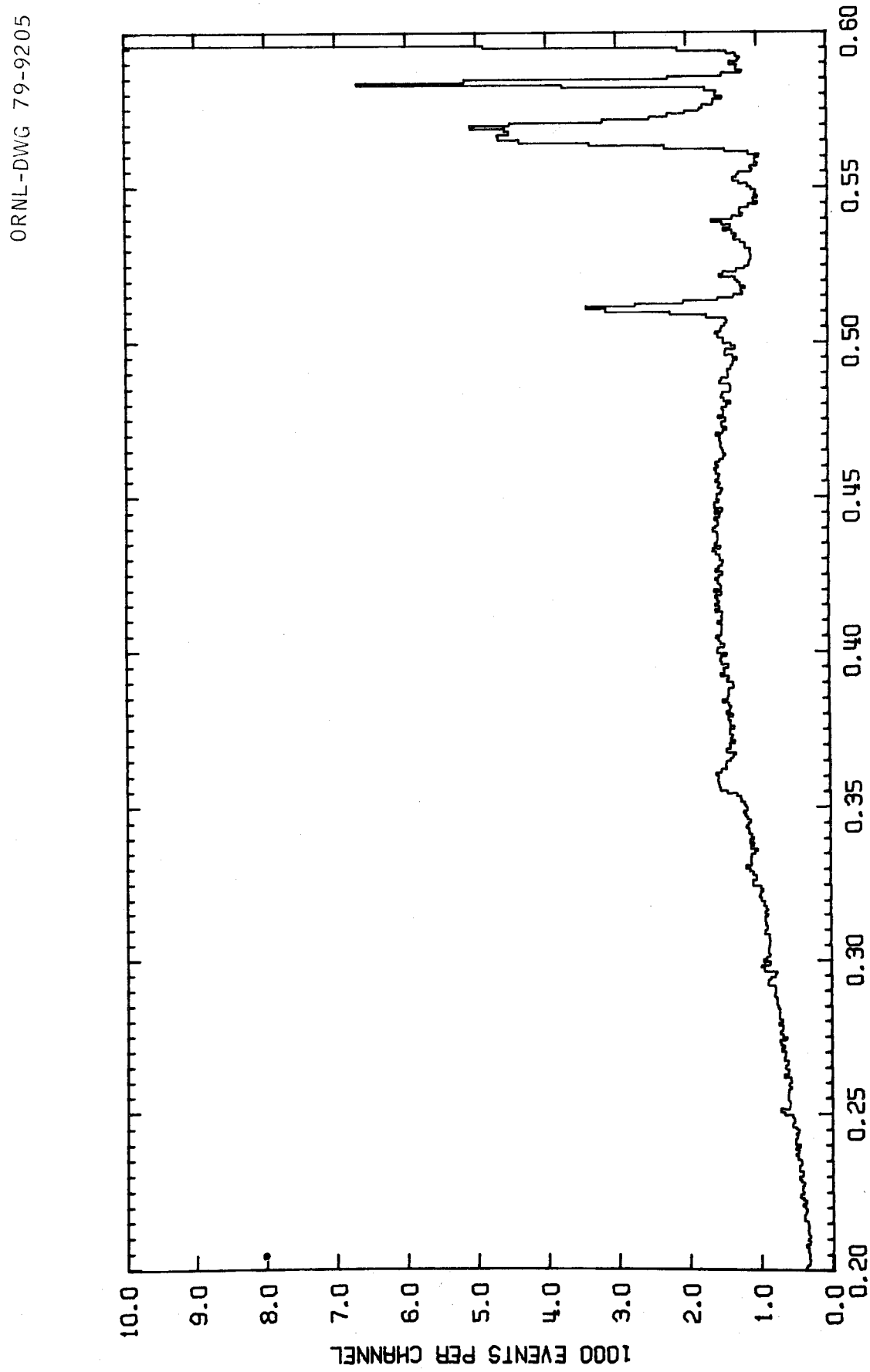

Fig. B6. Gamma-ray spectrum from 0.67 to 1.00-MeV incident neutrons.

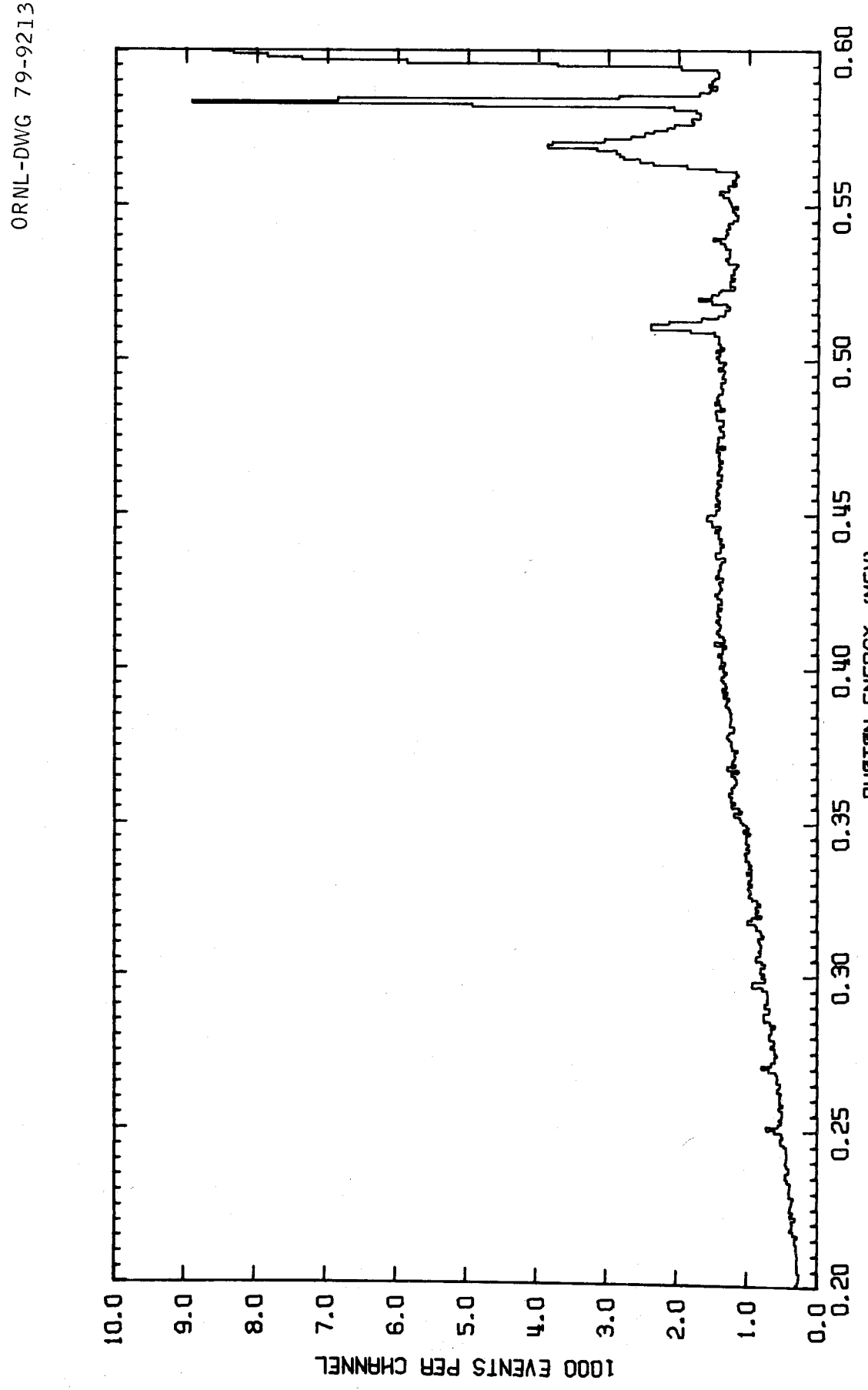

Fig. B7. Gamma-ray spectrum from 1.00 to 1.21-MeV incident neutrons.

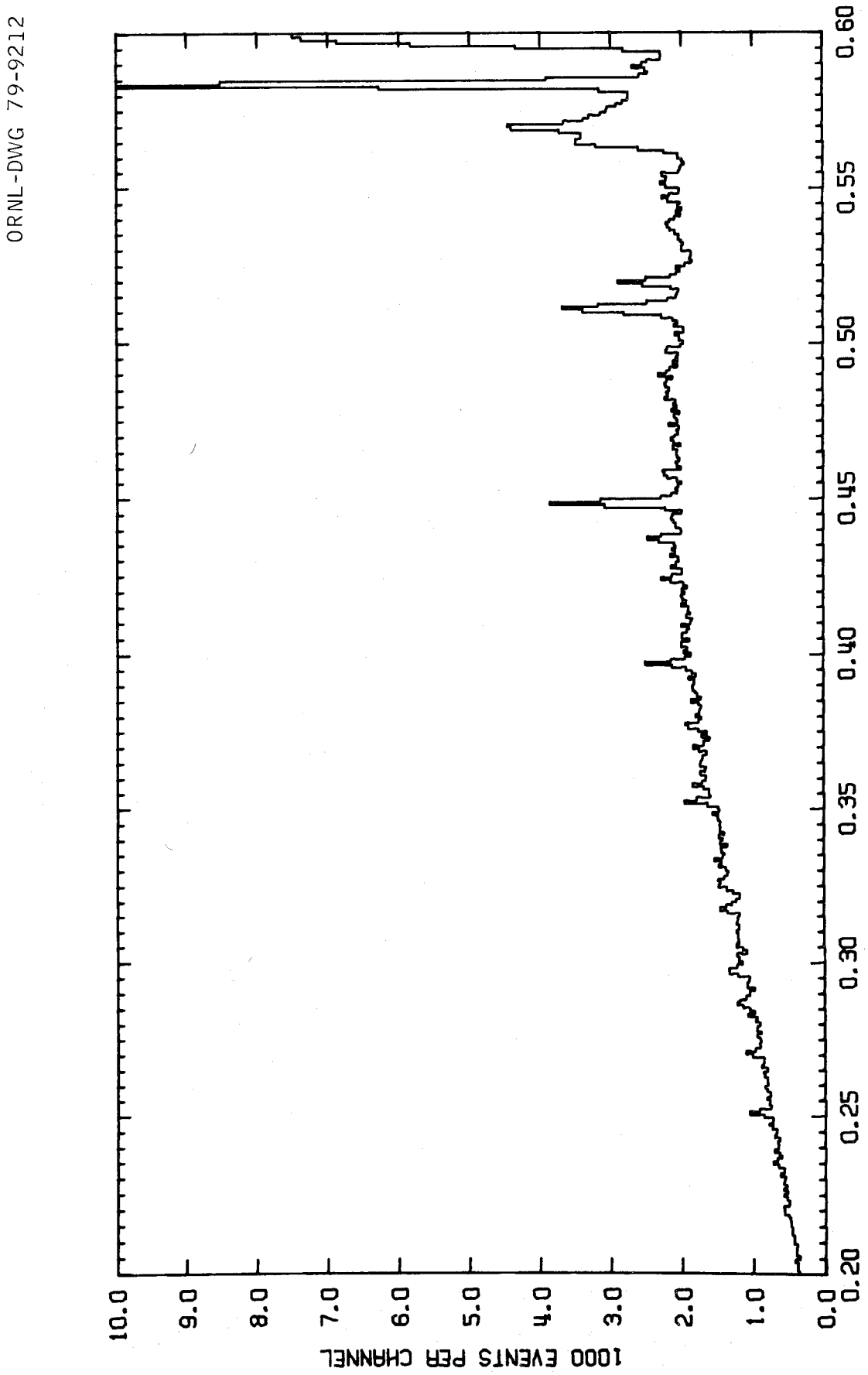

Fig. B8. Gamma-ray spectrum from 1.21 to 1.49-MeV incident neutrons.

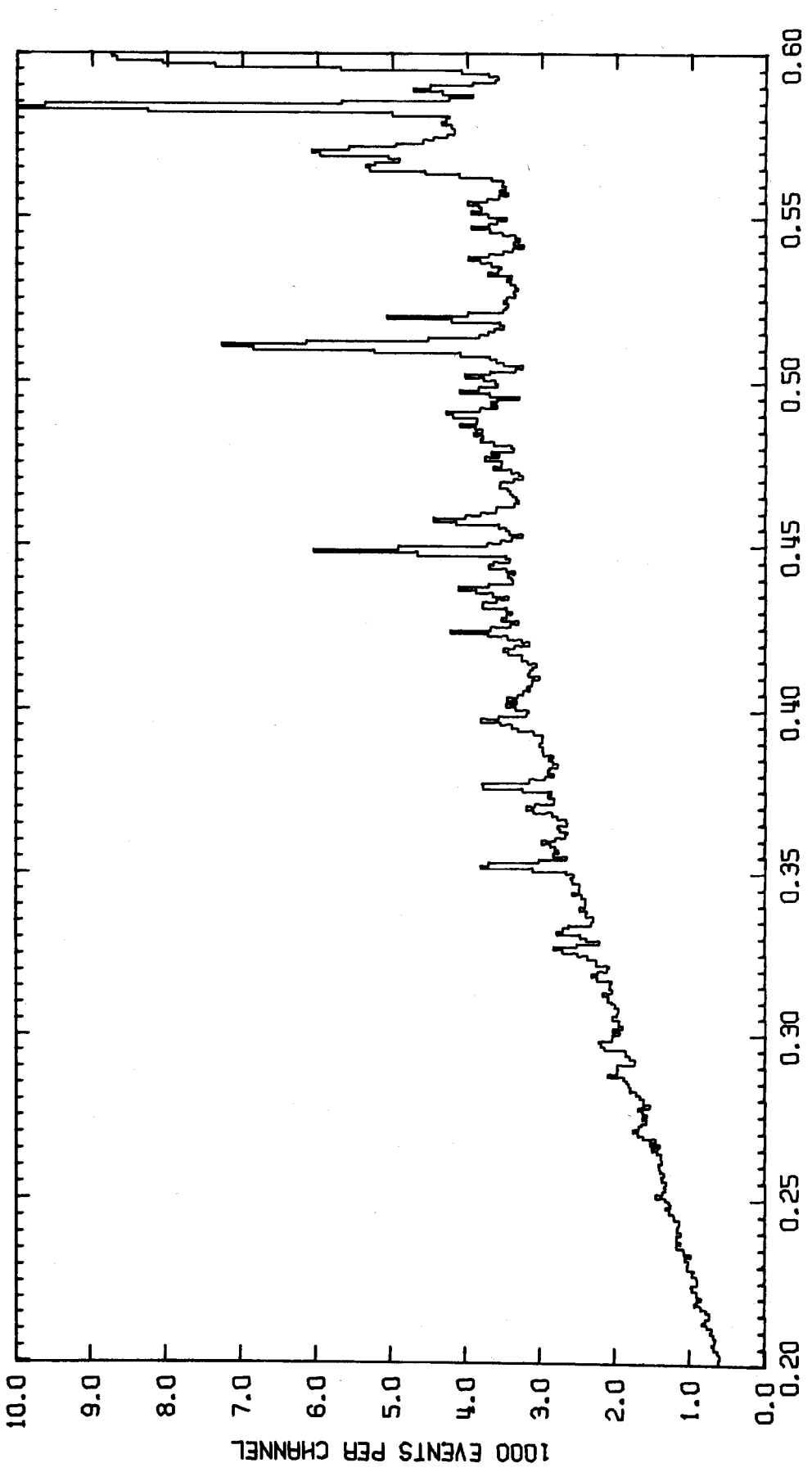

Fig. B9. Gamma-ray spectrum from 1.49 to 2.00-MeV incident neutrons.

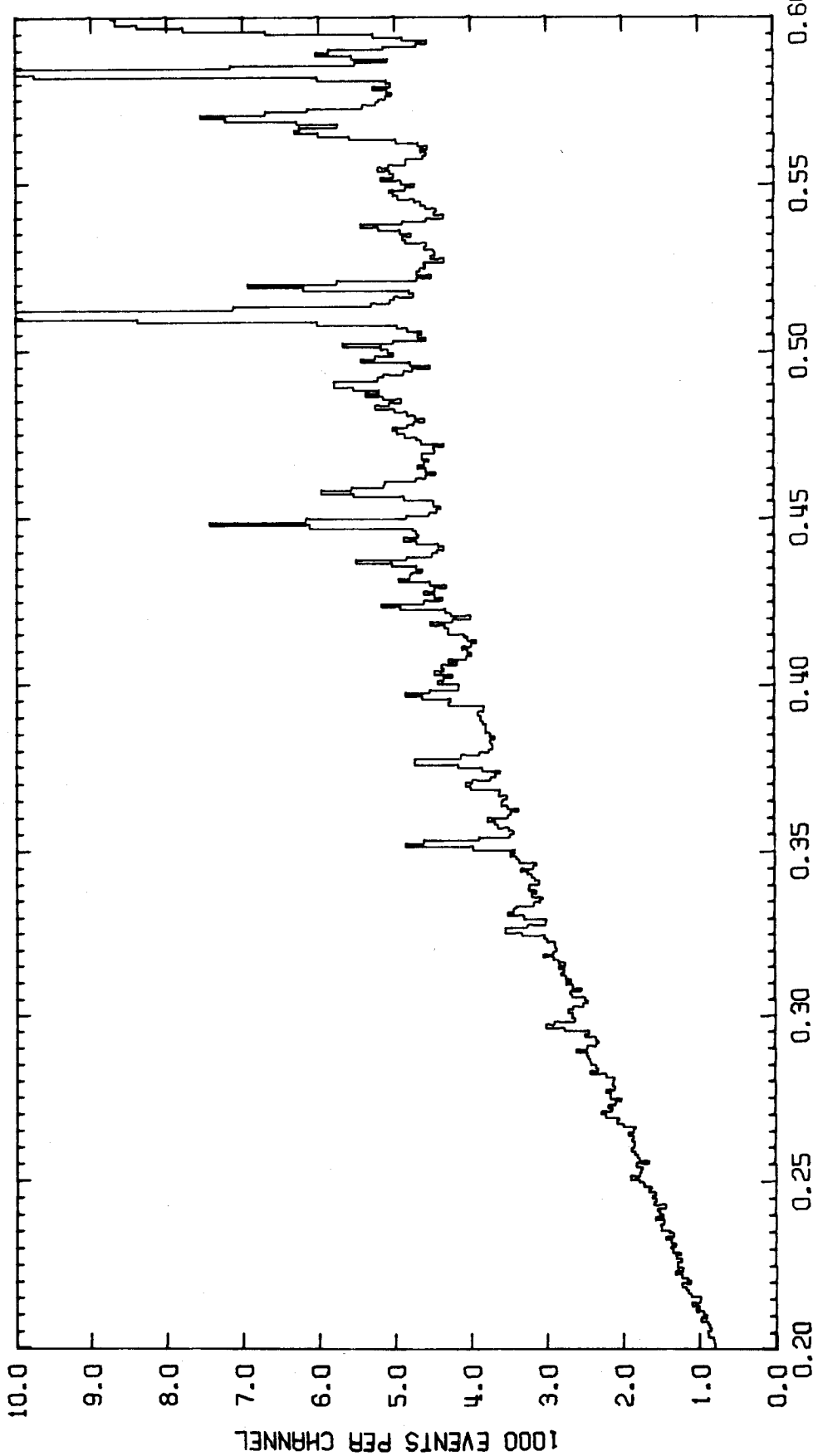

Fig. B10. Gamma-ray spectrum from 2.00 to 4.30-MeV incident neutrons.

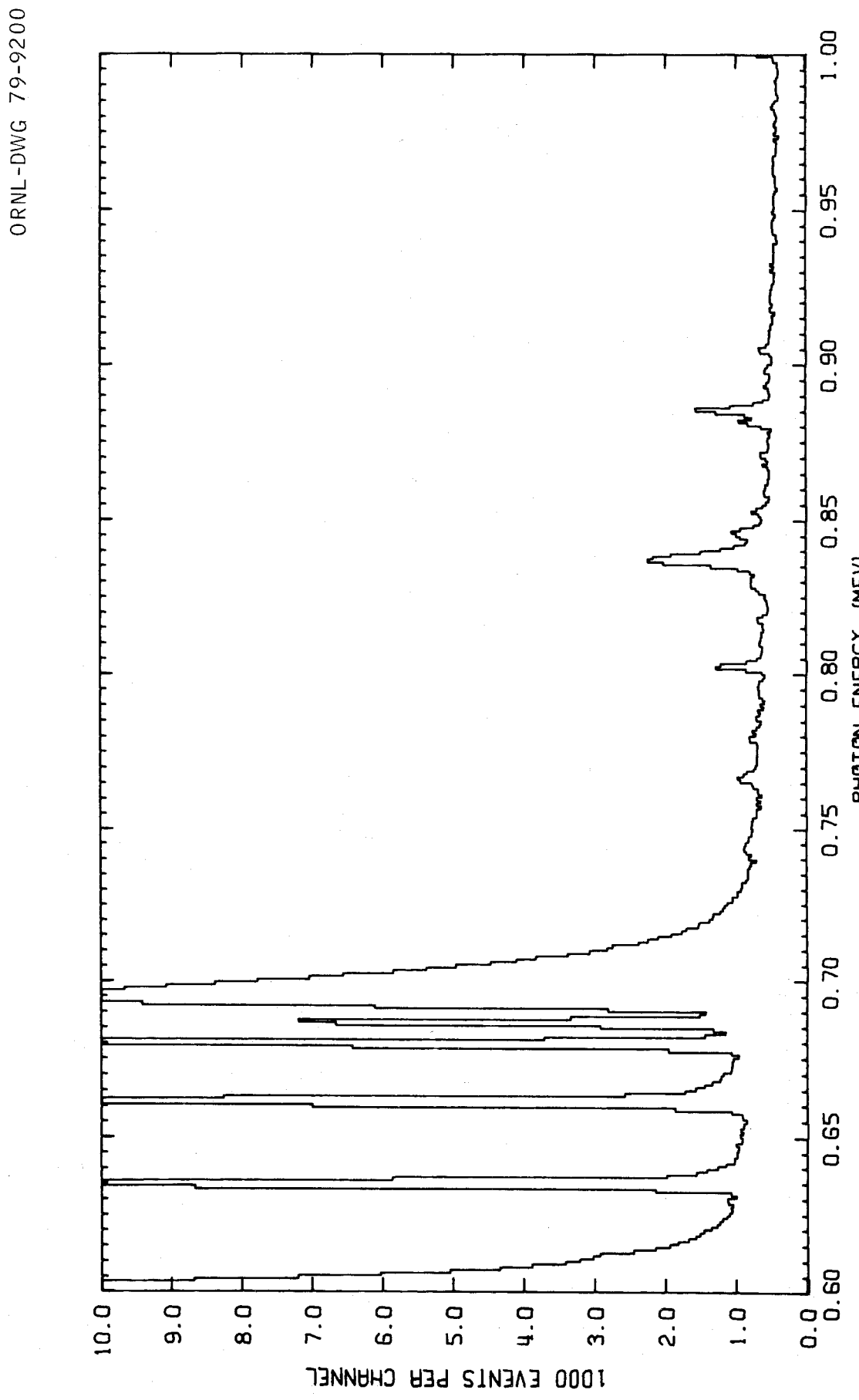

Fig. B11. Gamma-ray spectrum from 0.67 to 1.00-MeV incident neutrons.

ORNL-DWG 79-9198

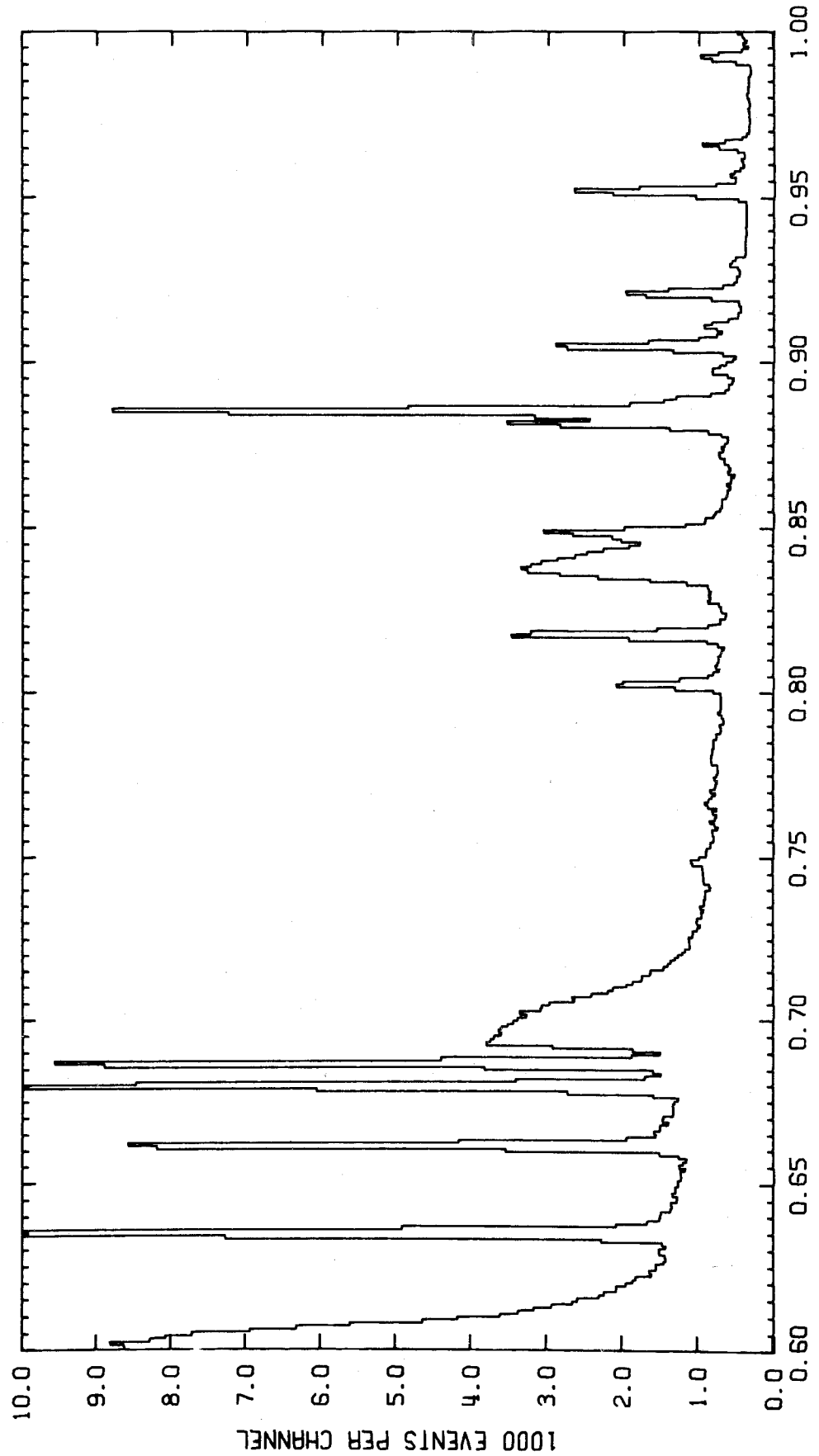

Fig. B12. Gamma-ray spectrum from 1.00 to 1.21-MeV incident neutrons.

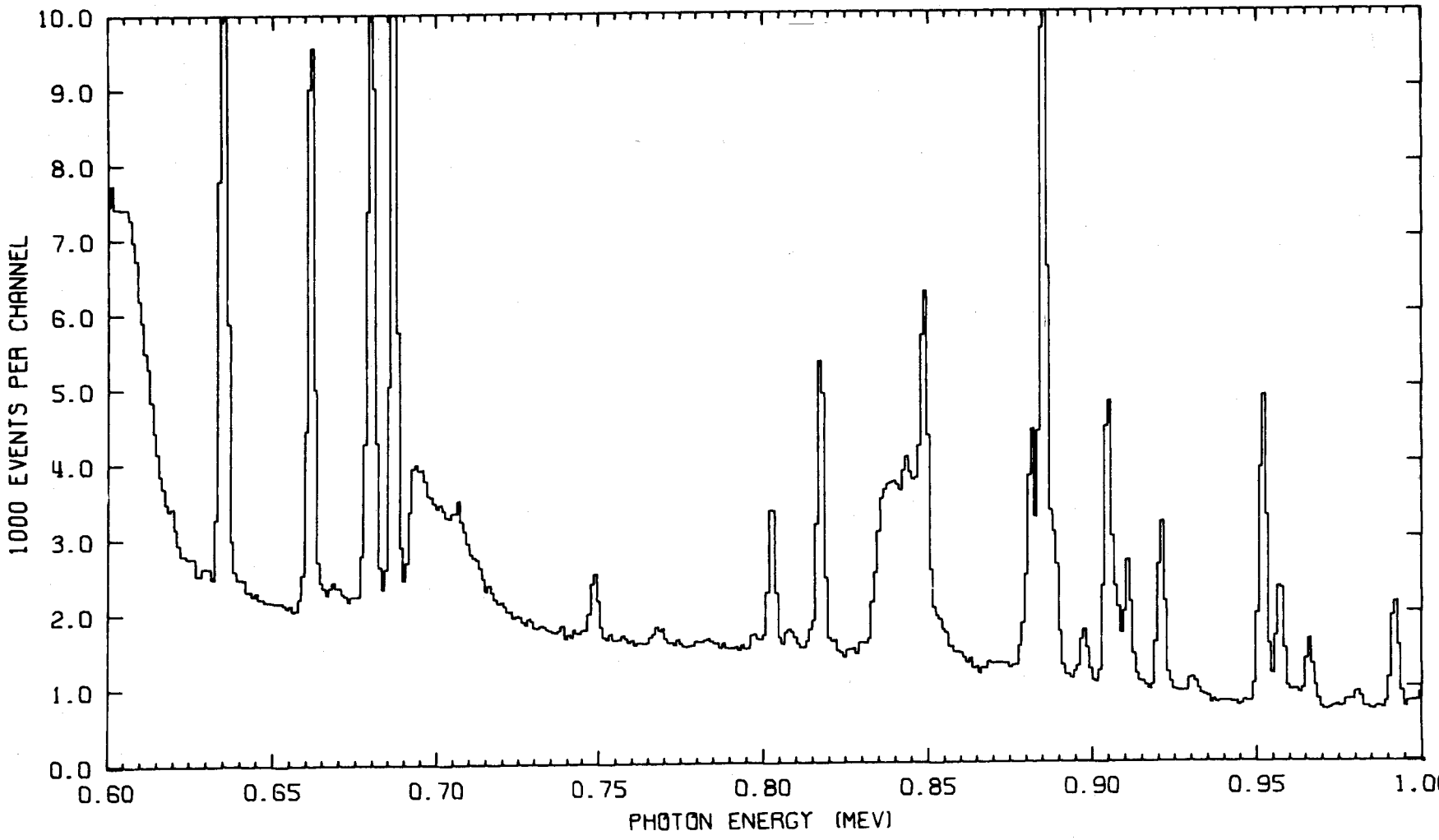

Fig. B13. Gamma-ray spectrum from 1.21 to 1.49-MeV incident neutrons.

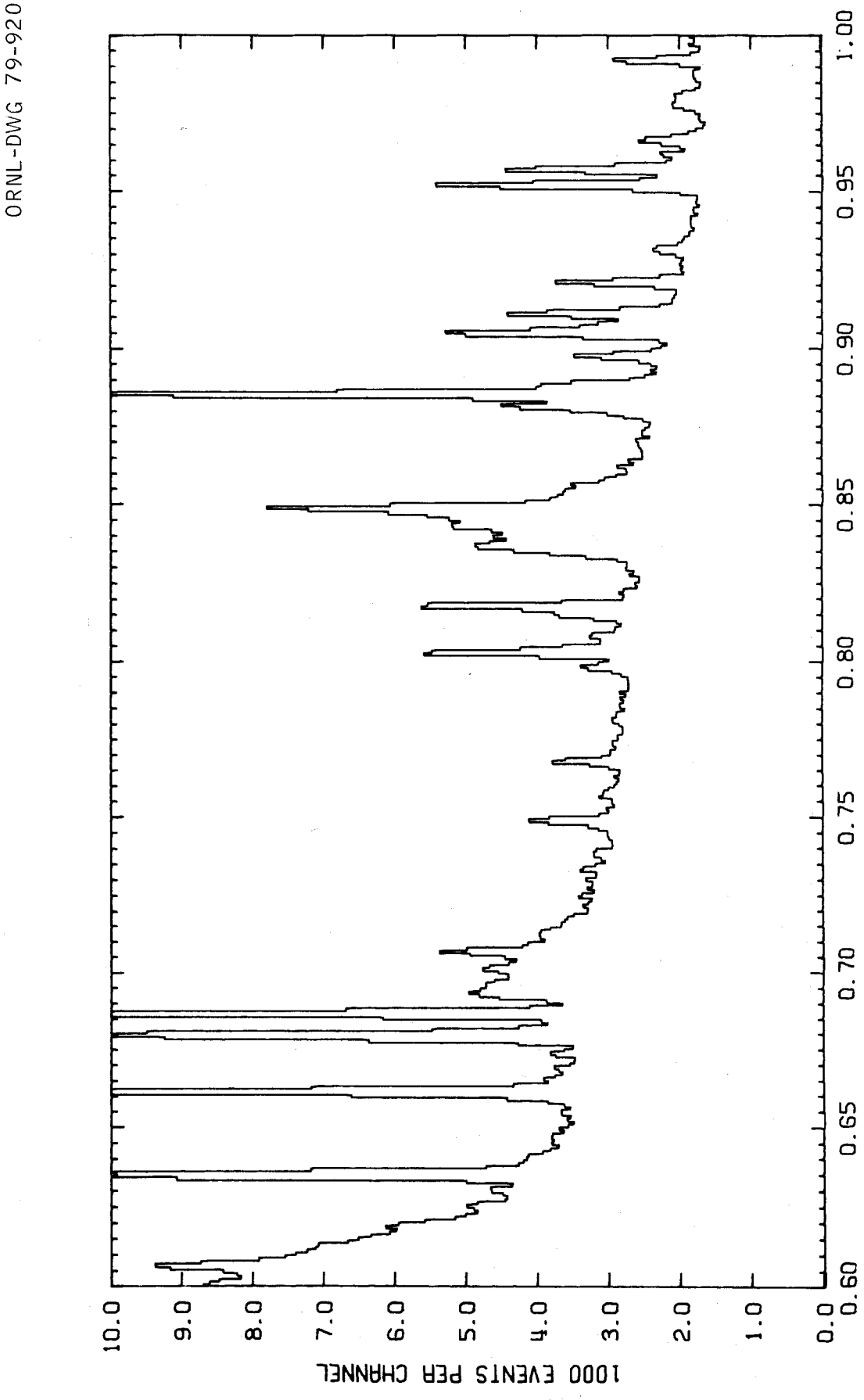

Fig. B14. Gamma-ray spectrum from 1.49 to 2.00-MeV incident neutrons.

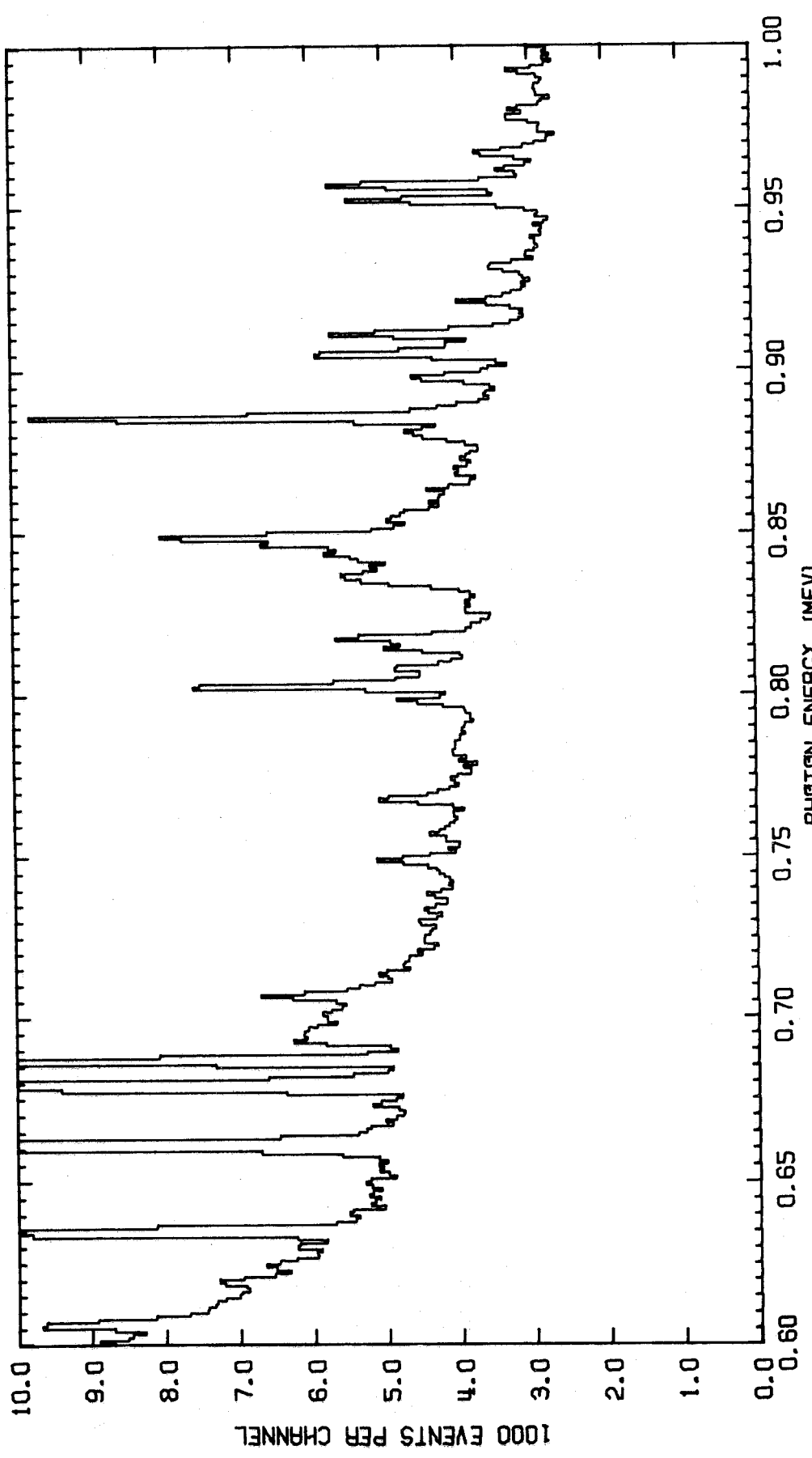

Fig. B15. Gamma-ray spectrum from 2.00 to 4.30-MeV incident neutrons.

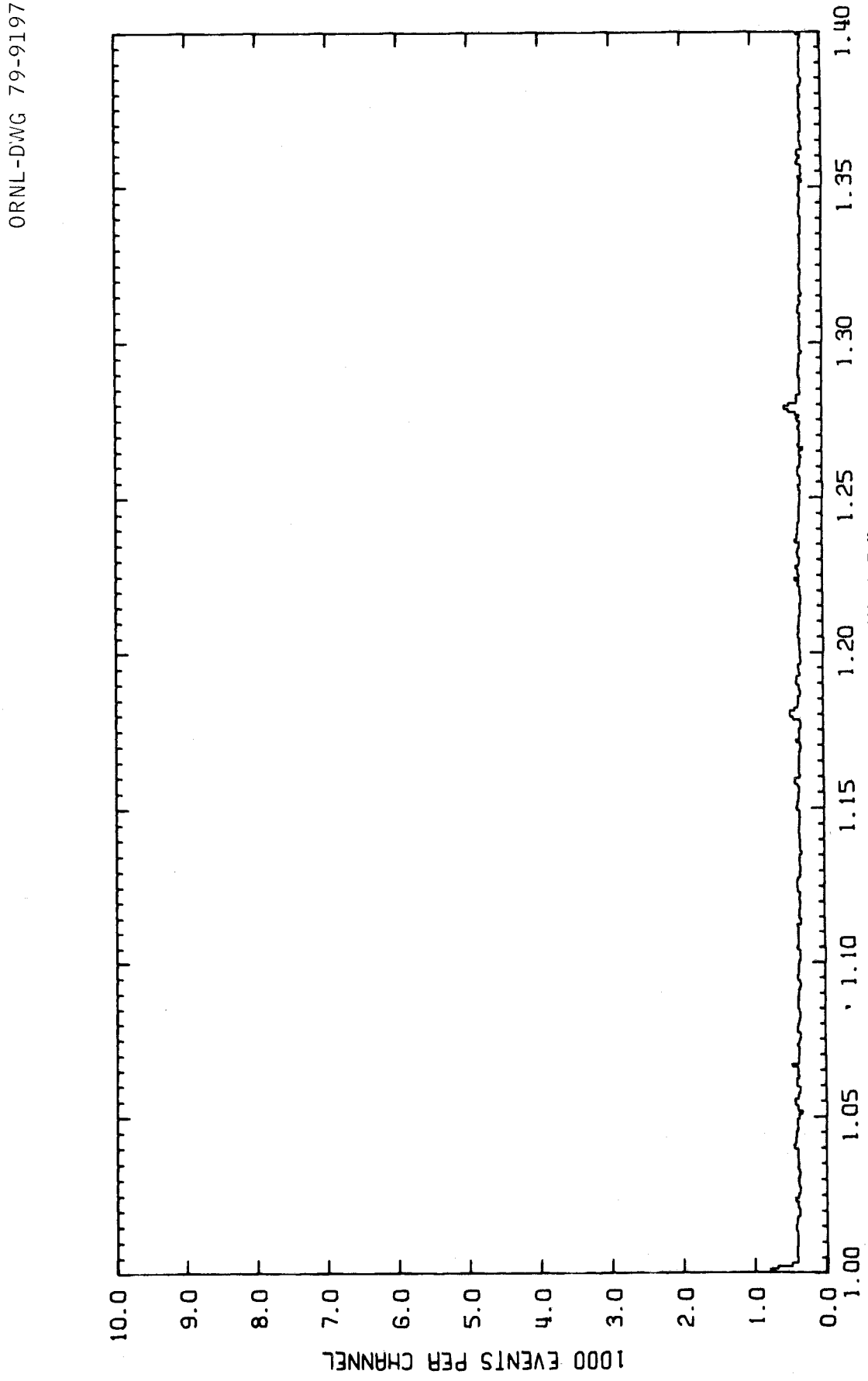

Fig. B16. Gamma-ray spectrum from 0.67 to 1.00-MeV incident neutrons.

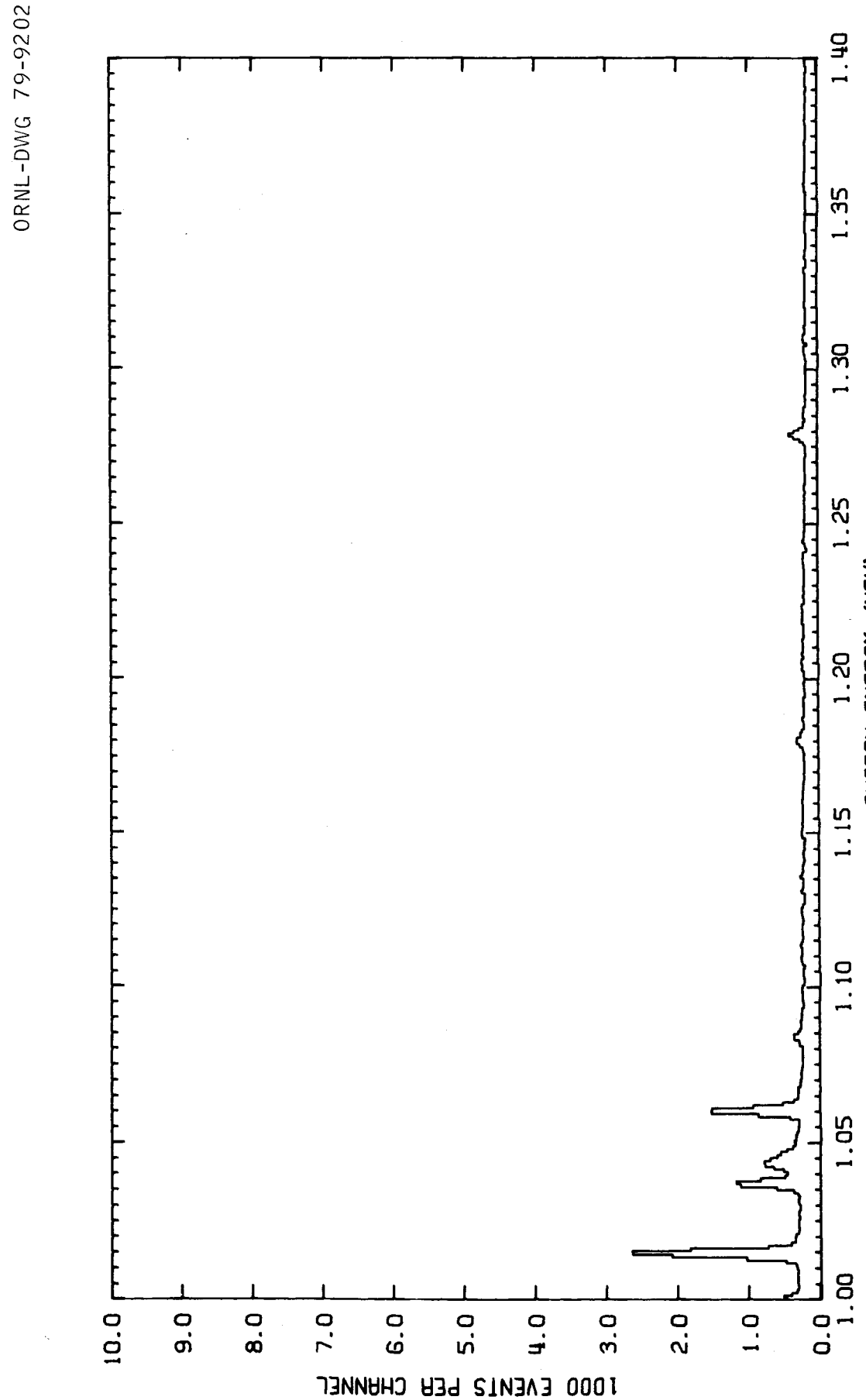

Fig. B17. Gamma-ray spectrum from 1.00 to 1.21-MeV incident neutrons.

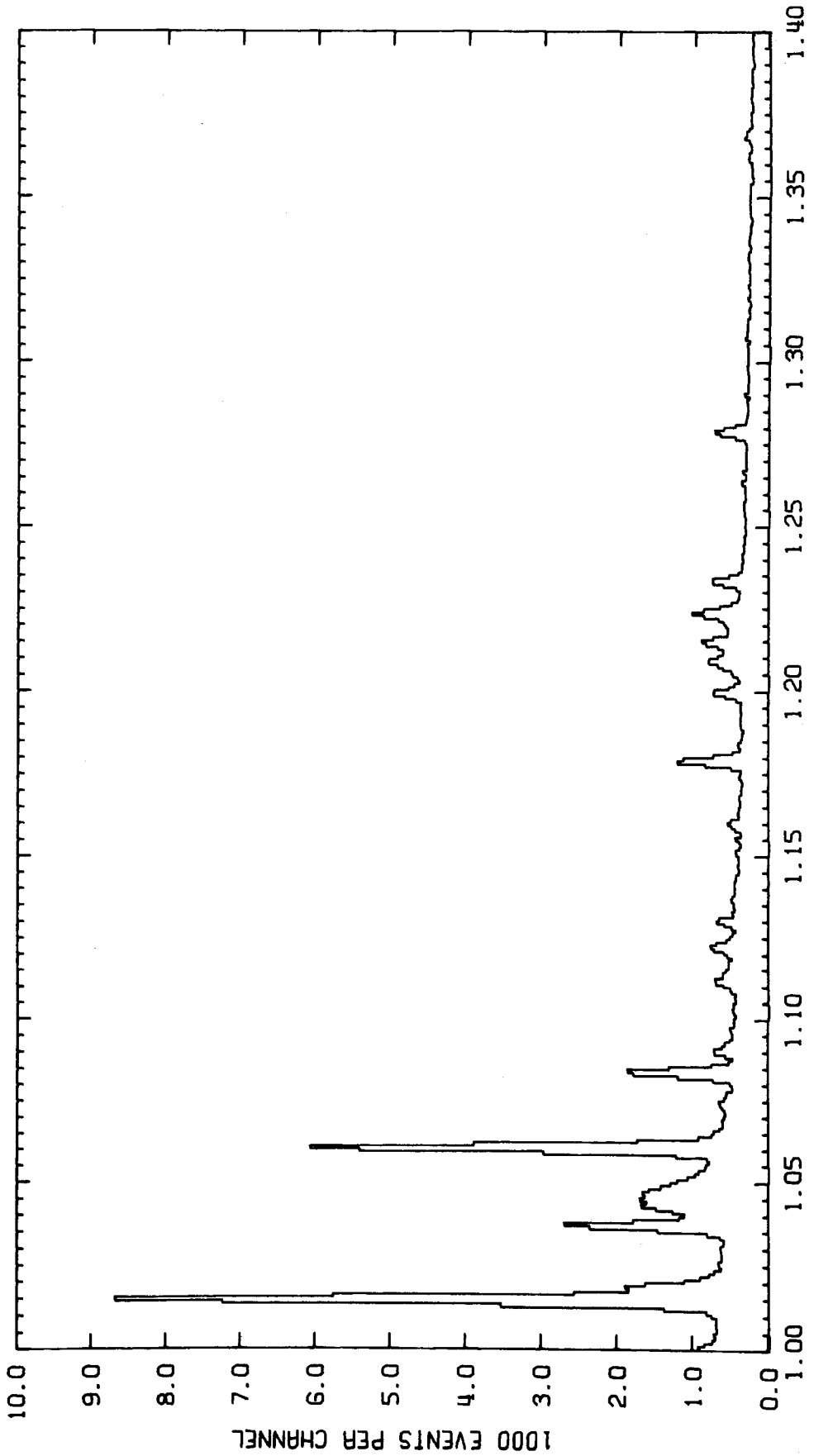

Fig. B18. Gamma-ray spectrum from 1.21 to 1.49-MeV incident neutrons.

ORNL-DWG 79-9211

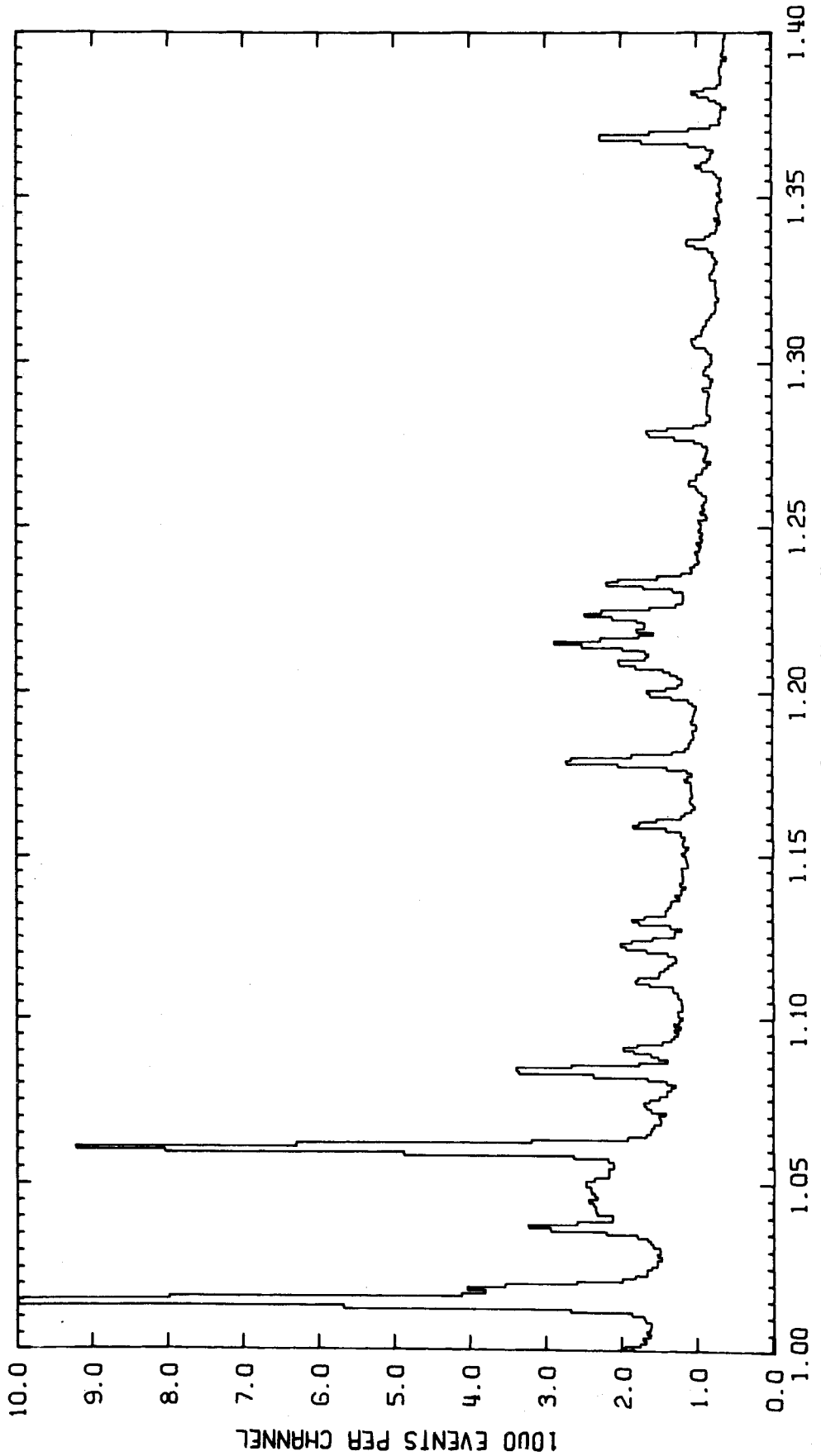

Fig. B19. Gamma-ray spectrum from 1.49 to 2.00-MeV incident neutrons.

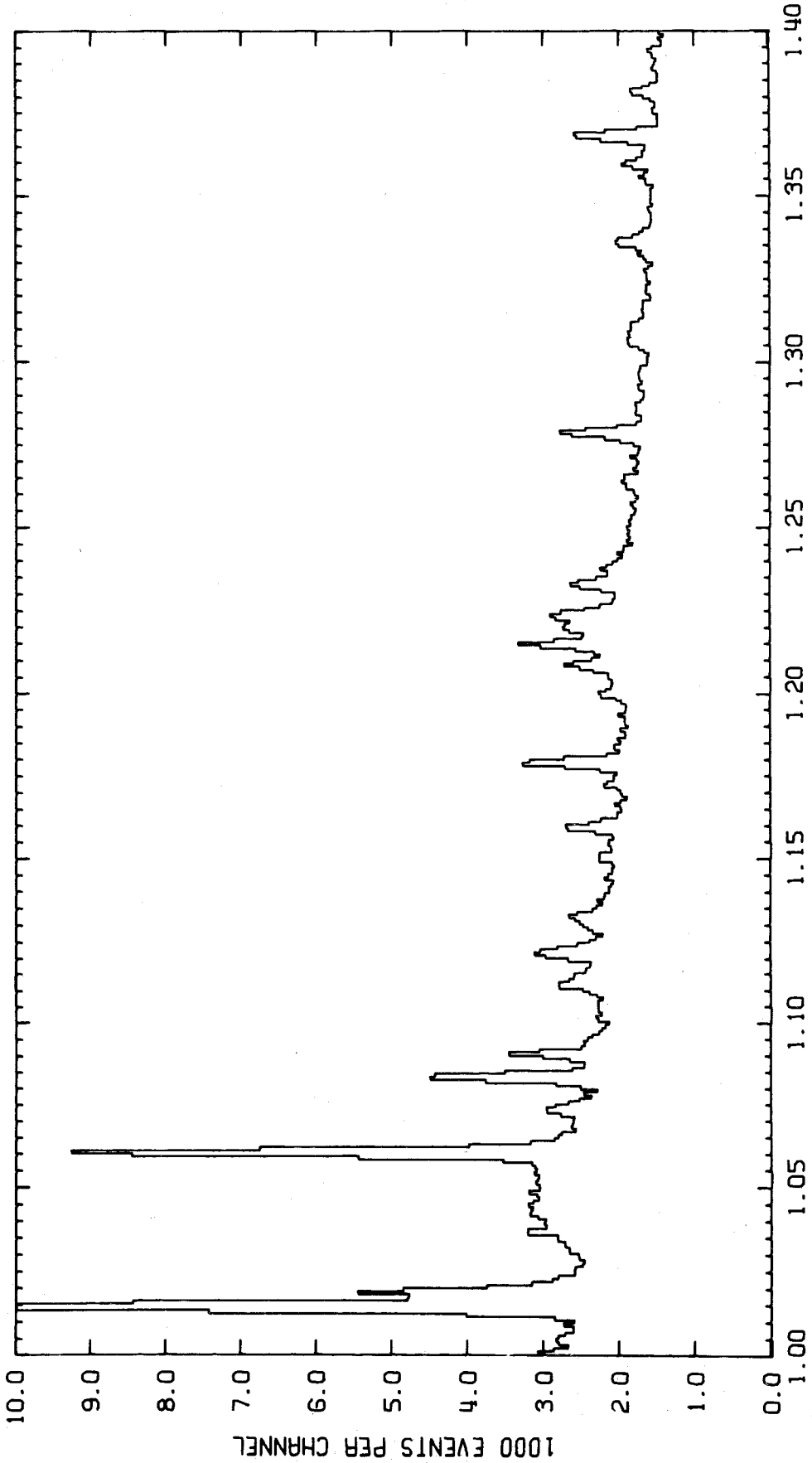

Fig. B20. Gamma-ray spectrum from 2.00 to 4.30-MeV incident neutrons.

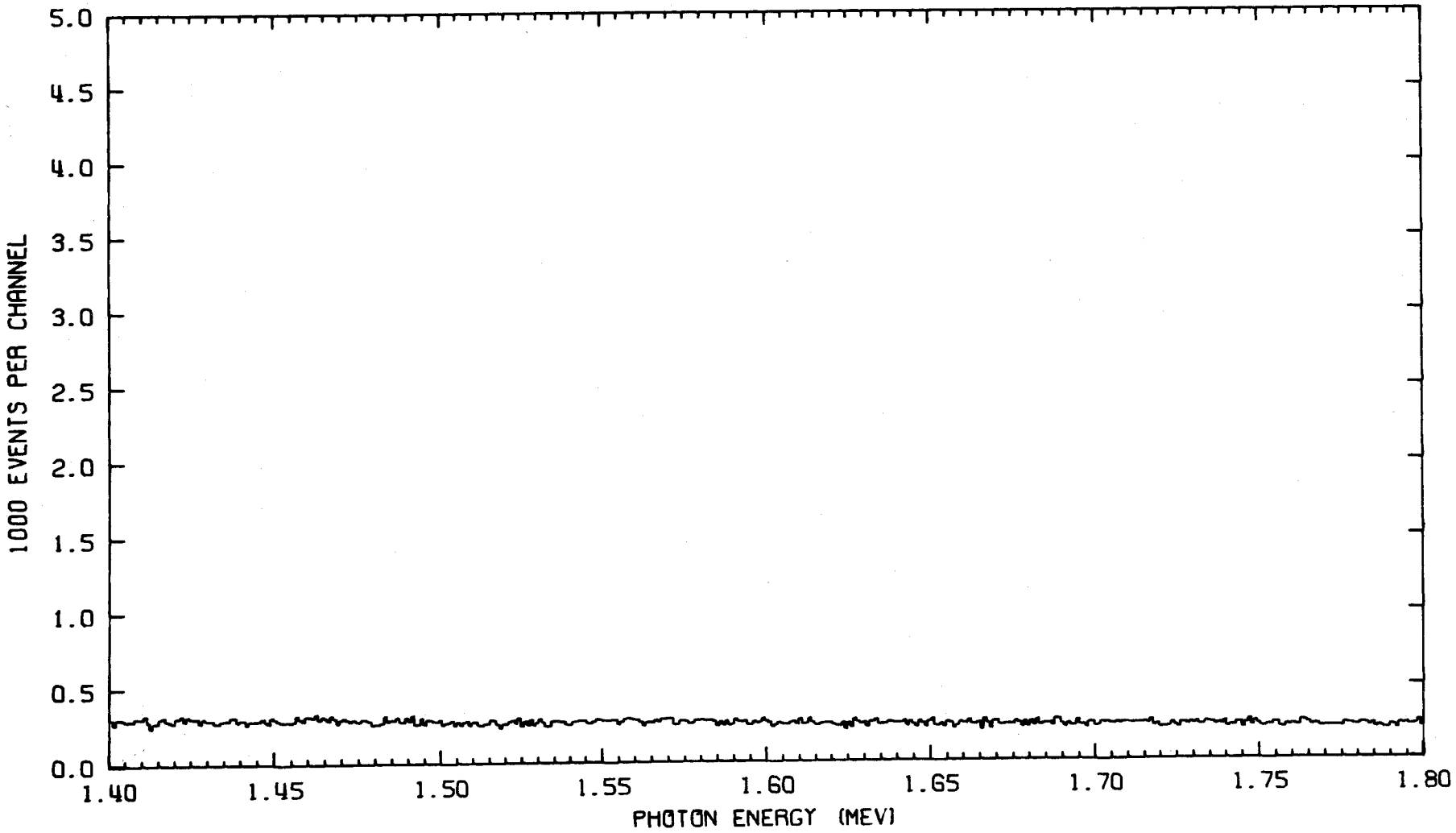

Fig. B21. Gamma-ray spectrum from 0.67 to 1.00-MeV incident neutrons.

ORNL-DWG 79-9214

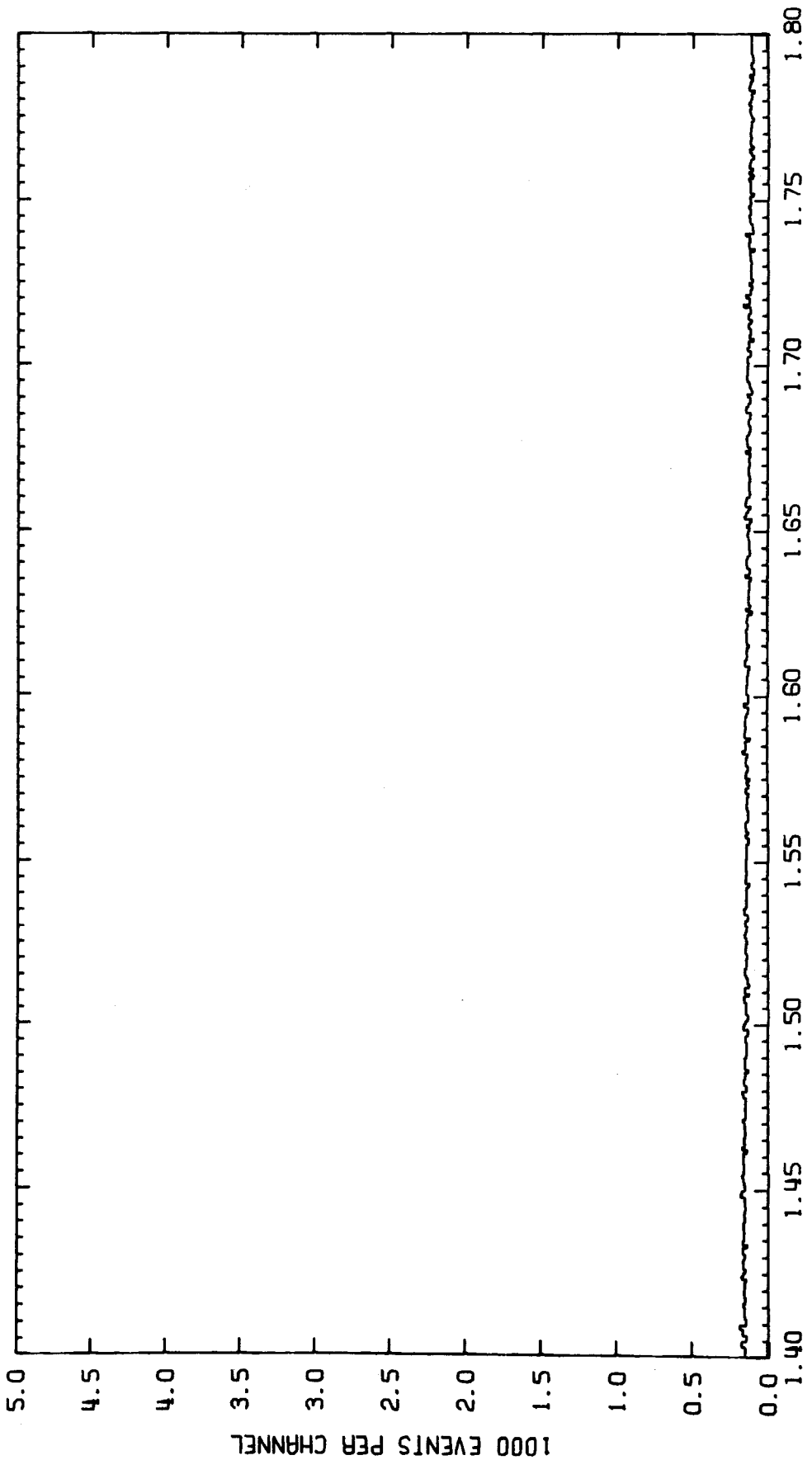

Fig. B22. Gamma-ray spectrum from 1.00 to 1.21-MeV incident neutrons.

ORNL-DWG 79-9203

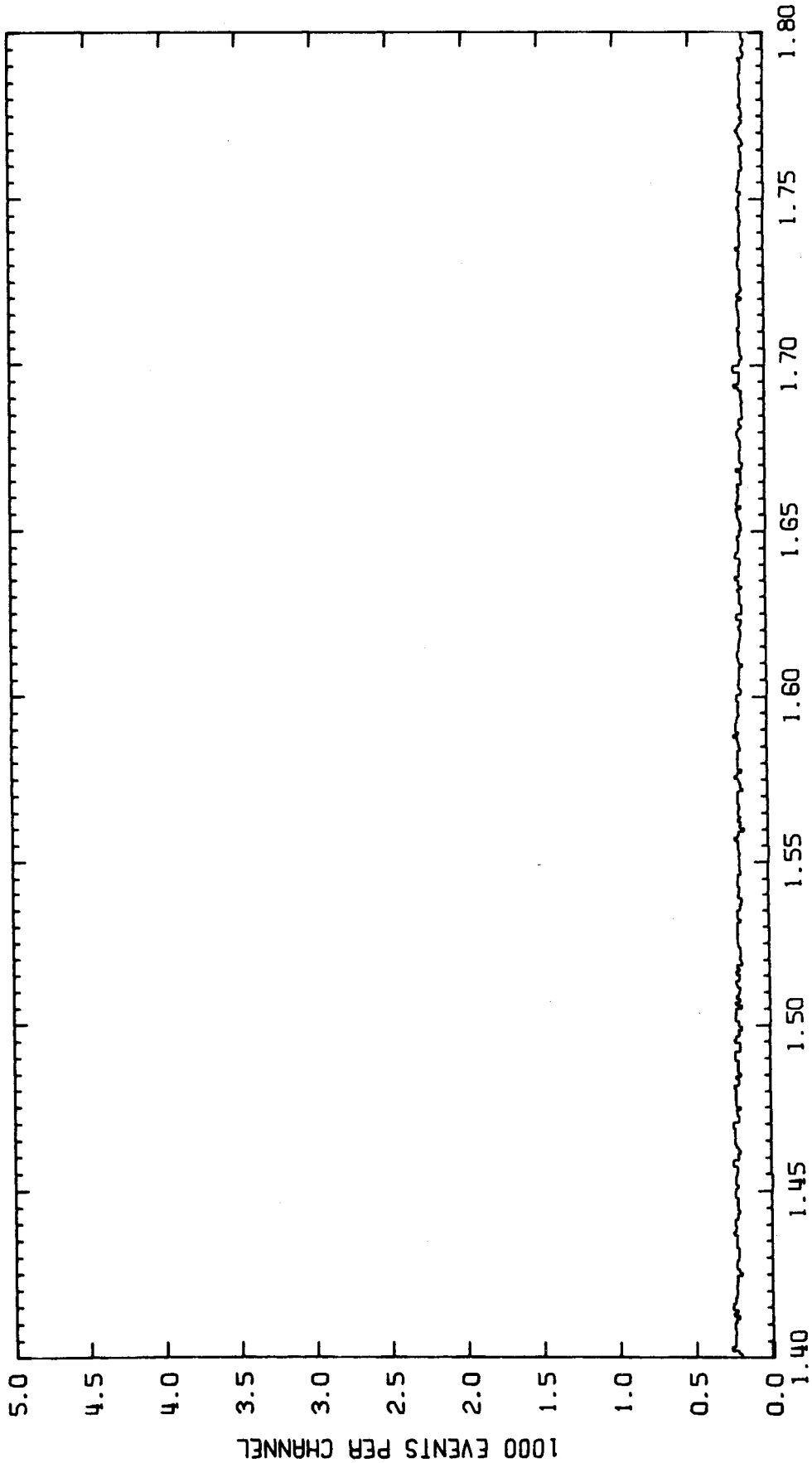

Fig. B23. Gamma-ray spectrum from 1.21 to 1.49-MeV incident neutrons.

ORNL-DWG 79-9204

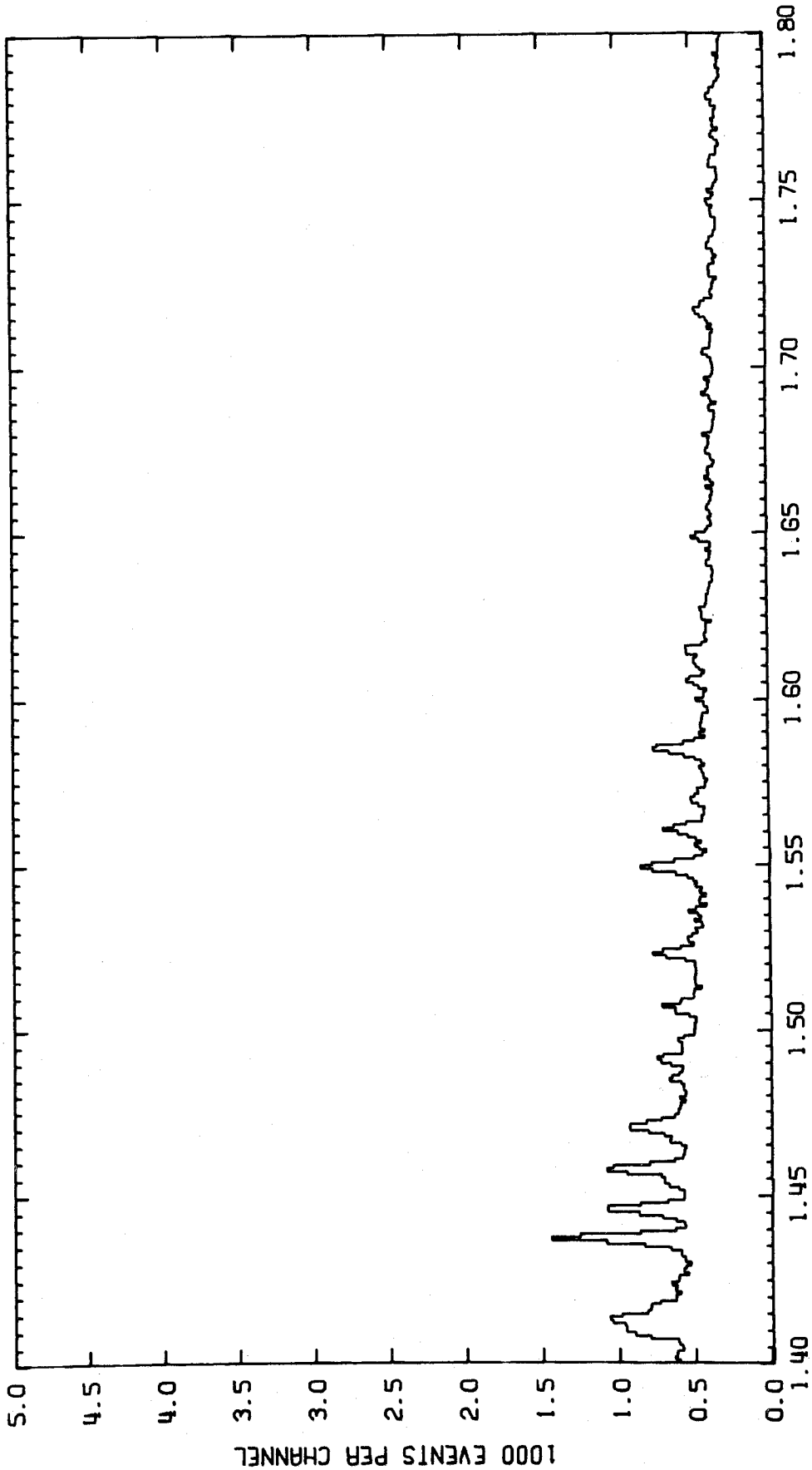

Fig. B24. Gamma-ray spectrum from 1.49 to 2.00-MeV incident neutrons.

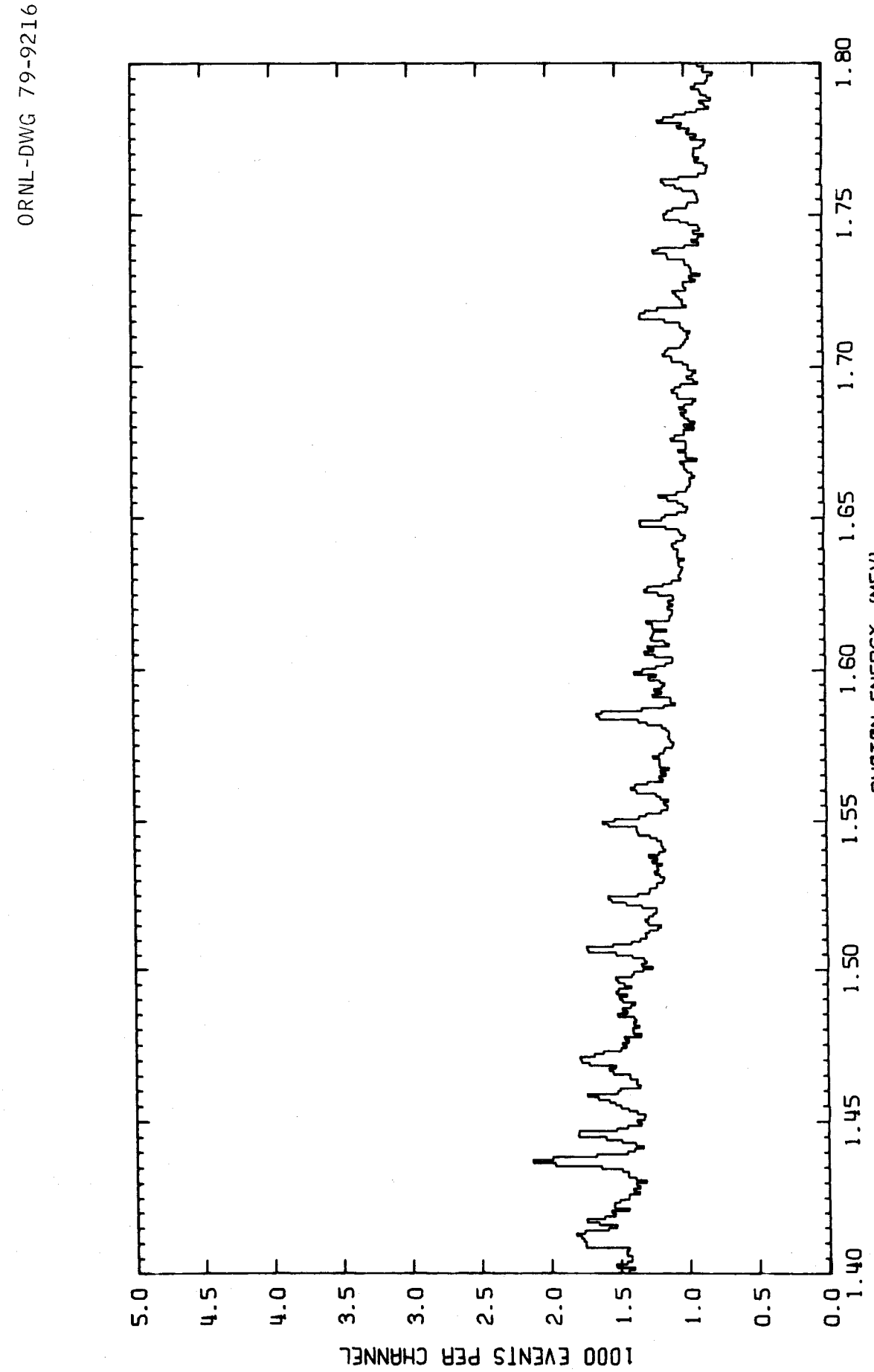

Fig. B25. Gamma-ray spectrum from 2.00 to 4.30-MeV incident neutrons.

ORNL/TM-6832
ENDF-281
Dist. Category UC-79d

INTERNAL DISTRIBUTION

1. L. S. Abbott
2. G. T. Chapman
3. G. de Saussure
4. J. K. Dickens
5. C. Y. Fu
6. C. H. Johnson
7. D. C. Larson
8. R. L. Macklin
9. F. C. Maienschein
10. B. F. Maskewitz
11-20. J. W. McConnell
21-30. D. K. Olsen
31-50. R. W. Peelle
51. F. G. Perey
52. R. B. Perez
53. R. R. Spencer
54. J. H. Todd
55. P. Greebler (consultant)
56. W. B. Loewenstein (consultant)
57. R. E. Uhrig (consultant)
58. R. Wilson (consultant)
59-60. Central Research Library
61. ORNL Y-12 Technical Library Document Reference Section
62-63. Laboratory Records Dept.
64. ORNL Patent Office
65. Laboratory Records (RC)

EXTERNAL DISTRIBUTION

66-75. G. L. Morgan, Los Alamos Scientific Laboratory, Physics Division, Los Alamos, New Mexico 87545
76. Office of Assistant Manager, Energy Research and Development, DOE-ORO, Oak Ridge, Tennessee 37830
77-78. DOE Division of Reactor Research and Development, Washington, D.C. 20545: Director
79-398. For distribution as shown in TID-4500 Distribution Category UC-79d, Liquid Metal Fast Breeder Reactor Physics - Base (60 copies - ENDF distribution)

☆U.S. GOVERNMENT PRINTING OFFICE: 1979-640-079- 205

UNITED STATES DEPARTMENT OF ENERGY
P.O. BOX 62
OAK RIDGE, TENNESSEE 37830

OFFICIAL BUSINESS
PENALTY FOR PRIVATE USE, $300

POSTAGE AND FEES PAID
UNITED STATES
DEPARTMENT OF ENERGY

ENDF

U.S. Department of Energy
ATTN: Dr. Stanley Whetstone
Nuclear Science
Div. of Basic Energy Sciences
Washington, DC 20545

PRINTED MATTER – BOOKS